UNIVERSITY OF CALIFORNIA, SAN DIEGO

Wave-driven beach sand level changes in southern California

A dissertation submitted in partial satisfaction of the
requirements for the degree
Doctor of Philosophy

in

Oceanography

by

Bonnie Cecily Ludka

Committee in charge:

R.T. Guza, Chair
Falk Feddersen
Sarah T. Gille
Myrl C. Hendershott
Geno Pawlak
Eric J. Terrill

2016

The dissertation of Bonnie Cecily Ludka is approved, and it is acceptable in quality and form for publication on microfilm and electronically:

_____

_____

_____

_____

_____

_____

Chair

University of California, San Diego

2016

DEDICATION

To my grandfather,

“Granddad” David Russell,

for inspiring me to be a scientist

EPIGRAPH

I seem to have been only like a boy playing on the sea-shore, and diverting myself in now and then finding a smoother pebble or a prettier shell than ordinary, whilst the great ocean of truth lay all undiscovered before me.

—-Isaac Newton, 1727

Earth and Sky, Woods and Fields, Lakes and Rivers, the Mountain and the Sea, are excellent schoolmasters, and teach some of us more than we can ever learn from books.

—-John Lubbock, 1894

Either a woman is a good scientist, or she is not; in any case she should be given opportunities, and her work should be studied from the scientific, not the sex, point of view.

—-Hertha Marks Aryton, 1919

Many words will be written on the wind and the sand, or end up in some obscure digital vault. But the storytelling will go on until the last human being stops listening. Then we can send the great chronicle of humanity out into the endless universe.

—-Henning Mankell, 2011

TABLE OF CONTENTS

LIST OF FIGURES

LIST OF TABLES

ACKNOWLEDGEMENTS

It has been a joy to learn how to be a scientist under the guidance of my brilliant advisor Bob Guza. This data set was born out of his vision for a long-term field campaign and sustained by his ability to bring together, manage, and continuously fund a talented team. Guza's exuberant enthusiasm is contagious and his commitment to his students is unwavering. He strikes the perfect balance of giving us freedom while always being there to help. His patience and delightful sense of humor has fostered both my personal and scientific growth. He has taught me the value of high quality observations, to think critically and write minimally. Thank you Guza. Words cannot fully express my gratitude.

Over the past 15 years, more than 800 long days have been spent collecting the sand level observations analyzed in this thesis. Four hundred and ninety of those days were ATV surveys. The other 310 days were part of "Jumbo" surveys, often conducted at ungodly hours to catch the best tide. For these surveys, in addition to riding the ATV, our crew spends hours on the jet-ski bouncing with the waves, and laboriously pushing the dolly through sometimes ripping alongshore currents. As I write the crew is in the field collecting more data. Futhermore, they built our technical survey equipment and somehow manage to maintain it through some of the harshest conditions; whether things are getting clogged by sand, corroded by salty ocean water, or slammed by waves. Despite the sometimes tough conditions, these folks are always having fun. I owe many thanks to our crew, Bill Boyd, Greg Boyd, Zoe Dagan, Dennis Darnell, Rob Grenzeback, Ian Nagy, Lucian Perry, Kent Smith, and Brian Woodward, as well as all of the volunteers who have helped collect the sand level data. Also thanks to Michele Okihiro, our organizational mastermind, who takes care of the (seemingly infinite) logistics for our ambitious endeavors. Lifeguard Captain Robert Stabenow ensured safe access to Imperial Beach. Kathy Weldon, City of Encinitas Shoreline Management Division Manager, facilitated work at Cardiff, while the aid of Kathleen

Ritzman, Scripps Assistant Director, was crucial in maintaining funding and survey continuity. It took a village to raise this dataset.

Bill O'Reilly coupled this rich set of sand level observations with essential wave data, and the members of CDIP (Coastal Data Information Program), including Julie Thomas, Randy Bucciarelli, Grant Cameron, Darren Wright, and Corey Olfe, have supported and made these data sets accessible.

I am thankful to have had the opportunity to build strong connections with the international coastal processes community. My advisor ensured I was able to present at international conferences, where I met talented scientists and engineers. Nathaniel Plant provided helpful insights regarding interpolation of bathymetric data and error estimation. Marissa Yates offered her expertise on equilibrium beach concepts and applications. Marcel Stive, Matthieu de Schipper and Sierd de Vries invited me to help with a field experiment in the Netherlands (MEGAPEX) at the massive sand replenishment site, "The Sand Engine", and have given me the opportunity to return this fall to learn how to use Dutch process-based morphological models. My advisor also generously sent me to a summer class at Woods Hole Oceanographic Institute, organized by Rocky Geyer, that further strengthened my fieldwork skills under the primary tutelage of Steve Elgar and Britt Raubenheimer. Combined with Scripps' Scientific Diver Training and the campaigns organized by our group in San Diego, Oregon and North Carolina, I have spent over 100 days in the field.

I would like to thank Falk Feddersen, Sarah Gille, Myrl Hendershott, Geno Pawlak and Eric Terrill for serving on my committee. Falk taught me about surf zone processes through reading group, his nearshore processes class, and informal discussions around CCS. Sarah helped build my data analysis foundation in her workshop-style class and was always available for troubleshooting or a discussion of analysis techniques. Myrl taught me fluid mechanics and waves, but I think he actually does more teaching at

TG where he is elated by talking to students about their work and offers us a wealth of knowledge. I have also valued Geno and Eric's insight as they both do exciting science in the nearshore.

I have thrived here because of the warm, vibrant and collaborative SIO community. Thanks to the professors, computing support team, diving officers, and graduate and business office staff who have helped me throughout my PhD. I am grateful that the "elder" CASPO students took me under their wing when I first arrived. My first year PO cohort became my study buddies, teachers, and friends. The graduate students and postdocs in the CCS "dungeon" basement have offered camaraderie, mentoring, and stimulating scientific conversations. Sean Crosby and Julia Fiedler were dedicated co-teachers of our self-designed, hands on Academic Connections class "The Physics of the Ocean World" and I look forward to teaching "Global Environmental Leadership and Sustainability" this summer with Veronica Tamsitt. We received a UC Ship Funds Award to take our students out on the R/V Sproul this summer! I am also thankful for the outreach opportunities, discussions and support from the SIO Team for Inclusion, Engagement, and Diversity in Science (TIDES).

In addition to all the amazing people I met at SIO, I was fortunate to befriend people in the greater San Diego community, whether through volunteering, ultimate frisbee, surfing, the community center-like house on Bonair St., or other activities. These wonderful folks keep me grounded by reminding me that while I am busy with science, there are good people taking care of everything else. My best friend Beth Kimball has heard about every high and low of graduate school and has been a pillar of support.

I am indebted to the many teachers and research mentors whose guidance led me to graduate school including Professors Paul and Debra Warne, David Schaefer, Deidre Hunter, Kevin Giovanetti, and Paola Cessi. Also, thanks to my friend Kate Ruck, for introducing me to the field of Oceanography.

My ability to engage in this academic pursuit is more a testament of my parent's hard work than mine. My mother made me fall in love with nature and my father made me wonder how things work, while my sisters were my partners in crime. My (Gramps) grandfather Ludka taught me "not to take crap from anyone" and to laugh about it if they do. My sweet (Grandma) grandmother Ludka gifted her perfectionism to my father who passed it on to me; a blessing and a curse, but in some ways necessary for science. My (Grammie) grandmother Russell not only taught me music, but to march to the beat of my own drum. My (Granddad) grandfather Russell inspired me to be a scientist and helped me with my math homework. He also taught me to fish and made me wonder what was happening beneath the water's surface.

This thesis was supported by the United States Army Corps of Engineers and the California Department of Parks and Recreation, Division of Boating and Waterways Oceanography Program (Program Manager Ron Flick). I am grateful to have received funding from the National Science Foundation's Graduate Research Fellowship, as well as NOAA grant NA10OAR4170060, California Sea grant project #R/RCC-01, through NOAA's National Sea Grant College Program, and the NOAA/Southern California Coastal Ocean and Observing System. The statements, findings, conclusions, and recommendations here are those of the authors and do not necessarily reflect the views of the aforementioned organizations.

The text of Chapter 2, in full, is a reprint with minor modifications of the paper "Field evidence of beach profile evolution toward equilibrium", *Journal of Geophysical Research: Oceans*, *120*(11), 75747597. doi: 10.1002/2015JC010893 (Copyright of the American Geophysical Union 2015). The dissertation author was the primary researcher and first author with guidance provided by R.T. Guza, W.C. O'Reilly and M. L. Yates.

The text of Chapter 3, in full, is a reprint with minor modifications of the paper "Mid-El Niño erosion at nourished and unnourished southern California beaches",

Geophysical Research Letters, 43, 45104516, doi:10.1002/2016GL068612., (Copyright of the American Geophysical Union 2016). The dissertation author was the primary researcher and first author with guidance provided by R.T. Guza and contributions from T.W. Gallien and S.C. Crosby.

The text of Chapter 4, in full, is a reprint with minor modifications of the paper "The evolution of four southern California beach nourishments", to be submitted to *Coastal Engineering*. The dissertation author was the primary researcher and first author with guidance provided by R.T. Guza and W.C. O'Reilly.

VITA

2007	B.Sc. Physics, Minor Mathematics, *Cum Laude* James Madison University
2011	M.S. Oceanography, Scripps Institution of Oceanography, University of California, San Diego
2016	Ph.D. Oceanography, Scripps Institution of Oceanography, University of California, San Diego

PUBLICATIONS

Ludka, B. C., Gallien, T., Crosby, S., Guza, R.T. (2016), Mid-El Niño erosion at nourished and unnourished southern California beaches. *Geophysical Research Letters*, 43(9), 4510-4516.

Ludka, B. C., Guza, R.T., O'Reilly, W.C. and Yates, M.L. (2015), Field evidence of beach profile evolution toward equilibrium. *Journal of Geophysical Research: Oceans*, 120(11), 7574-7597.

Cessi, P., Wolfe, C. L., Ludka, B. C. (2010), Eastern-boundary contribution to the residual and meridional overturning circulations. *Journal of Physical Oceanography*, 40(9), 2075-2090.

Hunter, D. A., Elmegreen B. G., Ludka B. C., (2010). Galex Ultraviolet Imaging of Dwarf Galaxies and Star Formation Rates. *The Astronomical Journal*, 139(2), 447-475.

PRESENTATIONS

Ludka, B.C., Guza, R.T., OReilly, W.C., The Evolution of Four Nourished San Diego Beaches, The San Diego Association of Governments Shoreline Preservation Working Group Meeting, San Diego, CA, June 2, 2016

Ludka, B. C., Guza, R. T., OReilly, W.C., Wave-driven Beach Sand Level Changes in Southern California, Applied Ocean Physics and Engineering Seminar, Woods Hole Oceanographic Institute, Woods Hole, MA, January 27, 2016

Ludka, B. C., Guza, R. T., OReilly, W.C., Observations of Four Nourished Beaches. Coastal Sediments Conference, San Diego, CA, May 11-15, 2015.

Ludka, B. C., Guza, R. T., OReilly, W.C., Wave-driven Beach Sand Level Changes in Southern California, Deltares Seminar, Delft, Netherlands, October 14, 2014

Ludka, B. C., Guza, R. T., OReilly, W.C., Observations of Three Nourished Beaches. International Conference on Coastal Engineering, Seoul, Korea, June 16-20, 2014.

Ludka, B. C., Guza, R. T., OReilly, W.C., The Impact of Beach Nourishment on Three San Diego County Beaches. Headwaters to Ocean Conference, San Diego, CA, May 27-29, 2014.

Ludka, B. C., Guza, R. T., OReilly, W.C., Equilibrium Beach Profile Behavior: Observations and Modeling. Ocean Sciences Meeting, Honolulu, HI, February 23-28, 2014.

Ludka, B. C., Guza, R. T., OReilly, W.C., Observations of Three Nourished Beaches in San Diego County. Headwaters to Ocean Conference, San Diego, CA, May 28-30, 2013.

Ludka, B. C., Guza, R. T., McNinch, J., OReilly, W.C., Testing the Equilibrium Beach Hypothesis. AGU Fall Meeting, San Francisco, California, December 3-7, 2012.

Ludka, B. C., Guza, R. T., OReilly, W.C., Exploring Equilibrium Theory Performance. Meeting of Students in Physical Oceanography, San Diego, CA, September 26-28, 2012.

Ludka, B. C., Guza, R. T., O'Reilly, W.C., Exploring Equilibrium Theory Performance. International Conference on Coastal Engineering, Santander, Spain, July 1-6, 2012.

Ludka, B. C., Guza, R. T., Seasonal Sand Level Changes in Southern California: Beyond Wave Energy, International Meeting of Students in Physical Oceanography, Seattle, WA, September 22-24, 2010.

FIELDS OF STUDY

Major Field: Physical Oceanography

Studies in Fluid Dynamics
Professor M.C. Hendershott

Studies in Geophysical Fluid Dynamics
Professors J. A. MacKinnon, P. Cessi and J. R. Norris

Studies in Linear and Nonlinear Waves
Professors W. K. Melville, M. C. Hendershott, and R. T. Guza

Studies in Data Analysis
Professors D. L. Rudnick, R. Pinkle, and S. T. Gille

Studies in Applied Mathematics
Professors E. Lauga, S. G. Llewellyn-Smith, and W. R. Young

Studies in Physical Oceanography
Professors J. A. MacKinnon, U. Send, C. Winant, and D. Roemmich

Studies in Nearshore and Estuarine Processes
Professors F. Feddersen and S. N. Giddings

Studies in Biological Oceanography
Professor P. J. S. Franks

Studies in Community Based Science
Professor B. T. Werner

ABSTRACT OF THE DISSERTATION

Wave-driven beach sand level changes in southern California

by

Bonnie Cecily Ludka

Doctor of Philosophy in Oceanography

University of California, San Diego, 2016

R.T. Guza, Chair

Sand levels were monitored at five southern California beaches for periods of 3 to 15 years, spanning a total of 18 km alongshore. Every 3 months, GPS equipped vehicles measured sand elevations on cross-shore transects from the backbeach to 8 m depth, with 100 m alongshore resolution. Subaerial observations were collected monthly above the spring low-tide line. Wave buoys and a numerical model provided hourly wave estimates in 10 m depth at each site.

These observations show that beach profile shapes (depth versus cross-shore distance) evolve consistent with the equilibrium hypothesis: under steady wave conditions, evolution is toward a unique, wave condition dependent, equilibrium beach profile.

Beaches far out of equilibrium change rapidly, and as equilibrium is approached they change ever more slowly. At the sandy regions, a simple equilibrium beach state model has skill >0.5 (Chapter 2, [Ludka et al., 2015]).

Repeated nourishments over multiple decades, costing hundreds of thousands of dollars, are a primary beach management strategy worldwide, but the wave-driven redistribution of nourishment sand is poorly understood. At four survey sites, 50,000-300,000 m^3 of imported sand was placed on the subaerial beach over alongshore spans between 300-1300 m. Wave conditions in the months after placement were similar at all sites, but the subaerial nourishment pads eroded and retreated landward at different rates. A pad built with native-sized sand washed offshore in the first few storms. In contrast, nourishments with coarser than native sand remained on the beach face for several years and protected shorelines during the significant wave attack of the 2015-16 El Niño (Chapter 3, [Ludka et al., 2016]). These relatively resilient and coarse subaerial pads stretched alongshore in a pattern consistent with seasonally shifting, wave-driven alongshore currents. Natural gains and losses in the total sand volume budget, integrated spatially over each site, are sometimes larger than the nourishment contributions (Chapter 4, in prep for Coastal Engineering).

Chapter 1

Introduction

Sandy beaches provide valuable recreation, drive tourism [Pendleton et al., 2012; WorleyParsons, 2013; Alexandrakis et al., 2015] and can protect infrastructure from flooding and erosion (Figure 1.1). As coastal populations grow [MacGrannahan et al., 2007], sea level rises, and storm characteristics transform [Stocker et al., 2013], understanding changes in beach sand levels will be increasingly important.

There are no accepted governing equations for sand transport in the turbulent surf zone (Figure 1.2). Currently granular physicists research the flow of grains moving under simpler conditions (e.g. the unidirectional flow of identical spherical grains under gravity down a chute, Figure 1.3 [Delannay et al., 2007]). There are many order-of-magnitude empirical formulations for surfzone sediment fluxes [Baillard, 1981; CERC, 1984; Kamphius, 1991; Ribberink 1998; van Rijn 2007ab; and others], and beach level changes are the result of the relatively small differences between these fluxes. Thus, morphodynamic models are diverse, parameterized, tunable, and inaccurate [van Rijn et al., 2003]. To build better morphodynamic models, observations are critical to rigorously test existing formulations and inspire new approaches.

Using a rich dataset of sand and wave observations, we found that beach profiles

evolve toward a wave-dependent equilibrium beach profile as hypothesized [Wright and Short, 1984; Wright et al., 1985]. In the future, the observed equilibrium behavior could be used as a simple test to validate whether process-based models produce realistic results. (Process-based models estimate sand level changes from the gradients of net sediment fluxes, e.g. XBeach [Reolvink et al., 2009], Unibest-TC [Ruessink et al., 2007; Walstra et al., 2012], COAWST [Warner et al., 2010], and others). Furthermore, a simple model using an equilibrium framework well described the cross-shore evolution of the beach state (both erosion and recovery) at sandy sites in southern California on time scales of months to years [Ludka et al., 2015]. When the few (3) free parameters were calibrated with a few years of quarterly beach profile data, the model could be used to predict the beach state given the wave forcing. Shoreline equilibrium models have been validated on beaches worldwide with diverse morphological characteristics and wave forcings [Miller and Dean, 2004; Yates et al., 2009, 2011; Davidson et al., 2013; Splinter et al., 2013, 2014; Castelle et al., 2014], suggesting that a calibrated equilibrium beach state model may be widely useful. However, both shoreline equilibrium models [Miller and Dean, 2004; Splinter et al., 2014] and the beach profile state model fail at Duck, North Carolina, for unknown reasons. (Investigating the different behavior of Duck compared to these other equilibrium-like beaches is an interesting area of future research.) The minimalist, computationally efficient, empirical equilibrium beach state model is a powerful tool for coastal managers in southern California (and potentially elsewhere), and should be used as a baseline performance standard for more complex process-based models.

Extreme events, the most damaging and most concerning for coastal planners, are inherently difficult to model because of infrequent observations. The equilibrium beach state model overpredicts erosion during the 2009-10 and 2015-16 energetic El Niño winters. Observations during extreme El Niño winters [Dingler and Reiss, 2002; Sallenger et al., 2002; Barnard et al., 2011, 2015; Revell et al., 2011] are essential to

understand the impact of successive energetic storms as well as the equally important recovery between storms. No existing numerical model accurately simulates erosion, recovery, and the potentially increased erosion resistance of bedrock or dense cobble layers sometimes exposed in winter on sediment poor beaches. Waves were similar during the 2009-10 and 2015-16 El Niños, and the equilibrium model predicted slightly more erosion during 2016 than 2010. Torrey Pines was indeed slightly more eroded in 2016 than in 2010, albeit not as eroded as predicted in either winter. Nourishments placed in 2012 complicated the beach response at the other monitored sites [Ludka et al., 2016].

During the observing period, four of the monitored beaches were nourished with mechanically placed imported sand. Despite the frequency and expense of nourishment practices worldwide [Clayton, 1991; Haddad and Pilkey, 1998; Trembanis and Pilkey, 1998; Valverde et al., 1999; Hanson et al., 2002; Cooke et al., 2012; Luo et al., 2015], the wave-driven redistrubution of nourishment sand is poorly understood. Sites nourished in 2012 were constructed with coarse sand relative to native and largely remained subaerial for several years. These sites maintained wider and more elevated beaches during the significant wave attack of the 2015-16 El Niño compared to unnourished sand levels experienced during the previous 2009-10 El Niño [Ludka et al., 2016]. This contrasts the evolution of the 2001 Torrey Pines nourishment pad, constructed with a grain size similar to native, that washed offshore during a storm with an unexceptional significant wave height [Seymour et al., 2005]. At all sites the subaerial nourishment pads were advected in the direction of the seasonally shifting mean alongshore currents. Natural gains and losses in the total sand volume budget, integrated over the entire survey domain, are sometimes larger than the nourishment contributions. These detailed observations will help to inform coastal managers, including those developing a 50-year plan for repetitive nourishments in north San Diego County that will cost $160 million [Diehl, 2015].

Figure 1.1: (a) Sandy beaches provide valuable recreation and drive tourist economies. Sandy beaches can protect coastal infrastructure from (b) flooding and (c) erosion.

Figure 1.2: Sand transport in the turbulent surfzone.

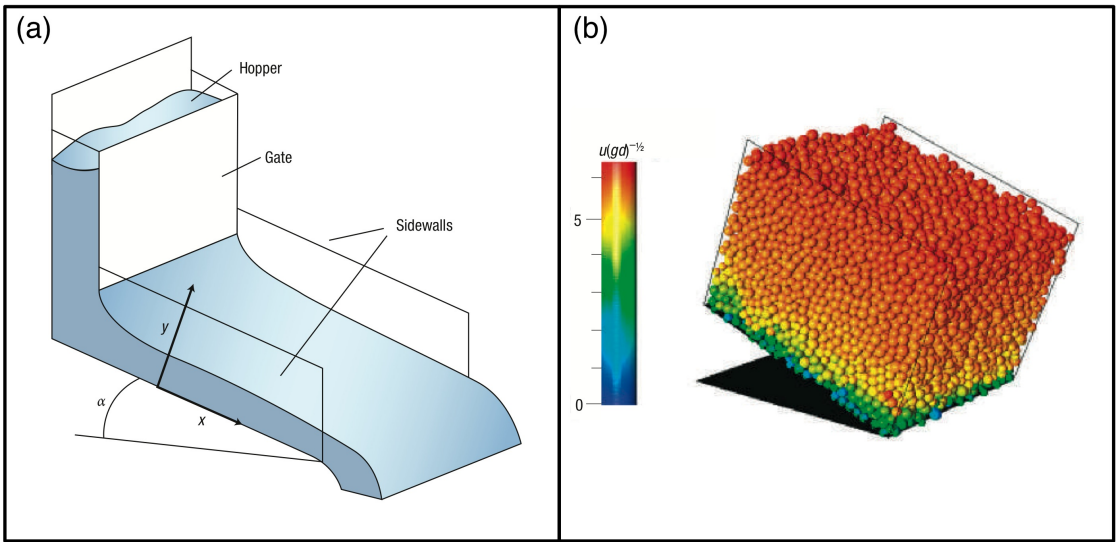

Figure 1.3: (a) A typical facility for studying the unidirectional flow of identical spherical grains under gravity down a chute. (b) Snapshot of a numerical simulation of 10,000 identical spherical grains flowing down an incline with frictionless sidewalls. Color represents dimensionless velocity (where g is the gravitational acceleration and d is the grain diameter) [Delannay et al., 2007].

Chapter 2

Field evidence of beach profile evolution toward equilibrium

2.1 Abstract

An equilibrium framework is used to describe the evolution of the cross-shore profile of five beaches (medium grain size sand) in southern California. Elevations were observed quarterly on cross-shore transects extending from the back beach to 8 m depth, for 3-10 years. Transects spaced 100 m in the alongshore direction are alongshore-averaged into nineteen 700-900 m long sections. Consistent with previous observations, changes about the time average profile in many sections are captured by the first mode empirical orthogonal function (EOF). The first EOF poorly describes sections with hard substrate (less than roughly 80% sandy bottom), and also fails near the head of a submarine canyon and adjacent to an inlet. At the 12 well described sections the time-varying amplitude of the first EOF, the beach state A, describes the well known seasonal sand exchange between the shoreline and offshore (roughly between 4-7 m depth). We show that the beach state change rate dA/dt depends on the disequilibrium between the

present state A and wave conditions, consistent with the equilibrium concepts of Wright and Short [1984] and Wright et al. [1985]. Empirically determined, optimal model coefficients using the framework of Yates et al. [2009a, 2011] vary between sections, but a single set of globally optimized values performs almost as well. The model implements equilibrium concepts using ad hoc assumptions and empirical parameter values. The similarity with observed profile change at five southern California beaches supports the underlying model equilibrium hypotheses, but for unknown reasons the model fails at Duck, N.C.

2.2 Introduction

Worldwide, almost one billion people live at elevations within 10 m of present sea level [Elko et al., 2014] and this population is increasing dramatically [McGranahan et al., 2007]. Sandy beaches provide recreational space, drive tourist economies, and protect coastal infrastructure from flooding and erosion. Sandy beaches are dynamic; in southern California, the beach width typically changes by 20 m between summer and winter. Understanding beach profile response to both energetic waves and calms will be crucial as rising seas encroach on coastal infrastructure and climate change modifies storm frequency and intensity [Stocker et al., 2013].

The time-averaged flux of sediment through a vertical cross-section, the relatively small difference between onshore and offshore fluxes, is difficult to measure or model accurately. Process-based models of cross-shore beach profile evolution estimate sand level changes from cross-shore gradients of the net fluxes [Roelvink and Brøker, 1993]. These models require extensive tuning because many processes involved are understood poorly. XBeach [Roelvink et al., 2009], a widely used process-based model [Callaghan et al., 2013], has limitations. McCall et al. [2010] applied a non-physical ero-

sion limiter to XBeach in order to reproduce barrier island evolution during a hurricane. Pender and Karunarathna [2013] used XBeach to model annual to decadal beach profile change, switching between the original storm erosion module when the arbitrarily predefined storm wave height threshold was exceeded, and a newly created recovery module during smaller wave conditions. Unibest-TC, another process-based model, allowed for net shoreward sediment transport, and reproduced on and offshore sandbar migration, growth and decay [Ruessink et al., 2007, Walstra et al., 2012]. However, the shoreline location was held fixed. Energetics models use parameterizations of hydrodynamic forcing and sediment response different from XBeach and Unibest-TC, and also successfully simulate cross-shore sandbar migration [Thornton et al., 1996, Gallagher et al., 1998, Hoefel and Elgar, 2003, Kuriyama, 2012, Dubarbier et al., 2015]. Process-based models are in continual development, and will ultimately provide quantitative understanding of profile evolution by coupling detailed understanding of each underlying process. Equilibrium profile models do not estimate sediment fluxes, and instead rely on the hypothesis that for given wave conditions, profiles tend asymptotically towards a unique equilibrium shape. If the equilibrium framework is shown to produce realistic macroscopic behavior, then equilibrium ideas can be used to evaluate and inspire process-based models.

Pelnard-Considere [1956] and Bakker [1968] coupled conservation of mass with a profile's tendency to maintain particular shapes to predict the spatial and temporal evolution of coastal contours. Bruun [1954] recognized recurring $x^{2/3}$ beach profile shapes (x is the cross-shore distance from the shoreline) in hundreds of observed beach profiles, and models designed to reproduce similar geometric shapes, using mass conservation fundamentally, have been used to describe profile evolution [Kriebel and Dean, 1985, Larson and Kraus, 1989, Dean, 1991, Kriebel and Dean, 1993]. Holman et al. [2014] superimposed sandbars on another profile shape. Davidson et al. [2009] constructed a profile evolution model using a different spatial shape and a constant wave threshold

to determine the sense (erosion or accretion) of profile evolution. Similar to Pender and Karunarathna [2013], the threshold does not depend on the present profile state or antecedent wave conditions. In the model developed below, the equilibrium shape, and the sense of profile evolution (shoreline erosion or accretion) is determined by the observations. Mass is not necessarily conserved in the observations or model.

Wright and Short [1984] identified descriptive two-dimensional equilibrium morphologies that depend on the value of the parameter, $\Omega = H_b/(w_s T)$, where H_b is the breaking wave height, w_s the sediment settling velocity, and T is wave period. Wright et al. [1985] noted that beach response to incident wave conditions is not instantaneous, but rather evolves toward the equilibrium state at a rate dependent on both the incident wave conditions and the present beach state (and hence the recent wave history). More recently this concept demonstrates skill at predicting the observed alongshore-averaged bar crest position [Plant et al., 1999, Pape et al., 2010], shoreline location [Miller and Dean, 2004; Yates et al., 2009a; Yates et al., 2011; Davidson et al., 2013; Castelle et al., 2014; Splinter et al., 2014], and beach three-dimensionality [Plant et al., 2006, Stokes et al., 2015] on a broad range of beaches.

Here the equilibrium hypothesis is further explored with up to 10 years of quarterly beach profiles at 5 southern California sites. Beach profile time series of this length, frequency, and spatial coverage, described in section 2.2, provide a unique opportunity to evaluate equilibrium profile models. In section 2.3, the state A of the evolving profile is characterized using empirical orthogonal function (EOF) analysis [Winant et al., 1975, Aubrey, 1979, Aubrey et al., 1980]. The relationship of A to incident waves is broadly consistent with the equilibrium framework of Wright et al. [1985] (section 2.4). Aubrey et al. [1980] and Larson et al. [2000] also related statistical modes to the wave field, although they did not employ an equilibrium response. An equilibrium beach state model following Yates et al. [2009a, 2011] is developed and tested in section 2.5 and alternative

model formulations are explored. In section 2.6, the model is extended from beach state *A* to the depth profile. As summarized in section 2.7, the similarity with observed profile change in southern California supports the underlying model equilibrium hypotheses, but for unknown reasons the model fails at Duck, N.C.

2.3 Observations

2.3.1 Field sites

Sand levels and waves are monitored at 5 beaches within an 80 km reach in San Diego County, southern California (Figure 2.1): Imperial Beach (IB), Torrey Pines (T), Cardiff (C), Solana (S), and Camp Pendleton (P). The sand is medium-grained (median D_{50} = 0.20 $\pm$ 0.05 mm), but with considerable alongshore and cross-shore variation (Table 2.1)[Haas, 2005, Yates et al., 2009b]. Hard substrate at some locations [Moffatt and Nichol, 2009] affects profile change. Imperial Beach has a few offshore cobble patches in the south, adjacent to the cobbly shoal of the Tijuana River mouth (1 km south of the southernmost considered transect). A 450 m recreational pier is located at the IB central section, and there are two short 100-150 m jetties in the northern region. Torrey Pines has some cobble patches and reef in the north (Figure 2.2a), where Los Peñasquitos lagoon mouth connects to the ocean (section T9, Figure 2.2a). Scripps submarine canyon is just offshore to the south (Figure 2.2a). Torrey Pines is the study location of Shepard [1950], Winant et al. [1975], Aubrey [1979], Aubrey et al. [1980], Yates et al. [2009a, 2009b], and others. Solana Beach has reef in the south and north (Figure 2.6a, discussed below), and the San Dieguito Lagoon mouth is a few 100 m south of the southernmost transect. Cardiff Beach has reef and cobble patches in the south (Figure 2.6a, discussed below), and the San Elijo Lagoon mouth is a few 100 m north of the northernmost transect. Beach width and shoreface slope vary seasonally and

alongshore. Typical values are in Table 2.1.

2.3.2 Waves

Waves are seasonal in southern California, with winter storms and summer calms. The offshore Channel Islands create coastal wave shadows [Pawka, 1983], and wave refraction over submarine canyons and other features contributes to alongshore variability in wave characteristics. Island blocking and refraction over local coastal bathymetry are modeled numerically (Figure 2.1). Swell wave (0.04-0.1 Hz) predictions are initialized with buoys near and seaward of the island system (triangles, Figure 2.1). Sea wave (0.08-0.5 Hz) propagation models are driven with nearby nearshore buoys (circles, Figure 2.1). Hourly directional wave properties are estimated every 100 m alongshore at Monitoring and Prediction (MOP) locations, in 10 m depth, and alongshore averaged within each 700-900 m long section (T8 is shown in Figure 2.2d). The swell model [O'Reilly and Guza, 1998] compares favorably with nearshore buoys in the present study area [Young et al., 2012].

2.3.3 Sand levels

Sand levels were measured on cross-shore transects spaced 100 m (50 m at Camp Pendleton) apart in the alongshore, from the backbeach to $\sim$8 m depth (Figure 2.2a), using GPS-equipped platforms [Seymour et al., 2005]. Bias and root mean square errors (RMSE, defined in Appendix 2.A) are each roughly 10-15 cm. Although labor intensive relative to remote sensing techniques, the errors are smaller [Wengrove et al., 2013]. Approximately quarterly surveys were acquired for 3 -10 years with alongshore spans between 1.4 km (Cardiff) and 7.3 km (Torrey Pines, Table 2.2). Profiles were created by bin-averaging elevation data in 20 m alongshore by

1 m cross-shore bins centered on the predetermined cross-shore transect lines, applying a 2 m cross-shore moving average, and splining to a 1 m grid wherever breaks in data do not exceed 20 m. Southern California beach profiles vary seasonally (Figure 2.2c). In summer an elevated subaerial berm forms, while in winter the subaerial beach erodes and an offshore bar develops [Shepard, 1950, Winant et al., 1975, Aubrey, 1979, Aubrey et al., 1980, Yates et al., 2009a, Yates et al., 2009b].

Subaerial sand levels were measured more frequently (approximately monthly) at low tide on alongshore transects, spaced approximately 10 m apart in the cross-shore (Figure 2.2b). Subaerial cross-shore transects with 1 m resolution were created by interpolating observations within 20 m-wide alongshore swaths around the pre-determined cross-shore transect line, onto the transect line. These subaerial measurements were not used in the analysis below but are sometimes shown to aid visual interpretation of the results.

On each transect, time series of sand level are created at the cross-shore locations with mean depths from -9 to +2 m (relative to MSL) at 1 m intervals. Transects missing more than half of the elevation data at these locations were discarded. Then, cross-shore locations missing more than half of the remaining time series were thrown out. Lastly, survey dates missing more than half of the remaining grid points were not used. The surveys were divided into 700-900 m alongshore sections, and elevation time series at each depth alongshore averaged, and the mean removed. After this, no more than 3% of the profile data was missing at each beach section and these gaps were linearly interpolated first in space and then in time for the analysis below. Torrey Pines sections (T1-T9) are shown in Figure 2.2a, and Cardiff (C1-C2) and Solana Beach (S1-S3) in Figure 2.6a (discussed below). The shoreline elevation for section T8 (green in Figure 2.2d, including both subaerial and profile surveys) shows the expected summer accretion and winter erosion. Not surprisingly, vertical changes are reduced over (intermittently

exposed) offshore reefs (e.g. Figure 2.3). Sand level changes are unusually large in the offshore portion of section T1 located near a submarine canyon (Figure 2.3).

2.4 Empirical orthogonal function analysis

Empirical orthogonal function (EOF) analysis (Appendix 2.B) [Lorenz, 1956] is used to decompose the profiles into the basis functions that most efficiently explain the data variance [Davis, 1976]. The first mode explains more variance than any other mode. Typical EOF mode 1 (hereafter EOF 1) temporal amplitude $A(t)$ (e.g. Torrey Pines section T8, Figure 2.4a) and spatial shape $W(x)$ functions (Figure 2.4b) correspond to a seasonal bar-berm rocking of sand between the shoreline (near mean sea level) and offshore (roughly 4-7 m depth) [Winant et al., 1975, Aubrey, 1979, Aubrey et al., 1980, Yates et al., 2009a]. In summer $A > 0$, and the profile is bermed. In winter $A < 0$, and the profile is more strongly barred. Observed and reconstructed profiles using EOF 1 only are generally similar (Figure 2.4c,d), with the highest skill (defined in Appendix 2.A) near the shoreline and offshore bar crest ($R^2 > 0.5$ near x=0 and -200 m, blue curve Figure 2.4e). Reconstruction skill is low offshore (x=-350 m), but elevation fluctuations are small (standard deviation $\sim$0.1 m, red dash-dotted line in Figure 2.4e). EOF 1 contains 56% of the total variance of all cross-shore locations at T8.

The empirical model for beach change developed below (sections 4 and 5) relies crucially on the existence of the spatially coherent fluctuations captured in EOF 1, similar to section T8 (Figure 2.4). Seasonal cross-shore rocking was at least weakly detectable at all sections (variation from purple to green in Figure 2.5a) except T1 just onshore of a submarine canyon. At T1, shaded grey in Figure 2.5a, the entire profile tends to rise and fall in tandem. Six additional sections were anomalous with either fewer than 5 substantially coherent cross-shore locations (purple diamonds in Figure 2.5c) and/or

less than half the total variance explained (purple diamonds in Figure 2.5d). Anomalous sections are rocky (Figure 2.6a,b) [Moffatt and Nichol, 2009], and/or near a canyon or lagoon mouth (labeled in Figures 2.5, and 2.6). Twelve sandy sites (IB1, IB2, IB3, T2, T3, T4, T5, T8, S2, C2, P1, P2, unshaded sections in Figure 2.5, and bold axis labels in Figure 2.5 and 2.6b), away from reefs, a lagoon mouth and a submarine canyon, were analyzed for equilibrium behavior.

2.5 Observational evidence of equilibrium beach profiles

The beach state change rate, dA/dt, and average wave energy, $\langle E \rangle$, between a pair of consecutive surveys are only weakly correlated (average $R^2 = 0.25$ at all 12 sections). This result is consistent with equilibrium theory: the beach state change rate depends not only on the incident wave energy, but also on the present state of the profile. In Figure 2.7a, the beach state change rate between surveys, dA/dt, depends on both $\langle E \rangle$ and the state of the beach of the first of the two consecutive surveys, $A(t_0)$. For a given $\langle E \rangle$, the profile can change towards a more or less barred beach (colorbar, Figure 2.7a), depending on $A(t_0)$. The observations are equilibrium-like, but the details are distorted by wave averaging between surveys [Yates et al., 2009a]. The equilibrium wave energy, E_{eq}, is the E for which a given initial beach state does not change (dashed black line drawn by eye, Figure 2.7a). If the beach is out of equilibrium with the incident waves, it moves toward the equilibrium shape. For example, with $\langle E \rangle = 0.068$ m^2, (black dotted horizontal line Figure 2.7a), a beach with an initially eroded shoreline and developed offshore bar (left black dot, $A = -0.28$ Figure 2.7a, blue profile with circles Figure 2.7b) will move toward the equilibrium profile (black line Figure 2.7b) with offshore bar erosion and beach face accretion (blue arrows with circle base Figure 2.7b). Conversely,

with the same $\langle E \rangle$ a beach with a well developed berm and no offshore bar (right black dot, $A = +0.28$ Figure 2.7a, red profile with diamonds Figure 2.7b) moves toward the same equilibrium profile (black line Figure 2.7b), with onshore berm erosion and offshore bar accretion (red arrows with diamond base Figure 2.7b). Although wave averaging between surveys blurs Figure 2.7, dA/dt appears to increase when $\langle E \rangle$ is farther from the equilibrium wave energy E_{eq}, (as the deviation from the dashed black line in Figure 2.7a, increases). Figure 2.7 is similar to Yates et al. [2009a] for location of the MSL contour, but extended to the profile state. The axes (flipped) of Figure 2.7 resemble the axes of Wright and Short [1984]'s Figure 12 and Wright et al. [1985]'s Figure 9, but instead of descriptive 2D beach states, the beach state is simplified to cross-shore profiles and quantified using the EOF. The present observations span intermediate states (Iribarren number 0.3-0.7), and $A > 0$ is more reflective than $A < 0$, according to Wright and Short [1984] and Wright et al. [1985]. The undistorted equilibrium energy relationship (solid black line in Figure 2.7a) is now estimated from the model using hourly wave conditions that resolve individual storms.

2.6 Equilibrium beach state model

2.6.1 State model formulation

A 1D equilibrium beach profile state model is developed that extends the shoreline model of Yates et al. [2009a, 2011], which was inspired by Wright and Short [1984], Wright et al. [1985] and Miller and Dean [2004]. The instantaneous beach state change rate dA/dt is assumed proportional to the instantaneous energy E and energy disequilibrium ΔE

$$\frac{dA}{dt} = C^{\pm} E^{1/2} \Delta E, \tag{2.1}$$

where $C^{\pm}$ are empirical change rate coefficients for accretion (C^{+} for $\Delta E < 0$) and erosion (C^{-} for $\Delta E > 0$). The factor $E^{1/2}$ ensures small changes in A when E is small. The sign of dA/dt is determined by the sign of the energy disequilibrium,

$$\Delta E = E - E_{eq}(A). \tag{2.2}$$

For simplicity, a linear equilibrium relationship is assumed,

$$E_{eq}(A) = aA + b, \tag{2.3}$$

where a and b are empirical parameters. For a given beach state, A, the equilibrium energy E_{eq} is the wave energy that causes no profile change. Rearranging (2.3) yields the equilibrium beach state for a given wave energy,

$$A_{eq} = \frac{E-b}{a}. \tag{2.4}$$

With constant E, the approach to equilibrium is exponential,

$$A(t) = \left(A_0 - A_{eq}\right) e^{\left(-aC^{\pm}E^{1/2}t\right)} + A_{eq}, \tag{2.5}$$

where A_0 is the initial beach state, and $(A_0 - A_{eq})$ is the initial disequilibrium. The four free parameters, $C^{\pm}$, a and b, are found as a best fit (minimum root mean square error, RMSE, Appendix 2.A) between the observations and the model forced with hourly wave estimates. This non-linear optimization problem is solved with simulated annealing [Kirkpatrick et al., 1983, Barth and Wunsch, 1990], a simple method that can navigate many local minima.

2.6.2 State model skill and error

The equilibrium model for beach state, A, equations (2.1)-(2.3), was tested on the 12 beach sections where the first mode EOF well describes the profile observations (IB1, IB2, IB3, T2, T3, T4, T5, T8, S2, C2, P1, P2). At T8, modeled and observed A are well correlated (Figure 2.8b), and at all sites $R^2 > 0.75$ and NMSE < 0.25 (Figure 2.8c). (Skill or R^2, and NMSE are defined in Appendix 2.A.) The model A error is consistently and anomalously large during the energetic El Niño winter 2009-10 (Figure 2.9). Shoreface erosion (and offshore accretion) was overpredicted using model parameter values largely determined by more moderate conditions. The effect of varying the duration and intensity (e.g. including El Niño) of calibration periods on model performance is usually not strong, as discussed further below.

2.6.3 State model parameter values and transportability

Best-fit model free parameters vary between sites (Figure 2.10a-d). However, model performance is similar using a single set of parameters fit to all 12 sections (vertical dashed lines in Figure 2.10a-d). The NMSE for the universal parameters is generally only slightly larger than with section specific parameters (compare open circles with dark triangles Figure 2.10e). As in the Yates et al. [2009a, 2011] shoreline model, the free parameter values are not well constrained by the observations. For example, the horizontal bars in Figure 2.10d indicate the wide range of values for a for which the RMSE changes by less than 10% while holding other parameters constant. Furthermore, changes from optimal in one free parameter can be compensated by changes in other parameters such that the error minima in the 4-dimensional parameter space are even more broad (not shown). Spatial variability in model parameter values has been ascribed to sand grain size and other physical factors [Davidson et al., 2013, Splinter et al., 2014, Stokes et al., 2015],

but is only physically significant if the parameters are well constrained.

2.6.4 Alternative beach state model formulations

Beach state model performance is relatively insensitive to details. For example, modeled beach state NMSE is increased only slightly by setting $C^+ = C^-$ and solving for 3 instead of 4 free parameters for each section at Torrey Pines (compare gray X with filled black circles in Figure 2.11). Using the same 4 optimal free parameters for all Torrey Pines sections also only slightly degrades results (green square in Figure 2.11). However a constant E_{eq}, significantly degrades model performance (open black circles in Figure 2.11) because the observed dependence of the beach state change rate on the present beach state (e.g. the variation of color along a line of constant $< E >$ in Figure 2.7a) is not modeled. Constant E_{eq} here is similar in principle to the constant $\Omega_{eq} =< H_b/(w_s T) >$ ($<>$ is time average) equilibrium condition used by Davidson et al. [2009, 2010].

Model performance was insensitive to including wave period T in equation (2.1) when replacing $E^{1/2}$ (proportional to significant wave height H_s) with H_s/T, $H_s T$, and $H_s T^2$,

$$\frac{dA}{dt} = C^{\pm}\frac{H_s}{T}\left[\frac{{H_s}^2}{T^2} - (aA+b)\right], \tag{2.6}$$

$$\frac{dA}{dt} = C^{\pm}H_s T\left[{H_s}^2 T^2 - (aA+b)\right], \tag{2.7}$$

$$\frac{dA}{dt} = C^{\pm}H_s T^2\left[{H_s}^2 T^4 - (aA+b)\right], \tag{2.8}$$

where the parameters were recalibrated for each alternate formulation (Figure 2.11). Yates et al. [2009a] found their equilibrium shoreline model performed similarly for several formulations including replacing $E^{1/2}$ by E, E^2, the radiation stress component S_{xx}, or $\Omega = H_b/(w_s T)$ (H_b is the breaker height and w_s the sediment settling velocity). Miller and Dean [2004] showed that different rate proportionalities including H_b, ${H_b}^2$,

$H_b{}^3$, or Ω were more effective at reproducing shoreline change at different beaches. Davidson et al. [2009, 2010] employed Ω in their rate 'forcing' term, while Davidson et al. [2013], and Splinter et al. [2013, 2014] preferred a term proportional to $H\sqrt{T}$. Davidson et al. [2009, 2010, 2013] and Splinter et al. [2013, 2014] suggested Ω is an important parameter for modeling shoreline disequlibrium. Steeper waves (large H/T) may be more efficient at moving sediment; however, Stockdon et al. [2006] suggests that runup at the shoreline during storms increases as HT^2, suggesting a drastically different dependence on wave period. Although almost certainly important to sediment transport, there is no data-based reason to include wave period in the present model. A simple sinusoidal 3-parameter fit (amplitude, frequency and phase) to the temporal amplitude provides a baseline (black cross Figure 2.11) that is outperformed by all model versions except when E_{eq} is constant.

2.7 Discussion

2.7.1 Equilibrium beach profile model

The first mode EOF demonstrates some skill at profile reconstruction (Figures 2.4e and 2.5b), and the first mode temporal amplitude A is well modeled at the selected sections (Figure 2.8c).

Profile model formulation

As suggested by Yates et al. [2009a], the profile model uses the form of the first mode EOF reconstruction,

$$z(x,t) = W(x)A(t) + \langle z(x,t)\rangle, \tag{2.9}$$

where $\langle\rangle$ is the time mean, EOF analysis provides the spatial weights, W, and the temporal amplitude, A, is modeled with equilibrium equations (2.1)-(2.3). The profile model cannot outperform the skill of the first mode EOF reconstruction that it emulates. With N modeled cross-shore locations, W gives the $N-1$ additional empirical parameters that extend the state model to the profile ($W = 1$ at the shoreline). The equilibrium beach profile is calculated using equations (2.4) and (2.9),

$$z_{eq}(x,t) = W(x)\left(\frac{E(t)-b}{a}\right) + \langle z(x,t)\rangle. \tag{2.10}$$

Beach profile evolution at T8 for 4 months (period highlighted in gray in Figures 2.8 and 2.14) is shown in Figure 2.12. At the end of summer the mildly bermed beach is in equilibrium (the blue dashed modeled profile is approximately the same as the red dotted equilibrium profile in Figure 2.12b) with the low E waves (19 September, time t_1, Figure 2.12a). For 2 months, E is low (Figure 2.12a), only briefly exceeds E_{eq}, and little beach change is predicted (not shown). With the higher energy waves between 18 December and 10 January, $E > E_{eq}$ (Figure 2.12a), the bermed beach is out of equilibrium (Figure 2.12c) and evolves toward a barred profile (Figure 2.12d). After E subsides at t_4, the barred beach is predicted to recover (Figure 2.12e).

Equilibrium profiles from all beach sites (shown in Figure 2.13 for low and moderate E =0.01 m^2 and 0.2 m^2, $H_s = 0.4$ and 1.8 m, respectively) differ from the $x^{2/3}$ shape proposed by Bruun [1954] and others. Equilibrium profiles for higher E (not shown) often contain a non-physically large offshore bar. However, the non-physical bar is not predicted to develop for the field conditions, because high wave energy only persists briefly and equilibrium is not reached. For example at T8, with the present calibration, the offshore bar will exceed MSL if waves with E =0.5m^2 ($H_s = 2.8$m) persist on an initially accreted profile of beach state A = 1 for longer than about 4.5 months. During the

calibration period waves only exceeded $E = 0.5\text{m}^2$ during brief episodic storms (Figure 2.2d). The present model therefore cannot be extrapolated to periods of large waves much longer than used in the calibration. Given such observations the profile model response can be calibrated and adjusted as necessary by altering equations (2.1)-(2.3).

Profile model skill and error

Time series of modeled and observed sand elevations at various cross-shore locations are shown in Figure 2.14a-e at T8. Note that the time series detailed in Figure 2.12 (shaded gray in Figures 2.8 and 2.14) is relatively well modeled with small absolute error (Figure 2.14f). Model error (Figure 2.14f) and skill (dashed red line with squares, Figure 2.14g) vary across the profile consistent with the performance of the first EOF mode reconstruction (solid blue line with circles, Figure 2.14g). Model skill is high near the shoreline (mean depths 0, +1m) and at the typical winter bar location (mean depths -4m, -5m). Offshore (mean depth -8m) the skill is low, but changes are small (standard deviation in Figures 2.4e and 2.3).

The model fails most significantly mid-profile ($x = -100\text{m}$), where skill is low (Figure 2.14c,g) and signal (standard deviation of observed elevations, Appendix 2.A) is high (red dashed-dot curve, Figure 2.4e). Here the profile model fails because the EOF 1 reconstruction fails. EOF 1 reconstructs the data with a rocking motion, and the mid-depth profile tends to be at the node ($x = -125\text{m}$, Figure 2.4b), so the model reconstructed elevation fluctuations are small (red in Figure 2.14c). Extending the equilibrium profile model equations (2.1)-(2.10) with EOF mode 2 or complex EOF mode 1 (CEOF 1) did not show promise for improving overall model performance (Appendix 2.C).

The profile model performance is similar to T8 at all 12 sandy beach sections located away from significant sediment sources and sinks (Figure 2.15). The number of cross-shore locations with $R^2 > 0.5$ varies between 4-8 out of 11-12 (Figure 2.15a,b) and

global NMSE < 0.6 (Figure 2.15c). Global NMSE is calculated by concatenating the time series at all cross-shore locations and calculating the NMSE (Appendix 2.A).

Profile model calibration duration

Profile model performance changes with calibration duration (Figure 2.16). Both the beach state parameters, a, b, and $C^{\pm}$, determined by optimization, and the spatial shape function parameters, $W(x)$, determined by EOF analysis, are considered in the calibration. With 1 yr of calibration, global NMSE is close to 1, so the prediction is not better than predicting the mean profile. Global NMSE decreases with 2 and 3 yrs of calibration, but then flattens out, qualitatively similar to the results for shoreline model calibrations [Yates et al., 2009a, Splinter et al., 2013]. Including the El Niño winter in the calibration period reduces errors during El Niño, but slightly degrades model performance for the rest of the time series (not shown).

Non-conservation of mass

The cross-shore integrated difference between successive transects does not sum to zero, either in the observations or model. Mass on a transect is not conserved. The elevation fluctuation (Figure 2.12 b-e) of each observed and modeled profile is interpolated to a uniformly spaced cross-shore grid. The equivalent thickness is the cross-shore average of the interpolated elevation fluctuation, $\bar{z}'$ at each observed or modeled survey. An equivalent thickness of a uniform layer over the transect, $\bar{z}'$, is usually $< |10|$ cm at T8 (solid curve with large red circles in Figure 2.17), approximately the expected GPS bias error. Mass is less conserved at some other sections, and equivalent $\bar{z}'$ of 20-30cm, larger than the likely measurement errors, are not uncommon. The model $\bar{z}'$ (dashed curve with small red circles in Figure 2.17) can also reach 20-30 cm (not shown) but tends to be much smaller and noisy, and fails to simulate observed changes in mass on

a transect. In contrast, the model better reproduces the larger $\sigma_{z'}$, the standard deviation of the elevation fluctuation across the profile at each survey (between about 10 and 70 cm, blue curves with triangles, Figure 2.17). Modeled $\sigma_{z'}$ are smaller than observed $\sigma_{z'}$, because only spatially coherent fluctuations are modeled.

Changing water levels

Southern California water levels are dominated by tides with spring elevation changes up to 2.7 m. Storm surge is usually small, although wave-induced setup can raise water levels by more than a meter [Flick and Badan-Dangon, 1989], and El Niño events may raise water levels as much as 30 cm. The timing of wave events relative to water level can be important for profile change [Coco et al., 2014]. Here the EOF derived profile weights $W(x)$ allow the upper profile to move even if it is not wet. Observations with higher time resolution, that resolve changes with tidal level during storms, are needed to develop and test an equilibrium profile model extended to include changing water levels. A model modified to include variable water levels could use a coordinate origin ($x = 0$) that varies with water level (similar to Bruun [1962], and discussed conceptually in Castelle et al. [2014]), rather than the location of the shoreline on the average profile used here.

2.7.2 Model failure at Duck, NC

Shoreline equilibrium models succeed at beaches with a range of morphologies including multi-barred beaches with alongshore variations [Miller and Dean, 2004; Davidson et al., 2013; Splinter et al., 2013, 2014; Castelle et al., 2014], but fail at the alongshore non-uniform multi-barred Duck Beach, NC [Miller and Dean, 2004, Splinter et al., 2014]. The present *profile* model also fails. The profile model depends fundamentally on spatially coherent fluctuations across the profile, yet only locations

with mean depths 0, 1, and 2m are described well by the first EOF at Duck (Figure 2.18c). This contrasts with the southern California beaches, where offshore and near-shoreline locations are strongly coupled. In addition, the amplitude function A (Figure 2.18a) varies at longer than annual time scales and does not follow the present equilibrium framework (not shown). Even when averaging over longer alongshore spans and band passing to isolate the small annual signal, the Duck profile was not equilibrium-like according to the present model (not shown). Plant et al. [1999, 2001] showed that bars at Duck migrate toward an equilibrium location. Complex EOFs (CEOFs) better reconstruct the Duck observations [Ruessink, 2003] and their potential application in an equilibrium profile model similar to the bar crest position model of Plant et al. [1999] is discussed in Appendix 2.C.

The reasons for the dramatically different profile evolution at Duck and southern California are unknown. Although the Duck wave field is seasonal, similar to southern California (Figure 2.19a), the shoreline and other cross-shore locations (not shown) have a small annual signal, and are dominated by lower frequencies (Figure 2.19b) [Plant et al., 1999, Pianca et al., 2015]. The evolution of complex two-dimensional morphology (e.g. bar attachment, detachment, and straightening) has been studied extensively at several beaches, including Duck [Lippmann and Holman, 1990, Holland, 1998, Konicki and Holman, 2000, Plant et al., 2006]. The research pier also induces alongshore variations [Plant et al., 1999, Pianca et al., 2015]. Perhaps, even when alongshore averaged (with or without the vicinity of the pier excluded), these 2-D bar dominated morphologies are fundamentally different from southern California morphologies. The steep foreshore, cross-shore variations in grain size, and exposure to hurricanes and Nor'easters at Duck may also play a role [Larson and Kraus, 1994, Plant et al., 1999, Pianca et al., 2015].

2.8 Summary and conclusions

EOF analysis of profile evolution shows (consistent with previous work) that sandy southern California beaches located away from significant sediment sources and sinks exhibit an annual cross-shore rocking behavior, where the profile adjusts from barred in winter to bermed in summer. At these 12 (of 19) well-behaved sections, the temporal amplitude A of the first mode EOF is a measure of beach profile state. The observations suggest beach state change rate dA/dt depends on both incident wave energy and the present beach state. This is consistent with the equilibrium hypothesis; there is an equilibrium profile for every incident wave condition, and the profile evolves toward equilibrium at a rate proportional to the disequilibrium: the distance from the present to the equilibrium state. The same moderate wave conditions will erode an already accreted beach face (creating an offshore bar), and accrete an already eroded beach face.

A simple beach state model, driven by hourly wave energy, is used to quantify the equilibrium hypothesis at the 12 sections well described by the first EOF. The 3 or 4 parameter beach state model for A has high skill ($R^2 > 0.75$), although the model free parameters are not well constrained. Globally optimized parameters perform almost as well as section specific values. The beach state model is extended to describe the profile using the spatial weights of the first EOF. The EOF-based equilibrium beach profile differs from the classic $x^{2/3}$ profile. The profile model has high skill where the EOF reconstruction is also skillful and fails where the EOF reconstruction fails, most notably at mid-depths. After a few years of calibration with quarterly observations, skill does not increase with longer calibration. The model overpredicts shoreline erosion and offshore accretion during the anomalously energetic storms of the El Niño 2010, and cannot be extrapolated for use in persistent large wave conditions. Increasing the equilibrium model complexity may be problematic because equally plausible modifications to the

somewhat arbitrary modeling assumptions can yield similar (or no improvement in) model performance. The equilibrium profile model is crude and simplistic, and does not necessarily conserve mass or momentum. It does reproduce selected observations well (using empirical parameters), supports the equilibrium hypothesis, and provides a baseline skill level for comparable predictions by physics-based, process models. Physics-based process models are needed to quantify the complex fluid and sediment dynamics underlying the observed macroscopic equilibrium behavior, to determine the role of the neglected alongshore transport, and to explore causes of model failure.

2.9 Acknowledgments

Imperial and Cardiff Beach sand level data is available at http://cdip.ucsd.edu/SCBPS/regions/ and observations from the other southern California beach sites will be posted here in accordance with the AGU data policy. Southern California bathymetry and wave data collection was supported by the United States Army Corps of Engineers and the California Department of Parks and Recreation Division of Boating and Waterways (program manager Reinhard Flick). Bonnie Ludka was partially supported by a National Science Foundation Graduate Research Fellowship, NOAA Grant #NA10OAR4170060, California Sea Grant Project #R/RCC-01, through NOAA's National Sea Grant College Program and the NOAA/Southern California Coastal Ocean and Observing System. The statements, findings, conclusions and recommendations are those of the authors and do not necessarily reflect the views of the aforementioned organizations.

Kathleen Ritzman, Scripps Institution of Oceanography Assistant Director, was instrumental in maintaining funding and survey continuity for the Southern California monitoring program. Brian Woodward, Kent Smith, Dennis Darnell, Bill Boyd, Rob

Grenzeback, Ian Nagy, and Zoe Dagan built and maintained the surveying system and have collected more than 380 beach elevation surveys. The Coastal Data Information Program (manager Julie Thomas), maintained and operated the wave network. Michele Okihiro coordinated permits and logistics. Lifeguard Captain Robert Stabenow ensured safe access to Imperial Beach. It took a village to raise this data set. Thank you.

Jesse McNinch and the U.S. Army Corps of Engineers Field Research Facility generously provided all Duck, NC data.

The text of Chapter 2, in full, is a reprint with minor modifications of the paper "Field evidence of beach profile evolution toward equilibrium", *Journal of Geophysical Research: Oceans*, *120*(11), 75747597. doi: 10.1002/2015JC010893 (Copyright of the American Geophysical Union 2015). The dissertation author was the primary researcher and first author with guidance provided by R.T. Guza, W.C. O'Reilly and M.L. Yates.

Appendices

2.A Statistical definitions

With fluctuation $x' = x - \langle x \rangle$, where $\langle x \rangle$ is mean, definitions are,

$$\text{Standard Deviation: } \sigma_x = \sqrt{\langle x'^2 \rangle} \tag{2.11}$$

$$\text{Skill: } R^2 = \frac{\langle x'y' \rangle^2}{\sigma_x{}^2 \sigma_y{}^2} \tag{2.12}$$

$$\text{Root Mean Square Error: } RMSE = \sqrt{\langle (y-x)^2 \rangle} \tag{2.13}$$

$$\text{Normalized Mean Square Error: } NMSE = \frac{\langle (y-x)^2 \rangle}{\sigma_x{}^2} \tag{2.14}$$

$$\text{Percent Error: } \%\ \text{Error} = 100 \frac{y-x}{max(x) - min(x)} \tag{2.15}$$

2.B EOF analysis method

The data set is decomposed with standard methods as

$$\vec{z'}(t) = \sum_{i=1}^{N} A_i(t)\,\vec{\mathrm{w}}_i, \tag{2.16}$$

where $\vec{\mathrm{w}}_i$ are orthonormal basis vectors (EOFs),

$$\vec{\mathrm{w}}_i^T \vec{\mathrm{w}}_j = \delta_{ij} \tag{2.17}$$

with length N (the number of spatial locations). The temporal amplitudes

$$A_i = \vec{\mathrm{w}}_i^T \vec{z'}, \tag{2.18}$$

are also orthogonal

$$\langle A_i A_j \rangle = \delta_{ij} \langle {A_i}^2 \rangle. \tag{2.19}$$

With $\vec{W}$ a matrix with columns of the basis vectors $\vec{\mathrm{w}}_i$, and $\vec{D}$ a diagonal matrix with elements equal to the variance of each A_i, (2.16) is rewritten as the eigenvalue problem

$$\langle \vec{z'}\vec{z'}^T \rangle \vec{W} = \vec{W}\vec{D}, \tag{2.20}$$

where the diagonal of $\vec{D}$ are the eigenvalues, and columns of $\vec{W}$ are the eigenvectors, or EOFs. The EOF eigenvalue problem is solved with a singular decomposition [Kelly, 1988] and uses the convention that spatial weight $\vec{\mathrm{w}}_i = 1$ at the average shoreline position, $x = 0$. The first mode reconstruction, $A_1\vec{\mathrm{w}}_1$, explains the most variance in the dataset. Here, A and W refer to the first mode A_1 and $\vec{\mathrm{w}}_1$ respectively, unless otherwise specified.

2.C EOF mode 2 and CEOF mode 1

The profile model has poor skill at mid-depths and offshore because the first EOF does not well reconstruct the profile at these locations (Figure 2.4e, 2.5b, 2.14g, 2.15a). Vertical fluctuations at the deeper locations are small and relatively noisy. At mid-depths however, the elevation fluctuations are large (Figure 2.4e and Figure 2.3). The node of the EOF 1 standing wave is at the poorly modeled mid-depth part of the profile (Figure 2.4b,e, blue solid line 2.C.1b,c). If elevation changes are best described by a propagating wave, at least two EOF standing wave modes, or one CEOF mode would be necessary to describe the profile evolution. We explored the behavior of EOF mode 2 and complex EOF (CEOF) mode 1 for ways to extend the EOF mode 1 based equilibrium profile framework, but these modes did not show promise for improving overall model skill in southern California.

While EOF 2 does have large spatial amplitude (red dashed line Figure 2.C.1b) and some skill at mid-depths (red dashed line Figure 2.C.1c), the temporal amplitude does not behave in a manner consistent with well-organized cross-shore propagation (red dashed line Figure 2.C.1a) for which we expect the EOF 2 temporal amplitude (with positive spatial amplitude at mid-depth) to be large and positive where EOF 1 temporal amplitude is near zero (compare blue solid and red dashed lines in Figure 2.C.1a). (Similarly we would expect EOF 2 temporal amplitude to be large and negative where EOF 1 temporal amplitude is extreme.) This is not the case.

CEOF analysis [Horel, 1984] has been widely used to study sand bar migration, notably Ruessink [2003]. CEOF analysis is performed in the same manner as traditional EOF analysis (Appendix 2.B) except that $\vec{z'}$ is replaced by $\tilde{z'}$,

$$\tilde{z'} = \vec{z'} + iH\left\{\vec{z'}\right\}, \tag{2.21}$$

where H is the Hilbert transform. By considering only the first mode, which again explains the majority of the variance in the observations, an approximation for $\vec{z}$ is recovered,

$$\vec{z'}(x,t) \approx M(x)V(t)\cos\left[\theta(x) - \psi(t)\right], \tag{2.22}$$

where $M(x)$ is the spatial envelope of the bar amplitude, $V(t)$ represents the normalized temporal variations in $M(x)$, and $\theta(x)$ and $\psi(t)$ are the spatial and temporal phase respectively. $M(x)$ (thick black line, left axis, Figure 2.C.1b) and $V(t)$ (thick black line, left axis, Figure 2.C.1a) are the absolute values of the now complex first mode spatial eigenfunction, W, and temporal amplitude, A, respectively. Spatial phase θ (thin green line, right axis, Figure 2.C.1b) and temporal phase ψ (thin green line, right axis, Figure 2.C.1a) are defined as,

$$\theta(x) = \arctan\left[\frac{\Im\{W(x)\}}{\Re\{W(x)\}}\right], \tag{2.23}$$

$$\psi(x) = \arctan\left[\frac{\Im\{A(t)\}}{\Re\{A(t)\}}\right], \tag{2.24}$$

where $\Re\{\}$ and $\Im\{\}$ denote real and imaginary parts respectively. Bar length is defined as,

$$L(x) = \frac{2\pi}{\Delta\theta(x)}. \tag{2.25}$$

Time periods with relatively high temporal and spatial resolution at T2, T3, T4, T5, and T8 were used to compare EOF mode 1 and 2 to CEOF mode 1 in southern California. These observations were interpolated to uniformly spaced spatial and temporal grids. At T8, EOF modes 1 and 2 explain 54% and 21% of the data variance respectively, while CEOF mode 1 explains 70%. Compared with the barred beaches in Ruessink [2003], CEOF 1 temporal amplitude variations are large (Figure 2.C.1a), spatial amplitude is small (Figure 2.C.1b), and the reconstruction does not describe a large unbroken region of the profile (R^2 is fairly low, Figure 2.C.1c). Bar length (not shown) is noisy except

around $x = -150$ to -100 m (mean depth $\sim$ 2-3m) where $L(x) \sim 250$m, consistent with Ruessink [2003].

A possible way to extend the equilibrium framework by using the first CEOF is to assume that the temporal magnitude is constant and temporal phase is equilibrium like. The dotted line Figure 2.C.1c shows how CEOF 1 reconstruction skill is further degraded by assuming the temporal magnitude is constant. After this simplification, CEOF 1 is not a much better reconstruction than EOF 1. Furthermore, the temporal phase is only slightly correlated with the equilibrium-like EOF 1 temporal amplitude (Figure 2.C.1a). For these reasons we prefer the EOF model formulation in southern California. A CEOF based equilibrium profile model of this sort would be similar to the bar crest position model of Plant et al. [1999] and Pape et al. [2010] and would likely be more suited for the barred beaches similar to those described in Ruessink [2003] including Duck, NC.

Table 2.1: Survey site characteristics.

Survey Site	Beach Width[a] (m)	Beach Slope[b]	MSL D_{50}[c] (mm)
Imperial	30-60	.02-.03	0.25
Torrey Pines	20-100	.02-.03	0.23
Solana	10-50	.03-.04	-
Cardiff	20-40	.03-.04	0.16
Camp Pendleton	60-80	.03	0.20

(*a*) Beach width is the time averaged distance from the back beach to the MSL contour.
(*b*) Beach slope is calculated as the time averaged slope between -1m and +1 m elevations relative to MSL. The beach face is concave; beach slope steepens higher on the beach.
(*c*) D50 is median grain size diameter.

Table 2.2: Description of survey observations. In total, more than 4,000 km of survey tracks are analyzed.

Survey Site	Alongshore Length [km]	Date Range	# Subaerial Surveys[a]	# Profile Surveys[b]	# Transects/ Profile Survey
Imperial	2.1	01/2009 - 08/2012	32	16	21
Torrey Pines	7.5	04/2004 - 06/2014	138	36	74
Solana	2.3	05/2008 - 10/2012	36	18	23
Cardiff	1.4	06/2007 - 10/2010	44	16	14
Camp Pendleton	1.5	02/2007 - 10/2010	31	14	30

(*a*) For the regions and time periods considered, and assuming 6 alongshore lines per subaerial survey (the typical number of lines on a narrow beach with a weak spring low tide; twice as many lines are driven on a wide beach with an extreme spring tide), over 2,000 km of subaerial survey tracks have been driven.
(*b*) For the regions and time periods considered, and estimating 500 m as the typical length of a cross-shore profile transect, over 2,000 km of profile survey track have been acquired.

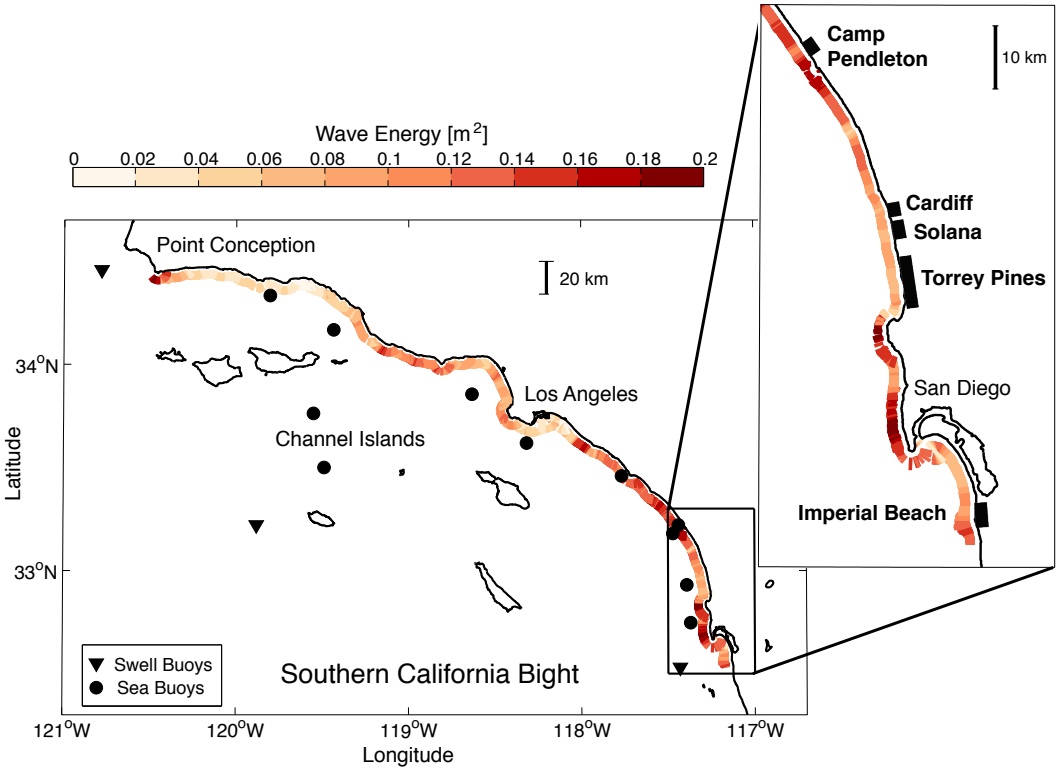

Figure 2.1: Map of southern California Bight. Wave buoys are used to initialize the swell wave propagation model (triangles), and to estimate local seas (circles). Inset shows zoom of region containing study beaches (black rectangles / bold labels). Colors show modeled wave energy every 100 m along the coast in 10 m water depth at 5:30AM on April 1, 2012. Island shadowing causes significant gradients in wave energy along the coast.

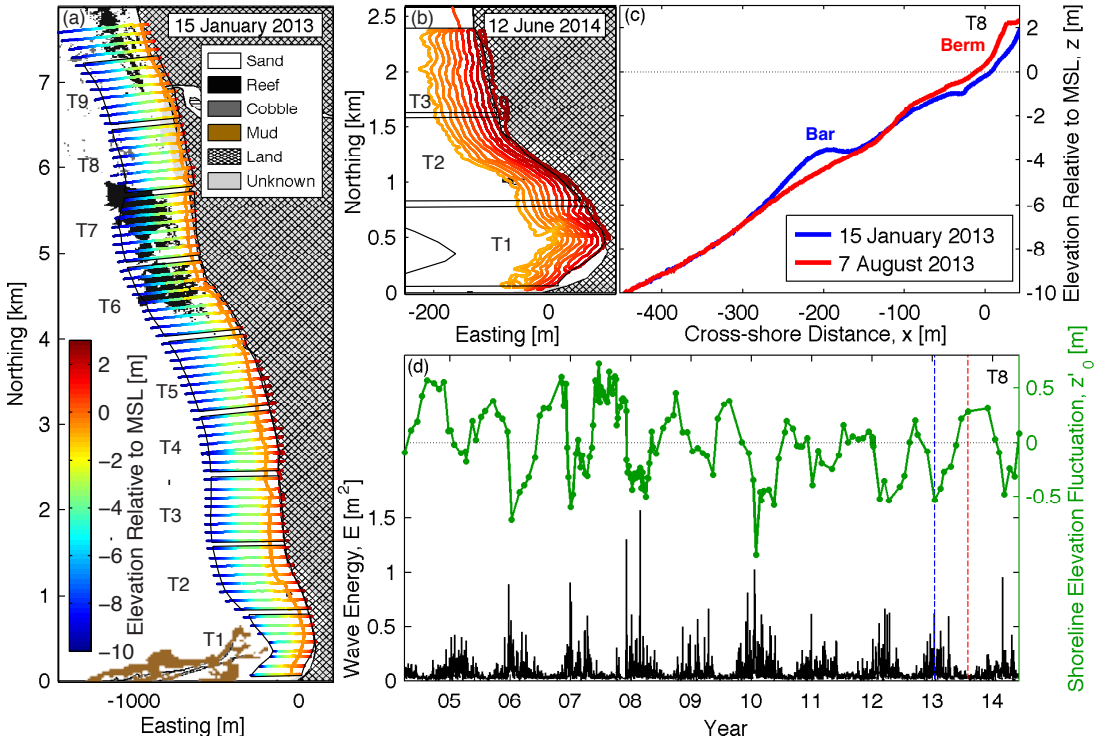

Figure 2.2: (a) Plan view of Torrey Pines Beach. Cross-shore survey transects (15 January 2013) are colored by depth (see color bar). Background colors/shading indicates substrate type (see legend) from multibeam and sidescan sonar [Moffatt and Nichol, 2009]. Sections T1-T9, are indicated. (b) Plan view of T1-T3 sections showing colored-by-elevation subaerial (all terrain vehicle) survey tracks (12 June, 2014). (c) Vertical elevation versus cross-shore distance for summer bermed (red) and winter barred (blue) profiles on a typical T8 transect. The shoreline $x = 0$ is the cross-shore location where the time-average sand elevation equals MSL. (d) Offshore (10m depth) wave energy (black, left axis) and sand elevation at $x = 0$ (green, right axis) versus time. Results are averaged over the 8 transects in section T8.

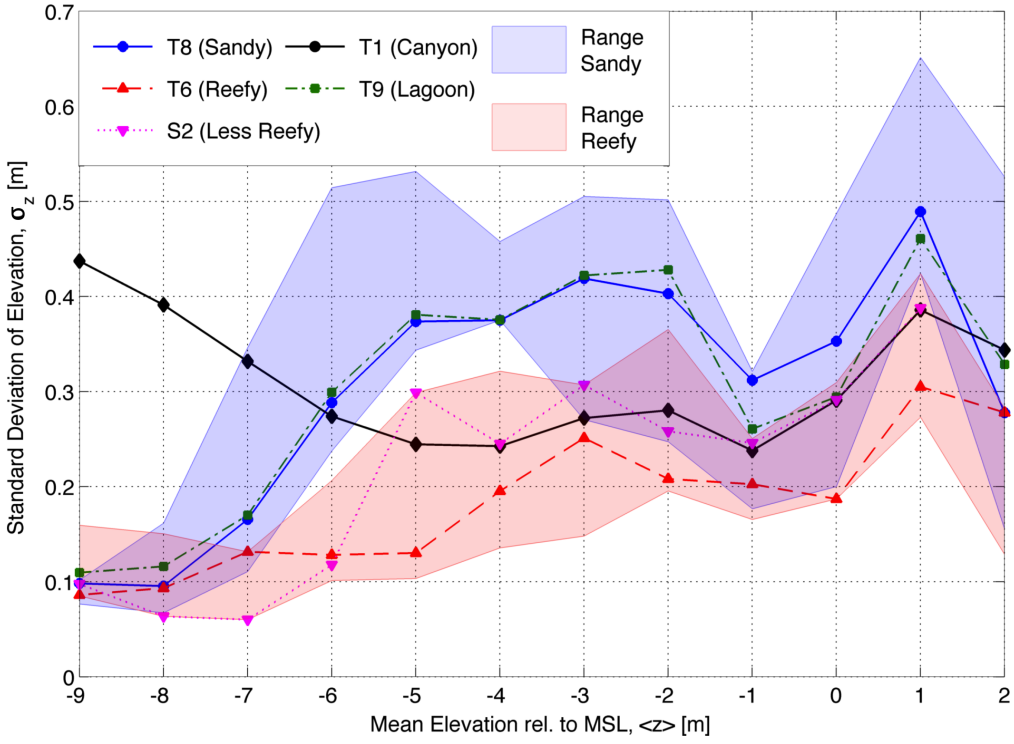

Figure 2.3: Standard deviation of elevation versus mean elevation for selected cross-shore transects (see legend). Standard deviation is lower at reefy (red swath) than sandy (blue swath) sections. Offshore (9m mean depth) sand level fluctuations are anomalously large near a submarine canyon (T1, black).

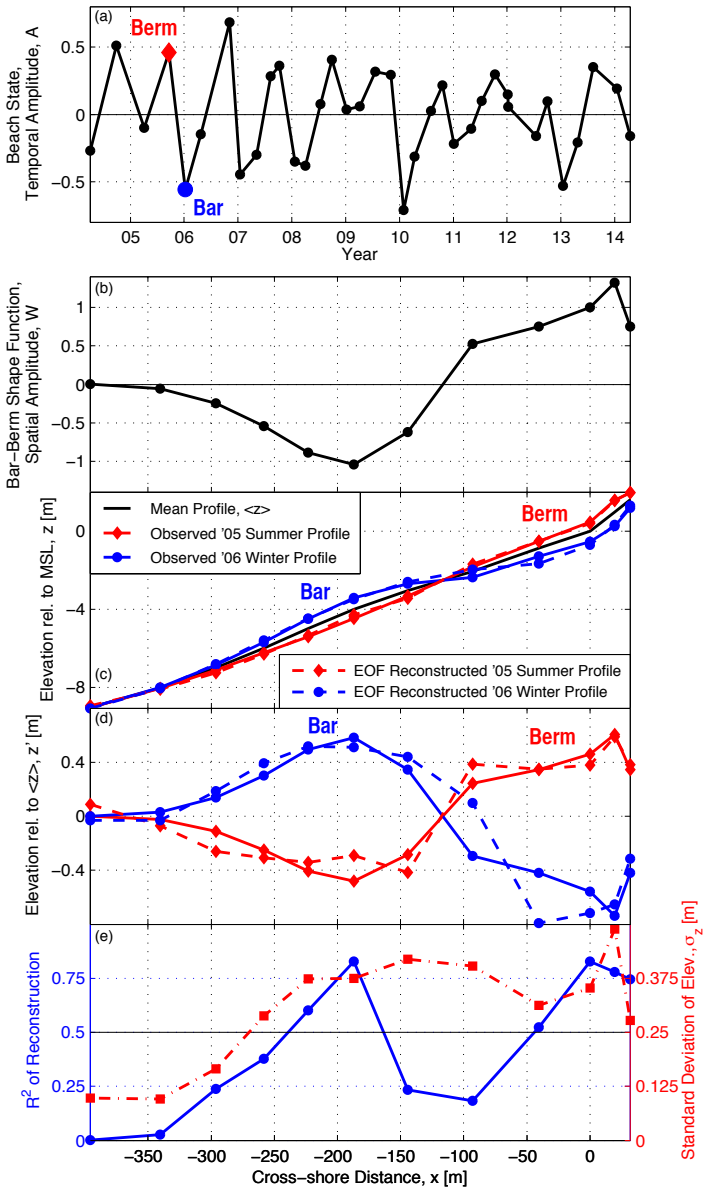

Figure 2.4: Torrey Pines, section T8. (a) Beach state (EOF 1 temporal amplitude A) versus time. (b) EOF 1 spatial weights W versus cross-shore distance x. (c) Elevation versus x for observed mean, summer, winter profiles (solid curves), and summer and winter EOF 1 reconstructions (dashed). (d) As in (c), but with the mean profile removed to increase visibility. The observed and reconstructed profiles are similar, and EOF 1 describes 56% of the total (over all cross-shore locations) variance. (e) R^2 between observed and EOF-reconstructed sand level (solid blue curve) and standard deviation of observed elevation (red dash-dot curve, right axis) versus x.

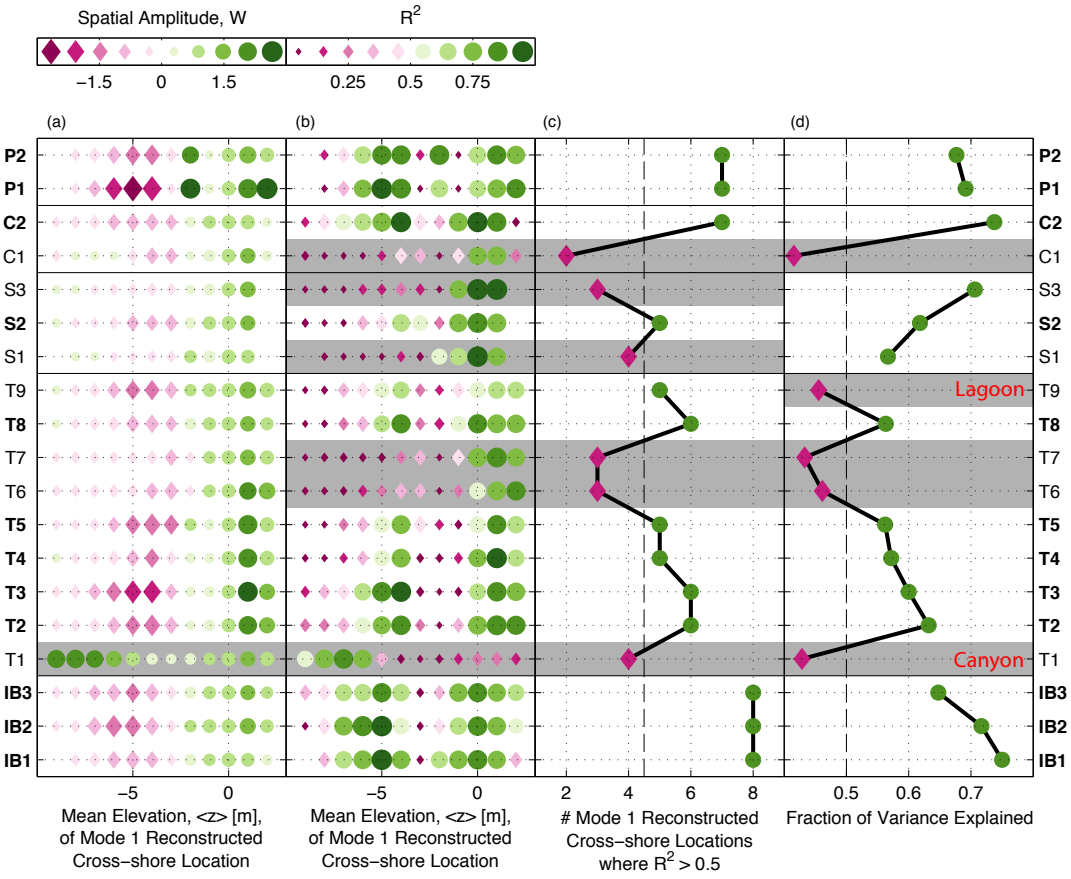

Figure 2.5: EOF performance at all sites. (a) EOF 1 spatial weights W versus mean elevation and section (W color bar at top). The anomalous W of T1 is shaded grey. (b) R^2 between observed and EOF-reconstructed sand level versus mean elevation and section (R^2 color bar at top). (c) Number of reconstructed cross-shore locations with $R^2 > 0.5$ at each section. In (b) and (c), sites with 4 or fewer cross-shore locations with $R^2 > 0.5$ are shaded grey. (d) Fraction of the total variance (all cross-shore locations) explained by EOF 1 at each section (ranging from 0.42-0.75, where shaded grey values are < 0.5). Analysis is focused on the 12 sections well described by EOF 1 (bold on vertical axis and lacking grey shading).

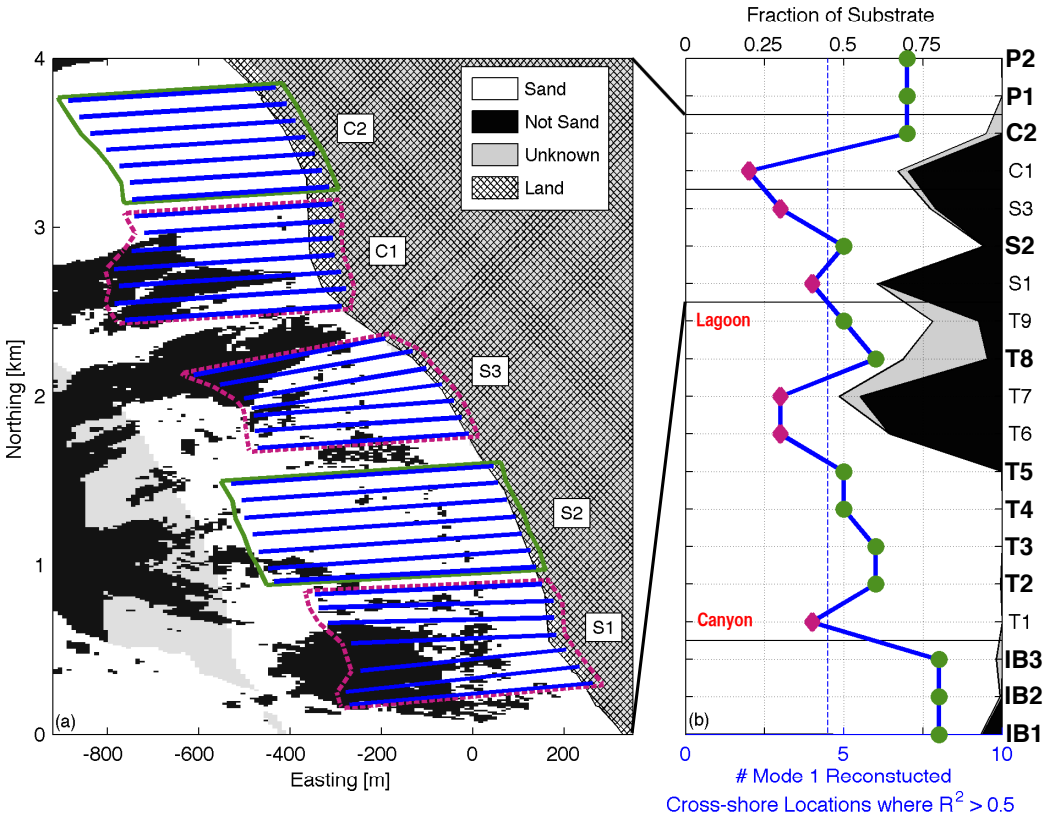

Figure 2.6: (a) Plan view of Cardiff (C1,C2) and Solana (S1, S2, S3) Beach sections and bottom type identified by multibeam and sidescan sonar [Moffatt and Nichol, 2009]. Blue lines are survey cross-shore transects. Sections C2 and S2 (green solid line boxes) are well described by EOF 1, and C1, S3, and S1 (purple dotted boxes) are not. (b) For all sections, substrate type (top black axis), and number of cross-shore locations well described ($R^2 > 0.5$) by the EOF 1 reconstruction (bottom blue axis) versus alongshore section. Sand substrate is white, unknown is grey and "not sand" is black as in the legend in (a). With the exception of slightly cobbly sections IB1 and T8, substrate classified as "not sand" is reef. Sections with relatively low % sand tend to have relatively few locations that are well described by EOF 1. For example, section C2 is almost all sand, and 7 (of 12) cross-shore locations are well reconstructed by EOF 1 (in (b), values greater than 5 are green circles). Section C1 is about 70% sand, and only 2 cross-shore locations are well reconstructed by EOF 1 (in (b), values less than 5 are purple diamonds). The sections well described by EOF 1 in general are labeled in bold on the right axis of (b). Well described sections have more than half their total variance explained by EOF 1 (see Figure 2.5d), *and* EOF 1 reconstructs 5 or more cross-shore locations with $R^2 > 0.5$ (as in (b) and Figure 2.5c). T1 is onshore of a submarine canyon and T9 contains a lagoon mouth.

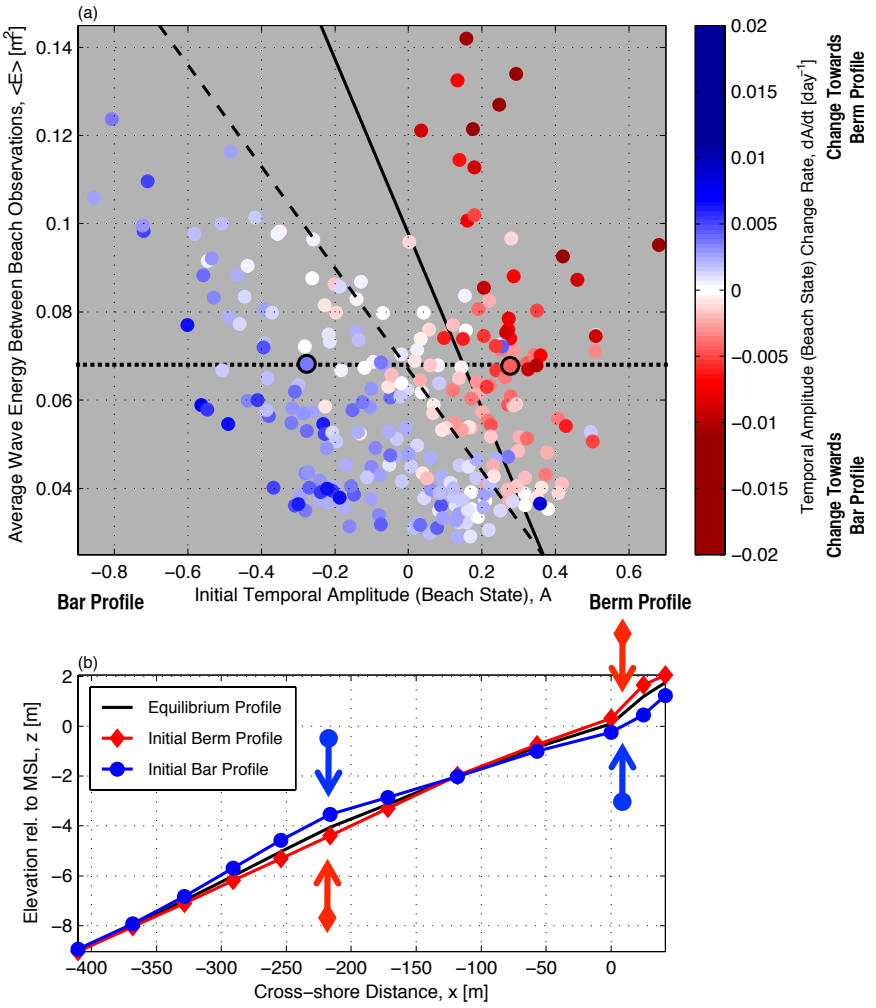

Figure 2.7: (a) Beach state change rate, dA/dt (see color scale), versus average wave energy between profile observations, $\langle E \rangle$, and initial beach state, A, for sections well described by EOF 1, where A is the temporal amplitude of EOF 1. The dashed black line (drawn by eye) separates change toward a barred profile (blue) from change toward a bermed profile (red). With $\langle E \rangle = 0.068\text{m}^2$ (significant wave height $H_s = 1.04$ m, dotted black horizontal line), all profiles evolve toward $A_{eq} = -0.01$, the equilibrium state given by the intersection of the dotted and dashed black lines. The solid black line is the more accurate equilibrium relationship, calculated by optimizing model parameters (i.e. dashed vertical lines in Figure 2.10) in equations (2.1)-(2.3) using hourly waves. (b) Example initial and equilibrium profiles for the scenarios circled in black in (a). Arrows show the direction of beach change toward the equilibrium profile. The rate and direction of profile change depends not only on the incident wave energy, but also on the present beach state.

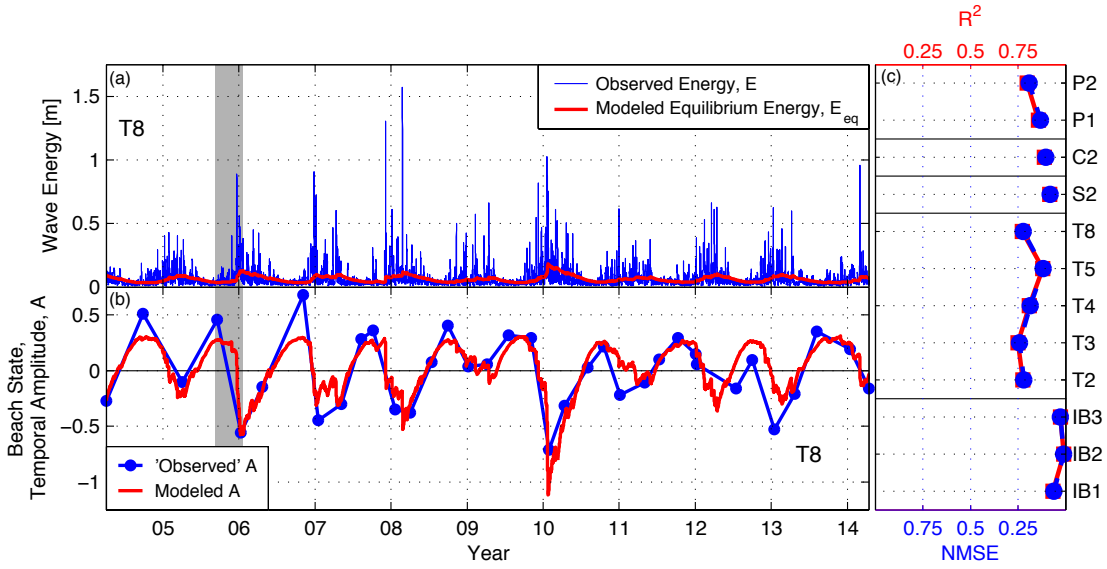

Figure 2.8: (a) Torrey Pines section T8 observed wave energy, E (blue), and modeled equilibrium wave energy, E_{eq} (red), versus time. (b) Observed (blue) and modeled (red) A (beach state) versus time at T8. When $E > E_{eq}$, the EOF temporal amplitude A decreases (the model beach face erodes and offshore bar accretes). When $E < E_{eq}$, A increases (beach face accretes and offshore bar erodes.) Gray vertical bar is time period detailed in Figure 2.12. (c) Beach state model normalized mean square error (NMSE, blue) and skill (R^2, red and on top axis) versus sections well described by EOF 1. Modeled A has NMSE < 0.25 and $R^2 > 0.75$ at all modeled sections.

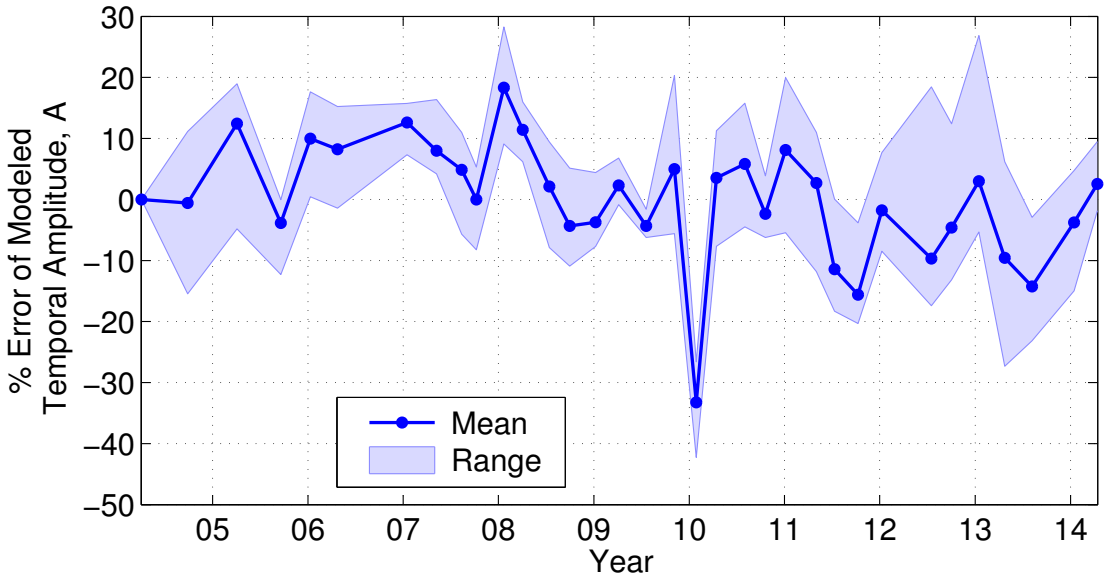

Figure 2.9: Percent error (Appendix 2.A) in modeled beach state (temporal amplitude, A) versus time. The percent error mean and range (see legend) are over the 5 sections at Torrey Pines (T2,T3,T4,T5,T8) that are well described by EOF 1. Mean errors are extreme during the energetic 2010 El Niño; shoreline erosion and offshore accretion are overpredicted.

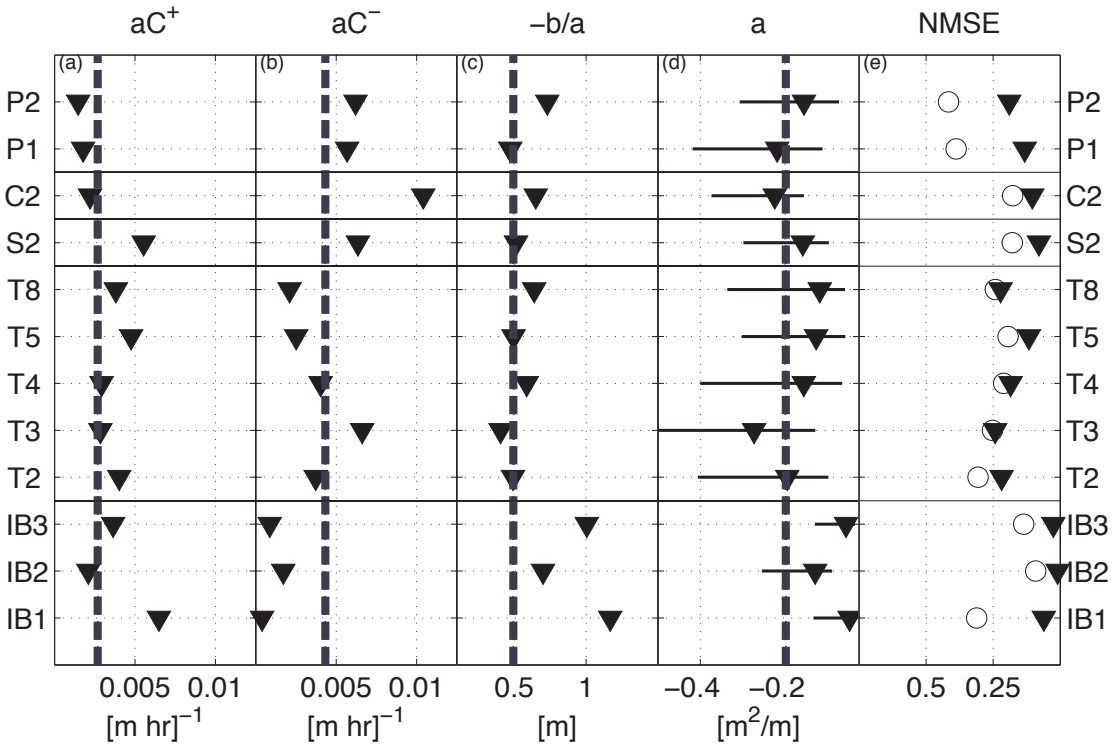

Figure 2.10: Optimal model free parameters and products (a) aC^+, accretion e-folding scale coefficient (b) aC^-, erosion e-folding scale coefficient (c) $-b/a$, maximum beach state (d) a, equilibrium slope. Results are shown for each individual section (triangles), and for all sections combined (dashed vertical lines). Horizontal lines in (d) show range of values of a for which RMSE is increased by less than 10% while holding other parameters constant. (Parameters are not well constrained.) (e) NMSE using free parameter values that are best fits for each individual section (solid triangles), and for all sections combined (open circles). Parameter b depends on the temporal mean removed from the time series and is not comparable between alongshore sections [Yates et al., 2009a, Yates et al., 2011]

.

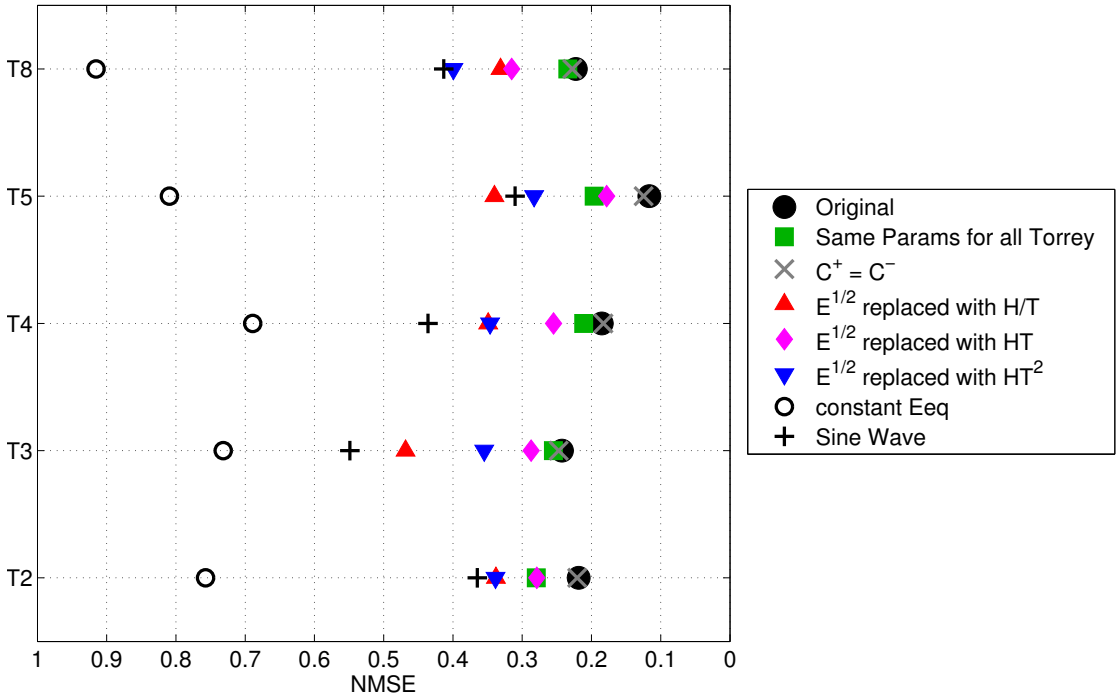

Figure 2.11: Modeled beach state NMSE (normalized mean square error) for Torrey Pines sections T2, T3, T4, T5 and T8, using different model formulations (see legend).

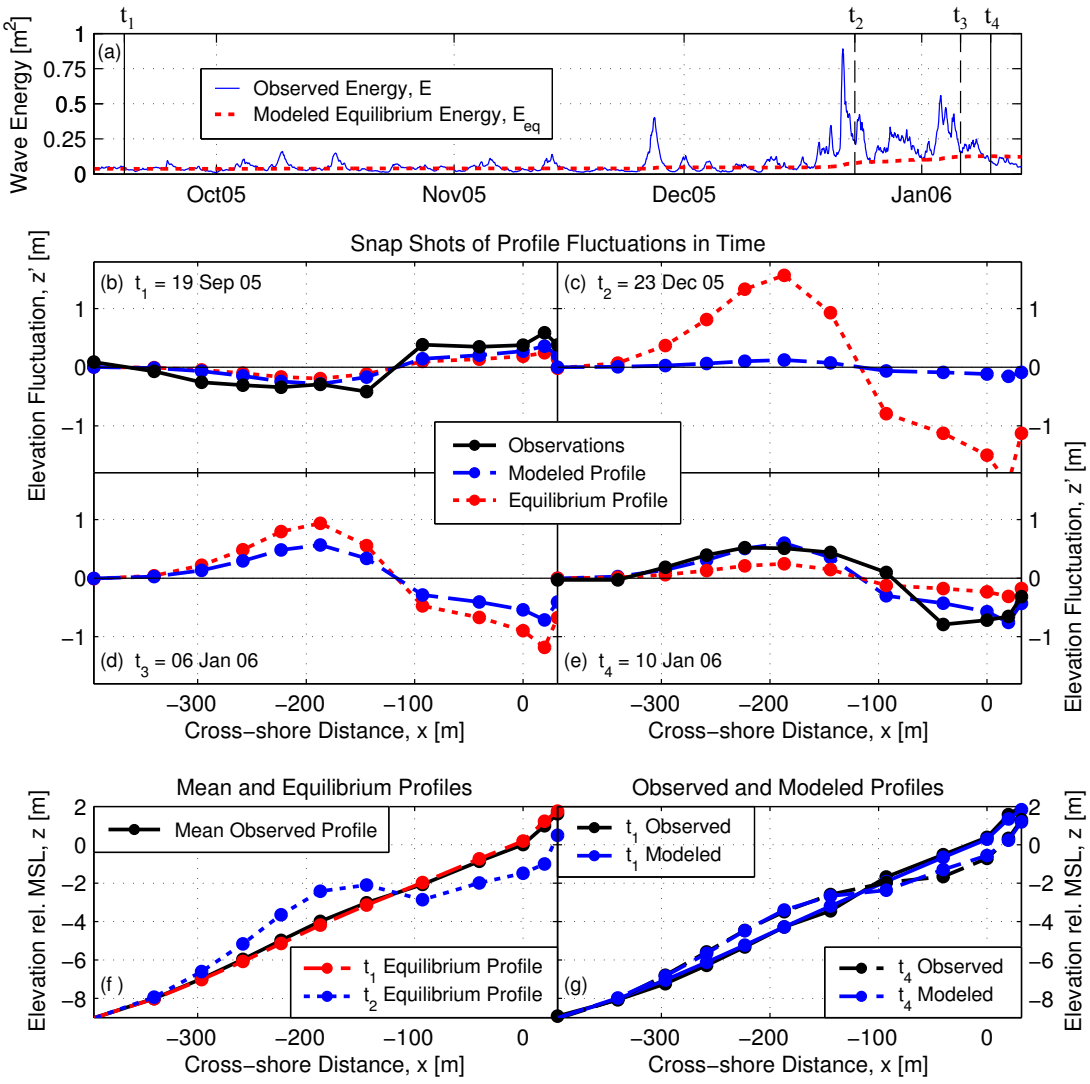

Figure 2.12: Torrey Pines section T8. (a) Observed and modeled equilibrium wave energy, E and E_{eq}, versus time for four months. Times t_1 through t_4 are labeled. (b-e) Modeled, observed (when available), and equilibrium profiles (demeaned) for times t_1 through t_4. The modeled profile (blue dashed) is evolving toward the equilibrium profile (red dotted) at each time step. (b) At t_1, the bermed beach is in equilibrium with the low E. (c) At t_2, the beach is out of equilibrium with the high E, and the beachface begins to erode while the offshore bar accretes. (d) By t_3, the barred beach is almost in equilibrium with the high E (e) At t_4, E is low, and the barred beach begins to recover. Observations were acquired at t_1 and t_4 (black in b and e). (f,g) Elevation versus cross-shore distance for (f) mean and equilibrium profiles and (g) observed and modeled profiles.

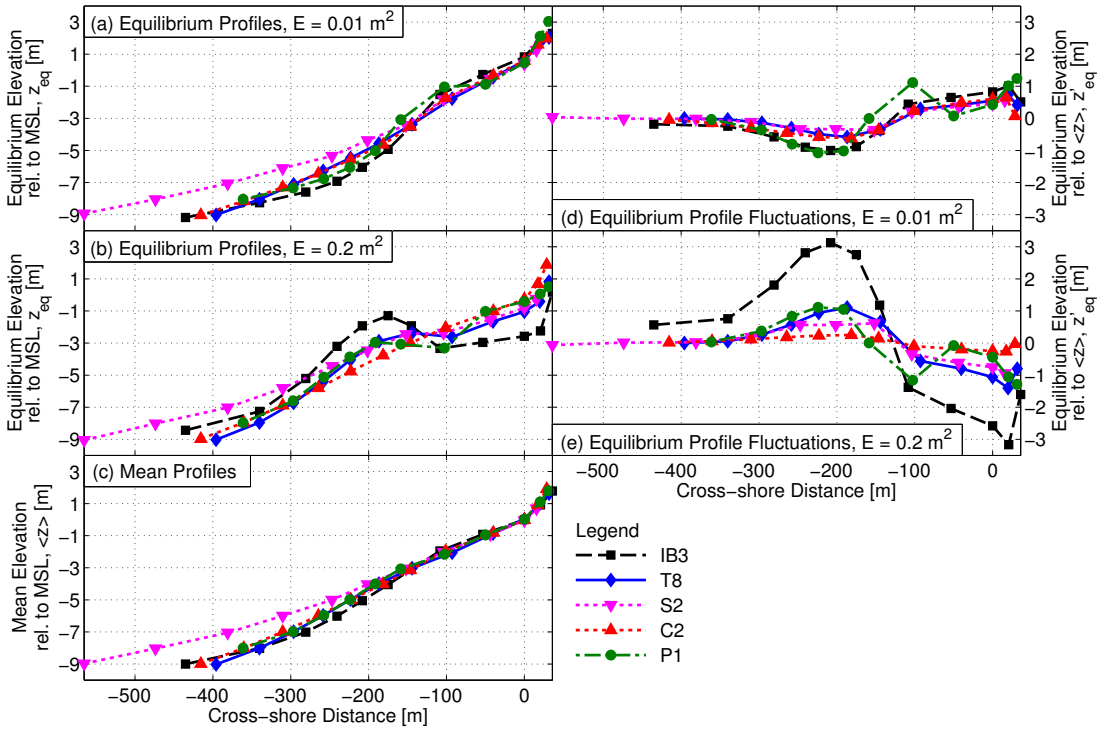

Figure 2.13: (a) Equilibrium beach profiles at sections representative of each beach site (see legend) for E = 0.01 m^2 (H_s = 0.4 m). (b) Same as (a) but with E = 0.2 m^2 (H_s = 1.8 m). (c) Mean profiles. (d) Same as (a) but with mean removed. (e) Same as (b) but with mean removed.

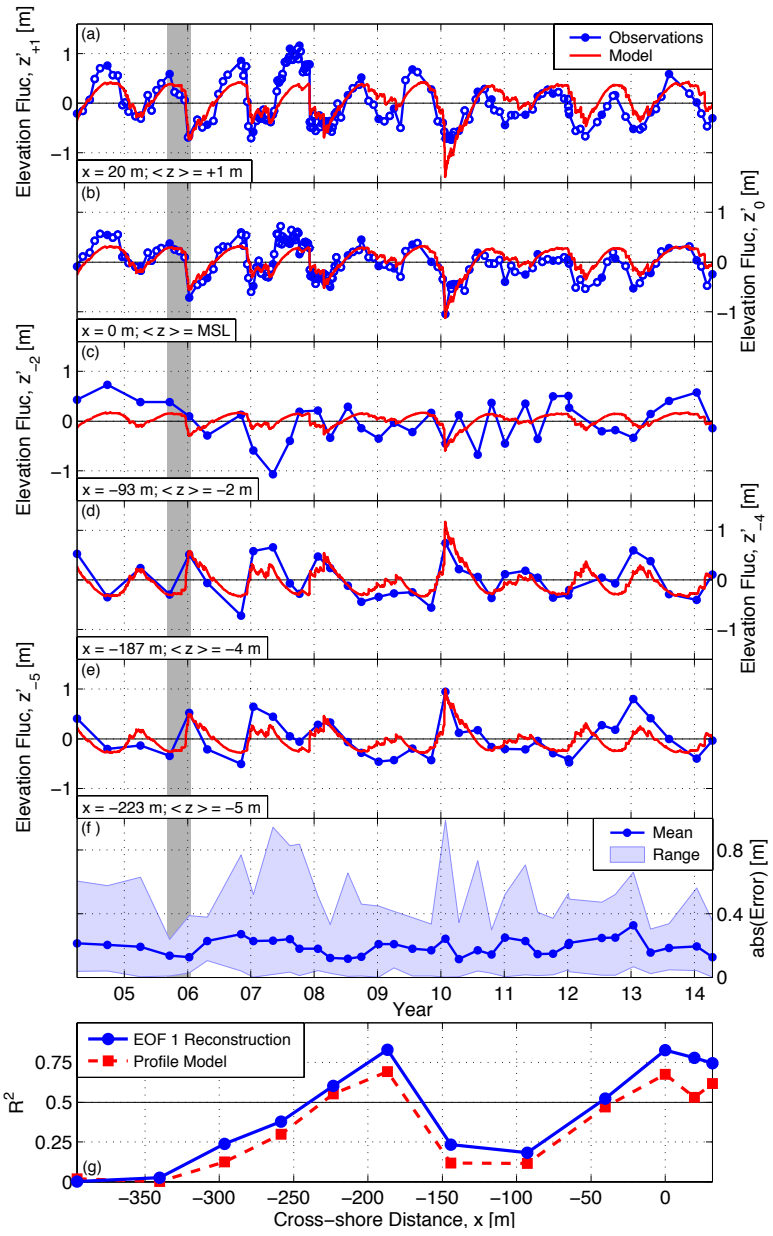

Figure 2.14: (a-e) Torrey Pines section T8 observed (blue curve with circles) and modeled (red) sand level fluctuations versus time. The mean sand elevations (see labels) range from +1m (a) to -5m (e). Open blue circles in (a,b) are subaerial surveys, not used in profile model calibration or evaluation. (f) Mean and range (see legend) of model misfit versus time. Gray bar is Figure 2.12 time period. (g) R^2 versus cross-shore distance. The profile model (red) works well ($R^2 > 0.5$) near the shoreline ($x = 0$) and in 4-5m mean depth ($x = -200$m), and generally follows the R^2 of the EOF reconstruction (blue curve is from Figure 2.4e). Additional errors from the imperfect modeling of the beach state, A, (Figure 2.8b,c) are relatively small.

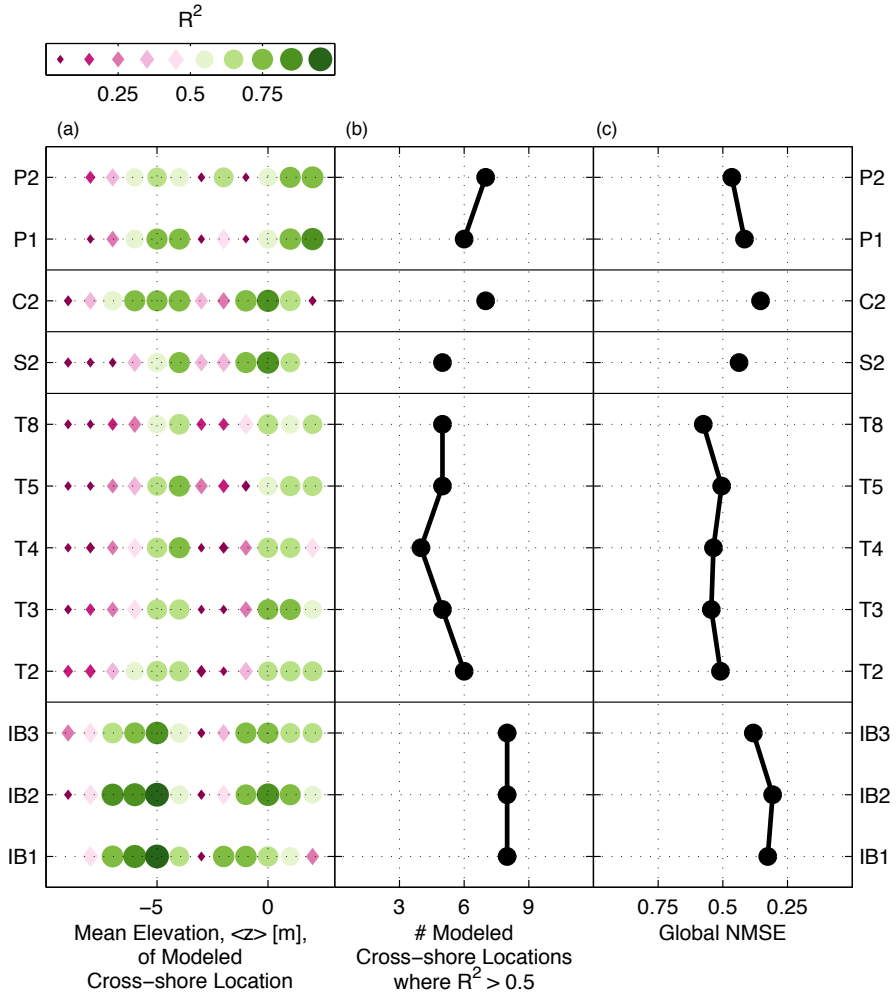

Figure 2.15: Profile model performance at the 12 modeled sections. (a) R^2 between observed and model sand level versus mean elevation and alongshore section (R^2 is coded by color and symbol, see bar at top). (b) Number of modeled cross-shore locations with total $R^2 > 0.5$, and (c) global NMSE (normalized mean square error).

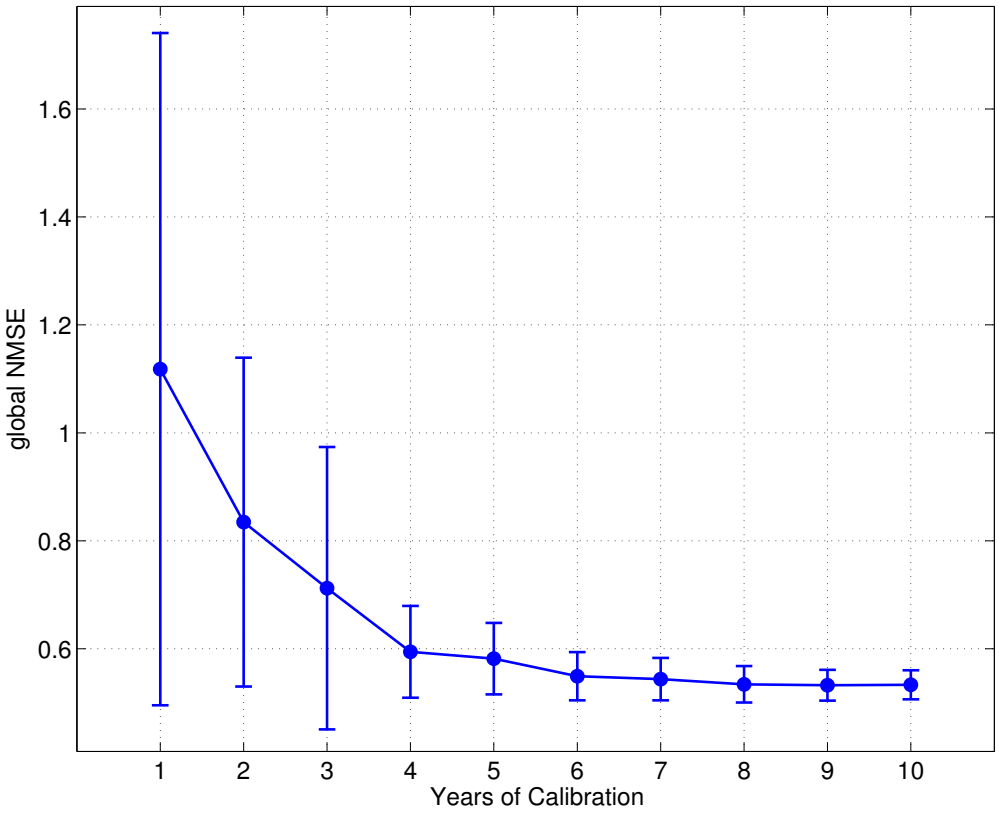

Figure 2.16: Beach profile model global NMSE versus years of parameter calibration. Standard deviation (scatter bars) includes variability from both different test periods and alongshore sections (T2, T3, T4, T5, and T8 are used). The number of cases for each years of calibration class are: 1-year (50), 2-year (25), 3-year (15) tests, 4-year (10), 5-year (10), and 6, 7-, 8-,9-, and 10- year (5).

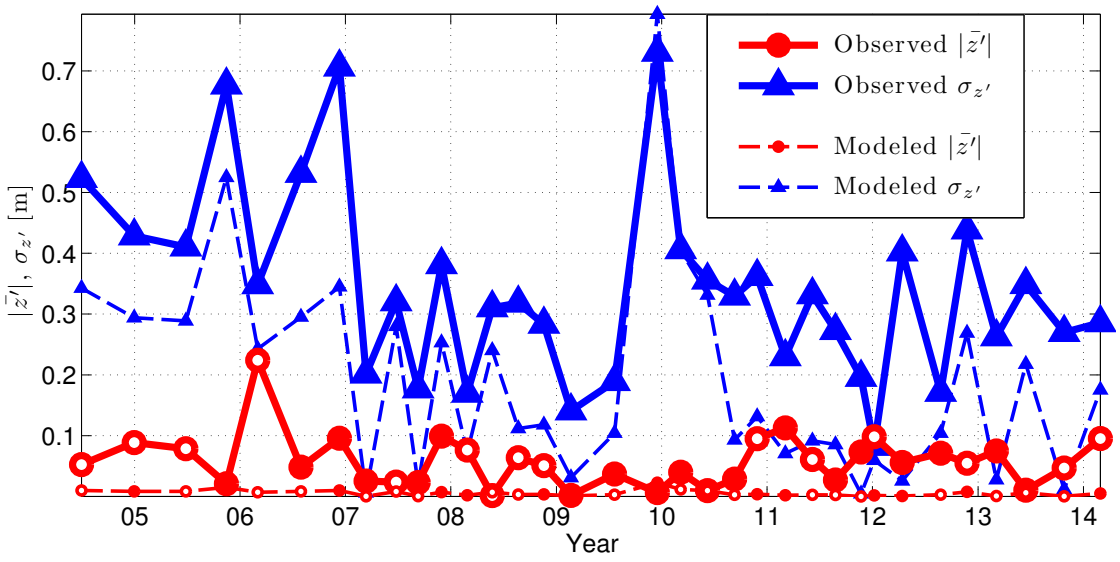

Figure 2.17: Equivalent sand level change versus time at T8. Curves are observed (solid) and modeled (dashed). Typically, the amount of sand exchanged between the bar and beach face (standard deviation of elevation change, $\sigma_{z'}$, blue triangles) is much larger than lost (or gained) integrated over the profile (mean change, $\bar{z}'$, red circles, where absolute value is plotted with negative values shown as hollow circles.)

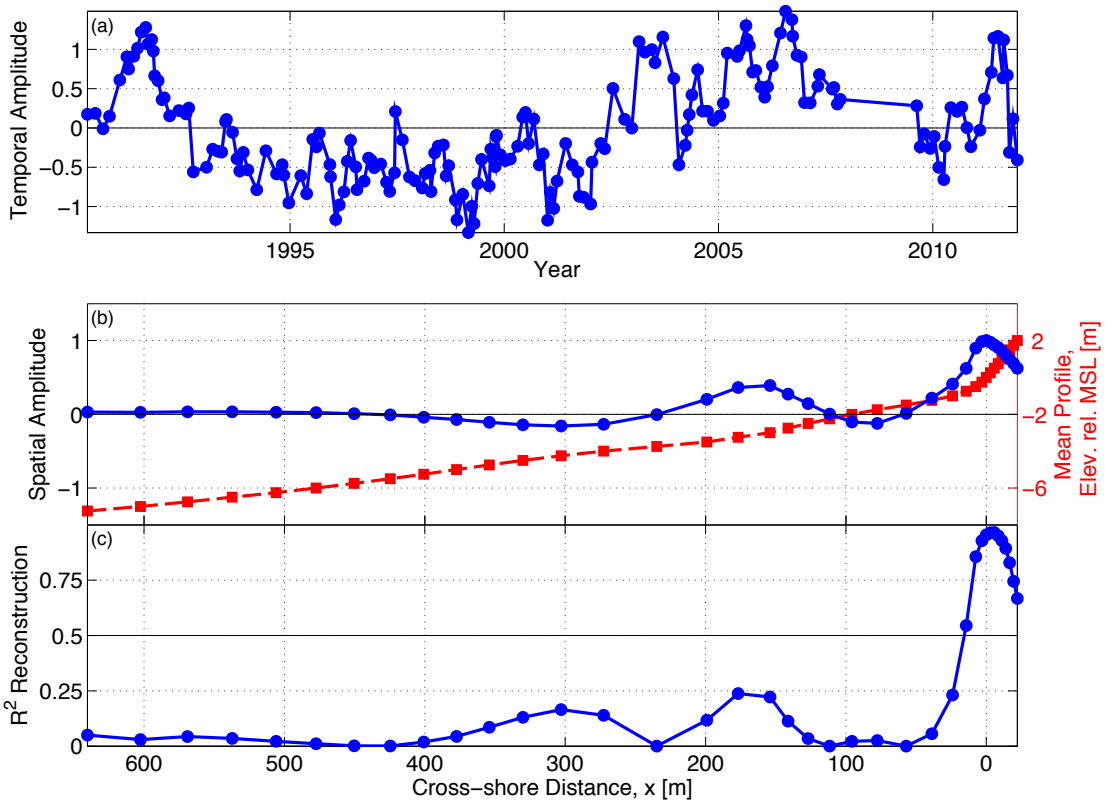

Figure 2.18: EOF 1 at Duck, south of the research pier. (a) Temporal amplitude (b) Spatial amplitude (solid blue curve with circles, left axis) and mean profile (dashed red curve with squares, right axis) (c) R^2 of reconstruction shows the first mode only well describes the upper beach; changes in the rest of the profile are incoherent with the upper beach. Analysis of various alongshore subsections and over the entire reach at Duck all yield similar results.

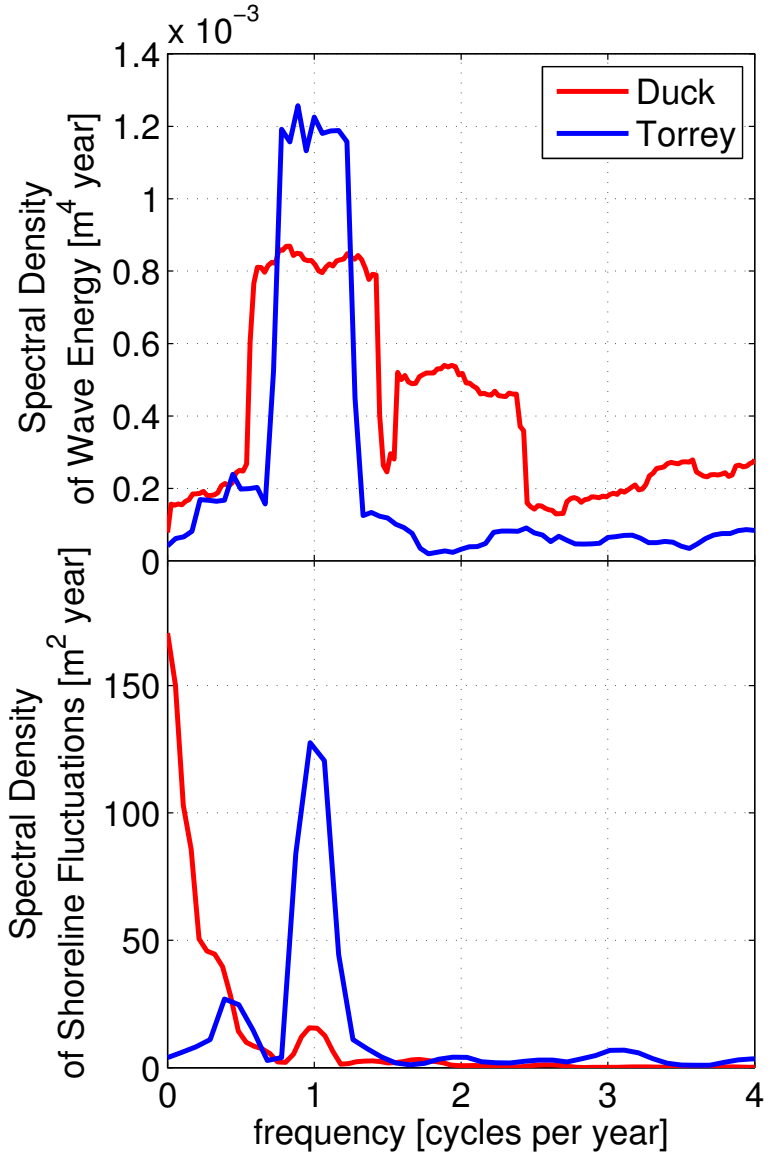

Figure 2.19: (a) Wave energy spectra of Duck waverider buoy (red) and T8 MOP model (blue). Both have energetic peaks at the annual frequency. (b) Shoreline elevation fluctuation spectra at Duck (south of the pier) and T8. Torrey shoreline fluctuations have a strong annual signal but the Duck shoreline is dominated by low frequency variability.

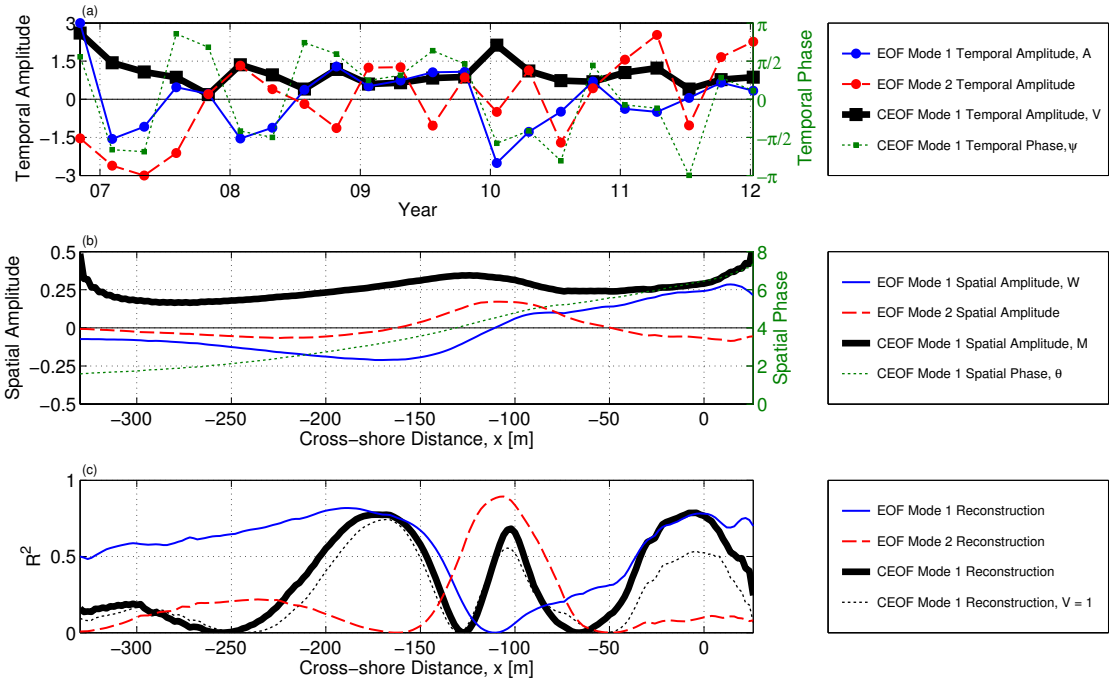

Figure 2.C.1: EOF modes 1 and 2 and CEOF mode 1 at T8. (a) Temporal amplitude (and CEOF temporal phase, right axis) versus time. (b) Spatial amplitude (and unwrapped CEOF spatial phase, right axis) versus cross-shore distance, and (c) R^2 of the reconstruction, versus cross-shore distance. The dotted black line shows CEOF 1 reconstruction skill when V (thick black line in (a)) is forced to equal 1.

Chapter 3

Mid El-Niño erosion at nourished and unnourished southern California beaches

3.1 Abstract

Wave conditions in southern California during the 2015-16 El Niño were similar to the 2009-10 El Niño, previously the most erosive (minimum beach widths and subaerial sand levels) in a seven-year record. As of February 2016, Torrey Pines Beach had eroded slightly below 2009-10 levels, threatening the shoulder of a major highway. However, Cardiff, Solana and Imperial Beaches, nourished with imported sand in 2012, were on average 1-2 *m* more elevated and more than 10 *m* wider than in 2009-10. Monthly subaerial sand elevation observations showed that the nourished beaches remained consistently wider than unnourished beaches under similar wave conditions. In contrast to a 2001 nourishment at Torrey Pines built with native sized sand that was removed from the beach face during a single storm [Yates et al., 2009c], these relatively coarse

grained nourishments protected shorelines for several years, and during the significant wave attack of the 2015-16 El Niño, as of February 2016.

3.2 Introduction

California's wave climate and beaches are altered substantially by the El Niño Southern Oscillation (ENSO), with greater wave energy flux and erosion during the warm phase El Niño [Dingler and Reiss, 2002; Sallenger et al., 2002; Barnard et al., 2011; Barnard et al., 2015; Revell et al., 2011]. While Pacific coastal regions are threatened by predicted long-term relative sea level rise averaging half a meter by the end of the century [Carson et al., 2016], ENSO is superimposed on this long-term trend, modifying regional coastal sea levels by a few decimeters on interannual time scales [Enfield and Allen, 1980, Huyer and Smith, 1985, Ryan and Noble, 2002, Hamlington et al., 2015]. Most significantly, ENSO modulates the locations of storms responsible for large wave events [Allan and Komar, 2006; Barnard et al., 2015] that can raise nearshore water levels through wave set up by a meter or more [Longuet-Higgins and Stewart, 1962, Bowen et al., 1968, Guza and Thornton, 1981]. Furthermore, regions exposed to anomalously energetic wave conditions experience intensified beach erosion, compounding flood risk and potentially depressing multi-billion dollar tourist economies [Pendleton et al., 2012, WorleyParsons, 2013, Alexandrakis et al., 2015]. The 1982-83 and 1997-98 El Niños were the highest sea surface temperature anomalies in the eastern equatorial Pacific since 1950, and the 2015-16 El Niño ranks alongside them [Climate Prediction Center, 2016]. Seven years of hourly wave data and monthly sand levels at Torrey Pines Beach, CA show that the winter 2015-16 conditions in southern California are similar to the 2009-10 El Niño. As of 29 February, 2015-16 winter significant wave heights had exceeded 2 m for 364 hours, comparable to the to 360 hours of exceedance by 28 February of

winter 2009-10. (Non-El Niño winters totaled less than 200 hours of 2 m exceedance.) Furthermore, at Torrey Pines the 2015-16 beach was slightly narrower and subaerial sand levels were slightly lower than in 2009-10.

Imported sand, mechanically placed on the beach, modifies the impact of the 2015-16 El Niño at the other monitored sites. This coastal management technique, known as beach nourishment, widens and elevates the beach to mitigate flooding and erosion, and promotes tourism and recreation. "Soft" sand based coastal management techniques (e.g. beach nourishment, shore nourishment [Hamm et al., 2002], scraped berms [Gallien et al., 2015]) are often preferred to hard structures (e.g. groins, jetties, breakwaters) that can stifle the sediment supply to adjacent coastlines [Bruun, 1995]. Beach nourishment is a primary erosion mitigation strategy worldwide, and non-opportunistic placements (placements not benefiting from sand available from a pre-existing project, e.g. a harbor dreging) are expensive [Clayton, 1991; Haddad and Pilkey; 1998, Trembanis and Pilkey; 1998, Valverde et al., 1999; Hanson et al., 2002; Cooke et al., 2012; Luo et al., 2015].

The wave-driven redistribution of beach nourishment sand is an important component of the complex cost-benefit analysis, but is poorly understood. On the U.S. Gulf and East Coasts, hurricanes most significantly redistribute nourishments [Browder and Dean, 2000; Gares et al., 2006; Elko and Wang, 2007]. However on the U.S. West Coast, tropical storms are rare and extreme erosion is dominated by repeated storms during El Niño [Barnard et al., 2015]. Elko et al. [2005] report increased nourishment erosion rates on the U.S. Gulf Coast during the 1997-98 winter El Niño. Our detailed observations of nourishment influence in the more severely affected southern California, during the 2015-16 El Niño, are unique.

In 2001, approximately 1.6 million m^3 of sand was placed on 12 San Diego County beaches [Coastal Frontiers, 2015] at a total cost of $17.5 million; the first non-

opportunistic nourishments in the region [Griggs and Kinsman, 2016]. The entire Torrey Pines pad, constructed with a sand grain size similar to native, washed offshore in a single storm [Seymour et al., 2005], partially returned to the beach face the following summer, and then became too dispersed to track [Yates et al., 2009c]. An additional 1.15 million m^3 of sand was placed on 8 San Diego County beaches in 2012 [Coastal Frontiers, 2015] at a total cost of $28.5 million [Griggs and Kinsman, 2016]. Based on comparatively sparse observations that included all the nourishments [Coastal Frontiers, 2015], Griggs and Kinsman [2016] stated that "Overall, the sand added to the relatively narrow San Diego County beaches [during the 2001 and 2012 nourishment campaigns] had a very short life span on the exposed subaerial beach." We present uniquely comprehensive observations showing that the impacts of three of the relatively coarse-grained nourishments placed in 2012 (Table 3.1) have remained detectable on the beach face for several years, and maintained a more seaward shoreline during the 2015-16 El Niño than the 2009-10 El Niño. February 2016 photos show the extreme erosion at Torrey Pines, unnourished since 2001 (Figure 3.1b), compared with Cardiff and Imperial Beach, both nourished in 2012 (Figure 3.1a,c).

3.3 Wave Observations

Waves are characterized with observations from the Torrey Pines Datawell directional wave buoy (NDBC 46225), located 12 *km* offshore of Torrey Pines Beach in 550m water depth [CDIP, 2016]. A few gaps in the observations during low waves (3% of the total record) are filled with a regional wave model. Although waves differ between the beaches [Ludka et al., 2015], wave observations at the Torrey Pines buoy are broadly representative. Waves are seasonal, with relatively low waves in summer (e.g. zero occurrences of wave heights above 2 *m*, Figure 3.2b). Winter wave heights are larger, and

elevated above 2 m most often during the 2009-10 and 2015-16 El Niños. The maximum wave height of 5.5 m was observed on 1 Feb 2016.

A simple 1D beach state model [Ludka et al., 2015] based on an equilibrium beach hypothesis [Wright and Short, 1984, Wright et al., 1985] previously calibrated on these beaches, characterizes the erosion potential of the observed waves, providing a comparison of different winters. The instantaneous beach state change rate, dA/dt, is assumed proportional to the instantaneous energy E and energy disequilibrium ΔE

$$\frac{dA}{dt} = C^{\pm} E^{1/2} \Delta E \tag{3.1}$$

where $C^{\pm}$ are empirical change rate coefficients for beach face accretion (C^{+} for $\Delta E < 0$) and erosion (C^{-} for $\Delta E > 0$). The factor $E^{1/2}$ insures small changes in A when E is small. The sign of dA/dt is determined by the sign of the energy disequilibrium,

$$\Delta E = E - E_{eq}, \tag{3.2}$$

where

$$E_{eq} = aA + b. \tag{3.3}$$

For a given beach state, A, the equilibrium energy E_{eq} is the wave energy that causes no profile change. Using modeled hourly waves at each site, and sand levels that excluded nourishments, reef, canyon and shoal sections of beach, the best-fit model four free parameters ($C^{\pm}$, a and b) are similar on these beaches. A single set of optimized free parameters for alongshore uniform sandy reaches at all study beaches reasonably predicts profile evolution [Ludka et al., 2015].

Waves at the Torrey Pines buoy are used with existing optimized equilibrium model parameters to solve (3.1) and (3.2) for the beach state, A (Figure 3.2c), quantifying

the time-integrated wave erosion potential, and neglecting site specific effects including beach nourishments, bedrock, cliffs, self-armoring of the eroded beach with cobbles, and riprap bordering Hwy 101. Modeled beach face erosion was extreme during the 2009-10 El Niño ($A = -1.03$) and was exceeded ($A = -1.17$) on Feb 2, 2016 (Figure 3.2c), suggesting that the 2015-16 El Niño had more erosion potential than the 2009-10 El Niño.

3.4 Sand Level Observations

Subaerial sand elevations at four San Diego County beaches were monitored monthly at low tide with a GPS-equipped vehicle [Seymour et al., 2005] driving shore-parallel tracks with ~ 10 m spacing. Quarterly beach and bathymetry surveys have 100 m shore-perpendicular transects, but only the subaerial portions of these surveys are considered in this analysis. Alongshore survey spans vary between 1.7 and 4.1 km depending on the site (Table 3.1, Figure 3.2). During the monitoring, three beaches were nourished with between 68,000-344,000 m^3 of coarse-grained sand ($D_{50} \sim$ 0.5-0.6 mm), over subaerial alongshore spans between 500-1500 m (Table 3.1, dotted black lines Figure 3.3).

Temporal fluctuations in beach width (Figure 3.2a) are estimated from changes in the cross-shore location of the mean sea level contour (MSL = +0.77 m NAVD88), averaged over the survey alongshore span. If a survey does not include observations of MSL on more than $2/3$ of the alongshore span, it is not considered. Beach widths vary seasonally due to seasonal fluctuations in wave energy, with punctuated erosion during El Niño. On average, all four beaches were relatively narrow during the 2009-10 El Niño. In February of 2016, Cardiff, Solana, and Imperial Beach, nourished in Fall 2012, were wider than 2009-10 by 10 m or more. Torrey Pines, nourished in 2001

[Seymour et al., 2005, Yates et al., 2009a], was eroded slightly below 2009-10 levels.

Plan view sand level difference maps (Figure 3.3) between the 2016 and 2010 surveys with minimum beach width (observed as of February 2016, Figure 3.2a), show the subaerial beach was relatively elevated over the entire alongshore span at Imperial, Cardiff and Solana Beaches. Relative sand levels were most elevated, by 1-2 m, at Imperial Beach, the site of the largest nourishment. Cardiff and Solana were elevated above 2010 by about 1 m. In contrast, at Torrey Pines, the subaerial beach was similar to, and in many locations slightly eroded relative to, 2009-10 levels.

Cross-shore profile evolution at the 2012 nourishment sites corroborate that these beaches were wider and more elevated in 2015-16 (thick red lines, Figure 3.4A,B,D,E) than in the 2009-10 El Niño (thick dashed black line, Figure 3.4A,B,D,E). The fall 2012 nourishment widened and elevated the subaerial beach (compare thin black dotted pre-nourish and thin light orange Nov 2012 profiles, Figure 3.4A,B,D). After placement, the pads retreated (Figure 3.4A,B,D), with partial recovery in the summer months (Nov 2015 Figure 3.4A,D, Figure 3.2a). As the nourishment pads retreated (Figure 3.4D), adjacent regions accreted (Figure 3.4E). Alongshore transport was especially pronounced at Imperial Beach; the southern region (Figure 3.4E) became (perhaps surprisingly) more elevated relative to Feb 2010 levels than the original placement region (Figure 3.4D). In contrast, on 27 January 2016 (when A= -0.57, Figure 3.2c) Torrey Pines was eroded similar to 2009-10 El Niño levels (Figure 3.4C).

3.5 Discussion and Conclusions

The 2015-16 and 2009-10 El Niños were the most energetic and erosive winters in the seven year record from 2009-2016 in southern California (black line Figure 3.2a, Figure 3.2b,c). Observations during extreme winters are essential to understand the

impact of successive energetic storms on sand levels, and the equally important recovery between storms. No existing numerical model accurately simulates erosion, recovery, and the potentially increased erosion resistance of the dense cobble layers (Figure 3.1b) often exposed on San Diego county beaches [Ludka et al., 2015].

As future El Niños and rising sea levels threaten coastal infrastructure, coastal managers must decide whether to protect, accommodate or retreat [Nicholls, 2011]. Beach nourishment is an important protection method worldwide, yet the wave-driven redistribution of nourishment sand is poorly understood. We observed three relatively coarse-grained nourishments that partially remained on the beach face for several years (Figure 3.4A,B,D,E). This evolution differed dramatically from a 2001 Torrey Pines nourishment with approximately 160,000 m^3 of imported sand with grain size similar to the native D_{50} $\sim$0.2 mm. This 500 m-long subaerial pad of native-grain-size sand completely washed offshore during a single storm with an unexceptional maximum significant wave height of 3.2 m during a neap tide (1 m range) [Seymour et al., 2005]. While these contrasting nourishment behaviors occurred on different southern California beaches, these beaches have been shown to respond similarly to incident wave conditions when not influenced by nourishment [Ludka et al., 2015]. Therefore, these results suggest that a larger than native grain size distribution is a primary factor in nourishment evolution in southern California, as at sites with different wave climates [Dean, 1991, Kana and Mohan, 1998]. Laboratory experiments (e.g. Dietrich [1982]) show that coarse grains have faster fall velocities than finer grains, minimizing the amount of time they are susceptible to suspended transport by currents.

Of the 20 total San Diego County beach nourishments in 2001 and 2012, we monitored only four in detail. In total 2.75 million m^3 of sand was placed [Coastal Frontiers, 2015], with total cost of about $44 million [Smith, 2016]. Future nourishments in southern California will be expensive (e.g. $160,000,000 over 50 *yrs* to nourish a

several *km* reach in San Diego County [Diehl, 2015]). Accurately assessing the evolution and impact of previous nourishment projects, in the context of long-term, high resolution, large scale monitoring, is essential. Based on comparatively sparse observations that included all the nourishments, Griggs and Kinsman [2016] concluded that "Most of the 2,600,000 m^3 sand added to the beaches of San Diego County during [the 2001 and 2012 nourishments] was essentially eroded from the exposed subaerial beach during the first year following nourishment." It should be anticipated that nourishment sand will leave the original placement region and analysis should include the impact of the nourishment sand on the surrounding region over many years [Stive et al., 2013, de Schipper et al., 2016]. While the assessment by Griggs and Kinsman [2016] is consistent with the observed evolution of the native-grain-sized 2001 Torrey Pines nourishment that completely washed offshore in a single storm [Seymour et al., 2005], it does not consider that sand partially returned to the beach face the following summer [Yates et al., 2009c]. While much of the sand placed in 2012 was indeed eroded from the original placement regions in the first year, the backbeach portions of the Cardiff and Imperial nourishment berms remained intact for several years (Figure 3.4A,D). Furthermore, much of the sand eroded from the original placement regions accreted adjacent subaerial regions (Figure 3.4D,E). Sand that was moved offshore in winters, partially returned in summers. Notably, at Solana, Cardiff and Imperial Beaches the (alongshore averaged) beach remained wider than pre-nourishment under similar wave conditions, including the energetic El Niño, observed thus far (Figure 3.2a).

The San Diego County nourishments were placed to increase tourism and recreation and reduce flooding and erosion. These public beaches are heavily used and include California State Beaches at Cardiff and Torrey Pines. The nourishments were expected to reduce Highway 101 closures at Cardiff and Torrey Pines by protecting it from flooding and erosion (Figure 3.1b). Owners and patrons of beachfront restaurants at Cardiff

(Figure 3.1a) and homeowners at Imperial Beach (Figure 3.1c) desired protection from wave overtopping. Detailed monitoring is crucial in order to estimate the extent that these goals were achieved, and to weigh the benefits against the monetary expense and potential negative ecological [Speybroeck et al., 2006, Baker, 2016, Wooldridge et al., 2016] and groundwater impacts [Hargrove, 2015]. Repetitive nourishments, perhaps augmented with retention structures, will be costly. Future El Niños, coupled with sea level rise, will inevitably increase pressure on already sparse sand resources [Roelvink, 2015]. Detailed monitoring of beach sand levels and storm damage over decades will be needed to inform coastal management during changing conditions.

3.6 Acknowledgments

Imperial and Cardiff Beach sand level data are available at http://cdip.ucsd.edu/SCBPS/regions/, and observations from the other southern California beach sites will be posted here in accordance with the AGU data policy. This study was supported by the United States Army Corps of Engineers and the California Department of Parks and Recreation, Division of Boating and Waterways Oceanography Program (program manager R. Flick). Bonnie Ludka was also supported by a National Science Foundation Graduate Research Fellowship, NOAA grant NA10OAR4170060, California Sea grant project #R/RCC-01, through NOAAs National Sea Grant College Program, and the NOAA/ Southern California Coastal Ocean and Observing System. The statements, findings, conclusions and recommendations are those of the authors and do not necessarily reflect the views of the aforementioned organizations. B. Woodward, K. Smith, B. Boyd, R. Grenzeback, G. Boyd, and L. Parry built, operated and maintained the surveying system. Lifeguard Captain Robert Stabenow ensured safe access to Imperial Beach. Kathy Weldon, City of Encinitas Shoreline Management Division Manager, facilitated work

at Cardiff. Kathleen Ritzman, Scripps Assistant Director, was essential to maintaining funding and survey continuity.

The text of Chapter 3, in full, is a reprint with minor modifications of the paper "Mid-El Niño erosion at nourished and unnourished southern California beaches", *Geophysical Research Letters*, 43, 45104516, doi:10.1002/2016GL068612., (Copyright of the American Geophysical Union 2016). The dissertation author was the primary researcher and first author with guidance provided by R.T. Guza and contributions from T.W. Gallien and S.C. Crosby.

Table 3.1: Beach statistics

Beach	Mean Beach Width [m]	Survey Alongshore Span [km]	Nourishment Alongshore Span [km]	Reported 2012 Nourishment Volume [m^3][a]	Reported Nourishment Grain Size [mm][a]	Native Grain Size [mm][b]
Cardiff	43	1.7	0.5	68,000	0.57	0.16
Solana	28	2.5	0.5	107,000	0.55	0.15
Torrey	38	3.1	-	-	-	0.23
Imperial	58	4.1	1.5	344,000	0.53	0.25

(a) Coastal Frontiers [2015]
(b) At MSL. Cardiff, Torrey and Imperial from Ludka et al. [2015]. Solana from Group Delta Consultants [1998]

Figure 3.1: Low-tide photos at (a) Cardiff, (b) Torrey Pines, and (c) Imperial Beach on 25 Feb 2016. Cardiff and Imperial Beaches, nourished in 2012, were relatively sandy and wide. Torrey Pines, unnourished since 2001, was primarily cobble, narrow, and backed by the eroding shoulder of Hwy 101.

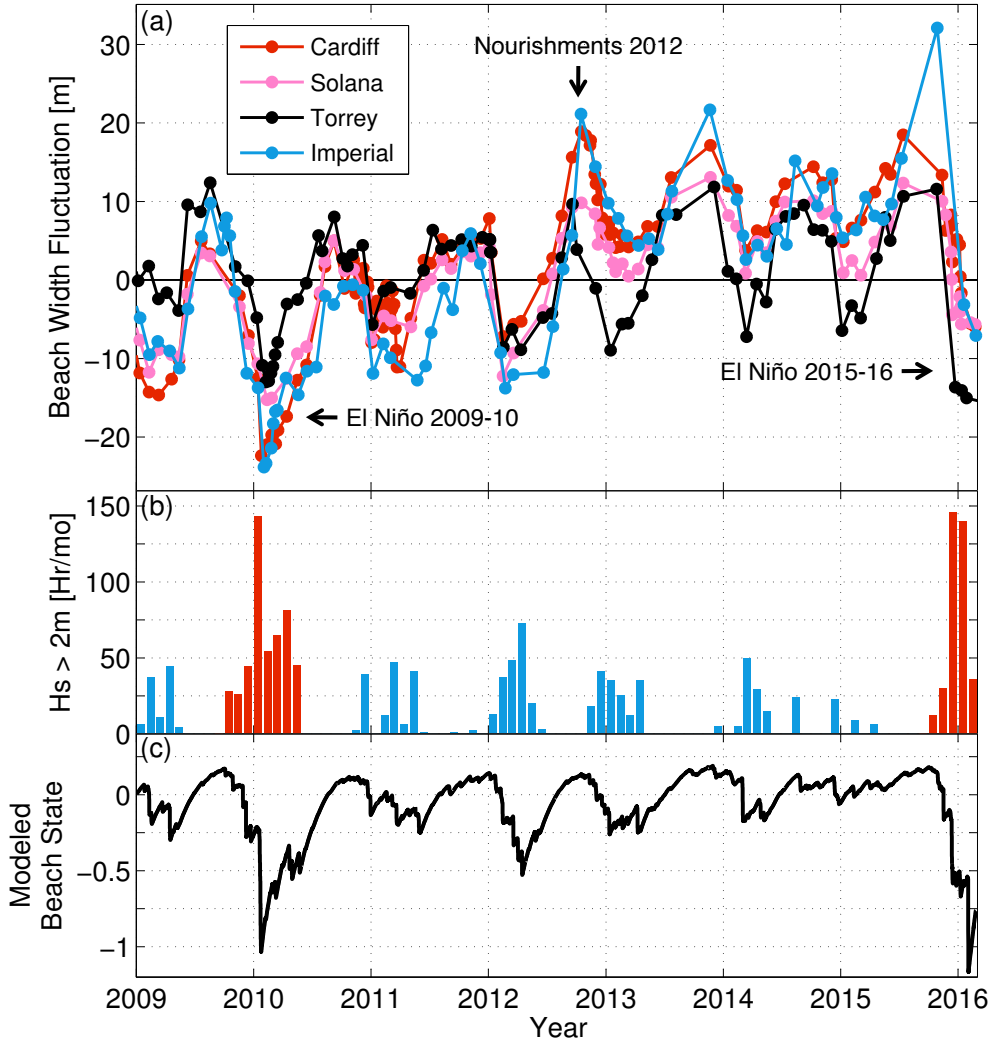

Figure 3.2: (a) Beach width fluctuation (about the mean, Table 3.1) versus time for four southern California beaches (legend). Each dot is an average over several *km* alongshore (Table 3.1, Figure 3.3). (b) Hours per month the observed significant wave height (Hs) exceeds 2 *m* (combined swell and seas, 0.04-0.25 *Hz*) at the Torrey Pines buoy (NDBC 46225) versus time. Red indicates El Niño winters. (c) Beach state estimated using observed waves and published model coefficients [Ludka et al., 2015]. The model, insensitive to initial conditions after a brief transient, is initialized with $A = 0$ on 1 January 2009.

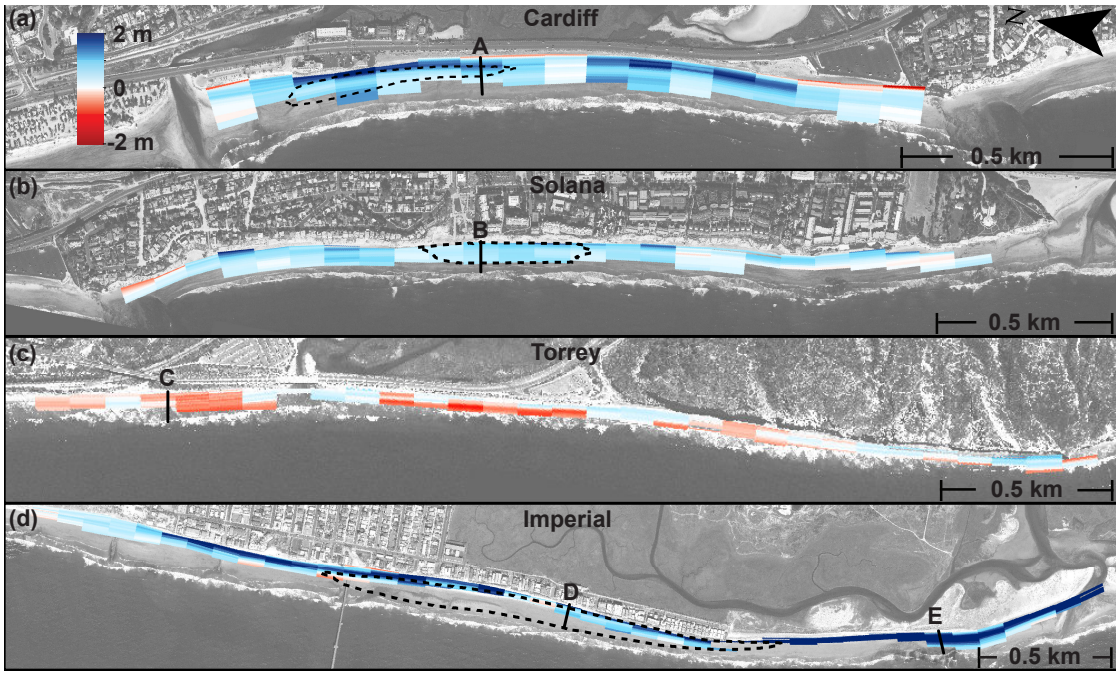

Figure 3.3: Sand elevation differences (color bar) between the winter 2016 and 2010 surveys with minimum beach widths. (a) Cardiff 23 Feb 2016 - 12 Feb 2010, (b) Solana 23 Feb 2016 - 12 Feb 2010, (c) Torrey Pines 27 Jan 2016 - 8 Feb 2010, (d) Imperial 25 Feb 2016 - 02 Feb 2010. Horizontal scale (bottom right) changes with panel. Black dotted lines outline the 2012 nourishment placement regions at (a) Cardiff (b) Solana and (d) Imperial Beach. (c) Torrey Pines, unnourished since 2001, has the smallest elevation difference, mostly less than 0.5 *m* of relative erosion (red). (d) Imperial Beach received the most imported sand in 2012 and almost the entire subaerial beach is elevated 1-2 *m* above the 2010 El Niño survey. (a) Cardiff and (b) Solana are elevated above 2010 by about 1 *m*. Black lines mark the locations of transect locations A-E in Figure 3.4.

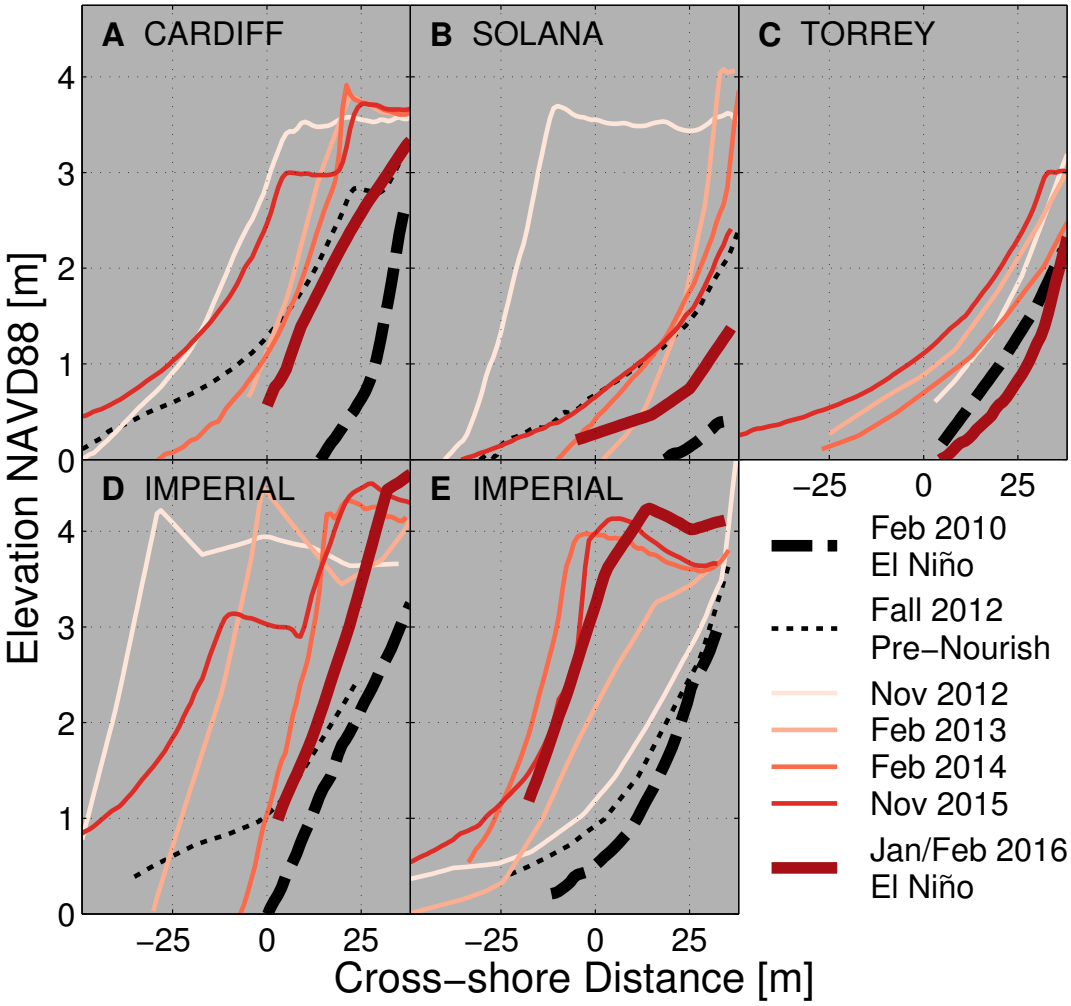

Figure 3.4: Sand level versus cross-shore distance at representative times (legend) at transects labeled in Figure 3.3. Erosion during the 2009-10 El Niño was extreme (thick dashed black lines). The recent profile (thick red line) at (C) Torrey is similar to Feb 2010, but at sites nourished in 2012 (A,B,D,E), the recent profile is elevated above Feb 2010. The pre-nourished profile is a thin black dotted line. At transects located in the original placement region (A,B,D), the nourished pad is evident in the Nov 2012 profile and retreats over time, with partial recovery in summer/fall as in Nov 2015 (A,D). As the Imperial Beach nourishment pad retreated (D), the southward region accreted (E).

Chapter 4

The evolution of four southern California beach nourishments

4.1 Abstract

Four southern California beaches were nourished with between 68,000-344,000 m^3 of offshore sand, placed as several meter thick subaerial pads spanning between 500-1500 m alongshore. The Torrey Pines pad, built in April 2001 with native-sized sand, was completely removed from the subaerial beach in a few days by waves with an unexceptional significant height (2.2m, daily average) [Seymour et al., 2005]. In contrast, the other nourishments, constructed with relatively coarse sand in 2012, elevated the subaerial beach face for several years even when exposed to waves more energetic than those that eroded the 2001 Torrey Pines nourishment [Ludka et al., 2016]. Here, the nourishment evolutions are described in detail. As the coarse-grained nourishment pads retreated, an accretionary crown formed at the seaward edge, causing the originally flat-topped pad to slope increasingly landward over time; the seaward edge of the pad became increasingly more elevated than the backbeach. At all four sites, the regions

adjacent to nourishment accreted, and formed tilted landward sloping subaerial profiles. The subaerial pads elongated alongshore in a direction consistent with seasonally shifting, wave-driven alongshore currents. At Imperial Beach, nourishment sand stretched several km alongshore and likely contributed to the closing of the Tijuana River mouth, causing hyper-polluted and anoxic conditions in the estuary. Natural gains and losses in the total sand volume budget (integrated spatially from the back beach to 8m depth and over the entire alongshore survey span) are sometimes larger than the nourishment contributions.

4.2 Introduction

Beach nourishment, placing imported sand to widen and elevate the beach, is used to mitigate flooding and erosion and promote tourism and recreation. The observations presented here detail the evolution of four nourished southern California beaches. The Torrey Pines nourishment was one of 12 San Diego County sand placement projects in 2001, with a combined cost of $17.5 million. Cardiff, Solana and Imperial Beaches were nourished in 2012, along with five other sites, at a total cost of $28.5 million [Griggs and Kinsman, 2016]. A 50-year plan is developing for repetitive nourishments in north San Diego County that will cost $160 million [Diehl, 2015]. A cost-benefit analysis of nourishment impacts is crucial as seas rise [Stocker et al., 2013] and global coastal populations continue to increase [MacGrannahan et al., 2007].

Despite the frequency and expense of nourishments worldwide [Clayton, 1991; Haddad and Pilkey, 1998; Trembanis and Pilkey, 1998; Valverde et al., 1999; Hanson et al., 2002; Cooke et al., 2012; Luo et al., 2015], the wave-driven redistribution of nourishment sand is understood poorly. Previous observations of nourishment evolution have provided important insights. However, wave conditions are often not observed [Cooper, 1998; Davis et al., 2000; Gares et al., 2006; Benedet et al., 2007; Park et

al., 2009; Roberts and Wang, 2012] or are only crudely approximated [Kuang et al., 2011]. Temporal resolution [Cooper, 1998; Browder and Dean, 2000; Gares et al., 2006; Benedet et al., 2007; Park et al., 2009; Bocamazo et al., 2011], duration [Elko and Wang, 2007], alongshore span [Anfuso et al., 2001] or cross-shore extent [Gares et al., 2006] is sometimes limited. The accuracy of the sand elevation measurements (e.g. scans of aerial photography, [Bocamazo et al., 2011]) is sometimes questionable. Here we present uniquely comprehensive, accurate wave and sand level observations of four nourished beaches (black boxes, Figure 4.1 inset), with relatively high temporal and spatial resolution, duration and extent. These detailed observations are used to describe the nourishment evolution, and to quantify the accumulation of instrument and interpolation errors in a volume time series.

The 2001 Torrey Pines nourishment grain size was similar to native, whereas the 2012 nourishment sand at Imperial, Cardiff and Solana Beaches was coarser than native. As Dean [1991] predicted, the relatively coarse-grained nourishments evolved to a steeper beach face than pre-nourishment, with an elevated subaerial profile [Ludka et al., 2016]. The slow erosion of the relatively coarse-grained 2012 nourishment pads, compared with the 2001 pad [Seymour et al., 2005] (Section 4.3.1), is also consistent with nourishment evolution at sites exposed to wave climates unlike southern California [Kana and Mohan, 1998]. As the relatively resilient coarse-grained nourishment pads retreated, an accretionary crown was formed on their seaward edge, causing the originally flat-topped pads to slope increasingly landward over time; the seaward edge of the pad became increasingly more elevated than the backbeach (Section 4.3.2). This cross-shore feature was not observed at the native-grain-sized Torrey Pines nourishment pad, which was not overtopped prior to the storm that washed it offshore [Seymour et al. 2005].

At all four sites, the regions adjacent to nourishment accreted, and formed tilted landward sloping subaerial profiles, similar to the diffusive spits observed by Elko and

Wang [2007] (Section 4.3.2). Rather than diffusing symmetrically [Pelnard-Considere, 1956; de Schipper et al., 2016], the subaerial elevation perturbations at all sites were advected [Castelle et al., 2009] in the direction of the seasonally shifting alongshore currents (Section 4.3.3). For the coarser than native nourishments, Dean and Yoo [1992] incorrectly (it turns out) speculated that the relatively coarse imported sand would act as a barrier, and native sand would accumulate on the updrift side, such that the pad elevation perturbation would move in a direction opposite of the alongshore current. When the entire survey domain is considered (Section 4.4.2), gains and losses in the sediment budget [Cooper, 1998; Browder and Dean, 2000; Park et al., 2009; Yates et al. 2009; and de Schipper et al., 2016] are sometimes larger than the nourishment contributions, and also larger than the estimated volume errors, at all sites. Possible impacts of the Imperial Beach nourishment are discussed in section 4.4.3. Section 4.5 is a summary.

4.3 Observations

4.3.1 Waves

Swell waves (0.04-0.1 Hz) were observed at offshore buoys (triangles, Figure 4.1) and propagated over the complex bathymetry of the Southern California Bight using a spectral refraction model that reproduces with significant skill the observations at nearshore buoys in the study area [O'Reilly and Guza, 1998; Young et al., 2012; O'Reilly et al., 2016]. The swell model was combined with a sea wave model (0.08-0.5 Hz) initialized with nearshore buoy conditions (circles, Figure 4.1) to provide hourly directional wave estimates every 100 m alongshore at Monitoring and Prediction (MOP) locations in 10m depth [O'Reilly et al., 2016]. Waves are seasonal, with energetic storms in winter, and milder summers (Figure 4.2).

4.3.2 Sand Levels

At all sites, quarterly bathymetric surveys, from the backbeach to 8m depth, were conducted using GPS equipped vehicles [Seymour et al., 2005] along cross-shore transects spaced 100m apart in the alongshore (black lines, Figures 4.3a, 4.4a, 4.B.3a). Relatively few surveys had finer alongshore resolution; 20m at Torrey Pines centered on the nourishment placement (Figure 4.3a), and 50m at Cardiff (black lines, Figure 4.B.1a). Additionally, monthly subaerial beach elevations were measured at all sites along shore-parallel tracks spaced 10m in the cross-shore (gray lines, Figure 4.3a, Figures 4.B.1a,4.B.3a). A coastline following coordinate system was created and the data from each survey were binned and mapped (Appendix 4.A). The monitoring spans 1.7-4.1 km alongshore and 8-15 years at each site. During the monitoring, all beaches were nourished with between 68,000-344,000 m^3 of sand, over subaerial alongshore spans between 500-1500 m (Table 4.1, Figures 4.3c,4.4c,4.5c,4.6c,4.B.1c,4.B.2c,4.B.3c,4.B.4c).

4.4 Description of nourishment evolution

4.4.1 Maps

The April 2001 nourishment at Torrey Pines (dark blue, Figure 4.3c), constructed with a grain size similar to native (Table 4.1), was placed on an eroded beach face (Figure 4.3b). In the following months, waves were calm (Figure 4.2a) and the beach surrounding the nourishment accreted (Figure 4.3d). Then, on 22 November 2001, a storm with peak daily averaged wave height of 2.2m (black dot, Figure 4.2a) completely washed the nourishment pad offshore (Figure 4.3e) [Seymour et al., 2005]. Sand was stored in an offshore bar (Figure 4.3e-f) and partially returned to the beachface the following summer (Figure 4.3g) [Yates et al., 2009]. The usual seasonal cross-shore exchange at Torrey

Pines [Shepard, 1950; Winant et al., 1975], was accentuated. The nourishment caused a super-elevation of the subearial beach (blue, Figures 4.4c,d,g) and a large offshore bar (light blue Figure 4.4f) compared to the maximum elevation observed at each grid point during unnourished times (Figure 4.4a).

In contrast, the relatively coarse grained (Table 4.1) September 2012 nourishment at Imperial Beach (dark blue, Figure 4.5c) was placed on an already accreted beach face (not shown), and largely remained subaerial for several years (Figure 4.5c-h) despite experiencing waves larger than the storm that washed the Torrey Pines nourishment offshore (Figure 4.2b, when waves exceed the horizontal black line) [Ludka et al., 2016]. The persistent super-elevation of the nourished subaerial beach is highlighted (blue Figure 4.6c-h) when compared to the maximum elevations observed prior to nourishment (Figure 4.6a). More similar to Imperial Beach than Torrey Pines, the coarse-grained nourishments at Cardiff and Solana Beaches were detectable as subaerial superelevations in July 2015, thirty months after nourishment (4.B.2g, 4.B.4g).

4.4.2 Cross-shore transects

The nourishment pads were constructed as flat-topped berms. As waves overtopped the berm, the 2012 coarse-grained nourishment pads retreated and an accretionary crown formed at the seaward edge, creating a landward sloping subaerial profile (Figure 4.7 B-D); the seaward edge of the pad became increasingly more elevated than the backbeach. Crowns were not observed in the original placement region at Torrey Pines (Figure 4.7A), as the pad was not overtopped until the storm of 22 November 2001, when the entire pad, constructed with a grain size similar to native, washed offshore. The wave and sand mechanics underlying crown formation are not understood. At all sites, landward sloping subaerial profiles formed downdrift from the nourishments (Figure 4.7E-H) similar to the diffusive spits observed by Elko and Wang [2007]. These features

are possibly due to relatively enhanced alongshore transport at the seaward edge of the pad compared to the backbeach.

4.4.3 Alongshore transport

Alongshore transport was most pronounced at Imperial Beach. The subaerial nourishment pad elongated over a few years to span several km alongshore (Figure 4.6c-h). The position of the center of mass (marked as a magenta x in Figure 4.6) of the subaerial sand "in play" (defined in Appendix 4.A as all sand above the minimum observed surface Figure 4.1.A) moves in different alongcoast directions in winter (southward) and summer (northward). The seasonal oscillation and net southward drift of the center of mass at Imperial Beach (thin blue in Figure 4.8a) is well correlated with the estimated S_{xy} (thick blue in Figure 4.8a, [Longuet-Higgens and Stewart, 1964]), suggesting that the nourishment pad was advected in the direction of the mean longshore current [Longuet-Higgins, 1970; Thornton and Guza, 1986; Ruessink, 2001]. This contradicts the prediction by Dean and Yoo [1992] that coarser than native nourishment sand would act as an erodible barrier, such that the center of mass would move in a direction opposite of the longshore current.

Although the nourishment pad at Torrey Pines only remained subaerial for one summer when alongshore currents were weak, the direction of the slight alongshore transport (thin red, Figure 4.8a) is consistent with the estimated cumulative S_{xy} radiation stress (thick red, Figure 4.8a). The center of mass and cumulative radiation stress curves at Cardiff (black, Figure 4.8b) and at Solana (magenta, Figure 4.8b) are not as well correlated. Future work will examine the sensitivity of results to the uncertainty and variability in the coastline angle, and other factors. Ultimately, the alongshore evolution will be modeled using gradients of S_{xy}.

4.5 Discussion

4.5.1 Subaerial sediment budget

Seasonal variability in wave forcing is apparent in the alongshore motion of the center of mass of the subaerial sand in play (subaerial region outlined with thin black line, Figure 4.3-6 b-h 4.A.1-4b). Seasonal variability in the wave forcing also influences cross-shore transport. The volume of subaerial sand in play at each site is divided by the subaerial survey area (Table 4.1), yielding an average thickness of subaerial beach sand in play. Winter storms remove sand from the subaerial beach and summer calms accrete the beach (Figure 4.2, Figure 4.9). The spring 2001 nourishment at Torrey Pines was placed on eroded beach, and during summer the adjacent beach accreted around it (red, Figure 4.9). Nourishment sand, completely removed from the beachface during the first storm [Seymour et al., 2005], partially returned to the beach the following summer [Yates et al., 2009]. Imperial, Cardiff, and Solana Beaches also experienced a seasonal cross-shore exchange of sand before and after nourishment; however, much of the relatively coarse-grained nourishment sand remained on the subaerial beach (blue, black and magenta curves, Figure 4.9). Subaerial sand volume was at a minimum at all sites during the significant wave attack of the 2009-10 El Niño winter. Wave energy was similarly energetic during the 2015-16 El Niño, and the Torrey Pines beach face was more eroded in 2016 than in 2010. In contrast, beaches nourished with relatively coarse-grained sand in 2012 maintained more subaerial volume than in 2010 [Ludka et al., 2016].

4.5.2 Full domain sediment budget

Total sand in play estimates for the entire survey domain divided by the survey area (Table 4.1) at each beach do not show strong seasonality because sand exchanged

between the subaerial beach and offshore sand bar is approximately conserved (Figure 4.10). Errors can accumulate over this large integration, and error estimates (Appendix 4.B) aid in interpreting results (error bars, Figure 4.10). The nourishment contributions at Torrey, Imperial and Cardiff Beaches are clearly visible and significant (increase in volume between squares on red, blue, and black curves, Figure 4.10). The expected nourishment volume contribution divided by the survey area is smallest at Solana Beach with a value of 8 cm (Table 4.1). This contribution is not observed in the total volume divided by survey area estimate. Instead the volume divided by survey area decreases slightly by 3.5 cm (magenta squares, Figure 4.10). The error bars during nourishment times span 12.5 cm at Solana Beach, suggesting that this decrease could be noise. Natural gains and losses in the system are sometimes larger than the nourishment contributions, and the noise. Future work will calculate volume estimates over different portions of the domain to attempt to identify where (offshore or alongshore) and when these large gains and losses occur.

4.5.3 Possible nourishment impacts at Imperial Beach

The landward sloping nourishment pad at Imperial Beach is backed by riprap, fronting houses (Figure 4.11a). At high tide, waves sometimes overtopped the berm (Figure 4.11a). Without the 20m wide, 1m tall, residual nourishment berm (Figure 4.5h), waves would have impacted directly onto the riprap. At low tide, surface water pooled in the low region behind the accretionary crown (Figure 4.11b). The perched water level contributed to ground water flows and the garages of the homes backing the nourishment pad flooded from below (Figure 4.10c, [Hargrove, 2015]). The garage elevation 1.4m MSL is almost 1.6m below the + 3m pad elevation.

Net transport at Imperial Beach was predominantly southward (Figure 4.6h, Figure 4.7f) and the accumulation of nourishment sand may have contributed to the

closing of the Tijuana River mouth in April 2016 that caused hyper-polluted and anoxic conditions in the estuary [Baker, 2016]. The blockage was mechanically removed (Figure 4.11d). The previous closure of the Tijuana River mouth occurred during a strong El Niño in 1983, so the additional nourishment sand may have contributed to other factors favoring closure in April 2016 (following an El Niño winter).

4.6 Summary

Four monitored southern California beaches received between 68,000-344,000 m^3 of imported sand placed as several meter thick subaerial pads spanning 500-1500m. The nourishment at Torrey Pines, constructed in 2001 with a sand grain size similar to native, washed offshore during a storm with an unexceptional significant wave height (2.2m, daily average) [Seymour et al., 2005]. Imperial, Cardiff and Solana Beaches received relatively coarse-grained sand in 2012 that largely remained subaerial for several years when exposed to wave conditions more energetic than the storm that eroded the pad at Torrey Pines [Ludka et al., 2016]. As these relatively hardy coarse-grained nourishment pads retreated, an accretionary crown formed on their seaward edge, tilting the originally flat-topped pad landward; the seaward edge of the pad became increasingly more elevated than the backbeach. Crowns did not form on the Torrey Pines pad, which was not overtopped until it encountered the storm that washed it offshore.

In some respects these nourishments evolved similarly. Enhanced alongshore transport, at the seaward edge of the pads relative to the backbeach, formed diffusive spits [Elko and Wang, 2007] that created landward sloping subaerial profiles in the regions adjacent to nourishment at all sites. The nourishments did not diffuse alongshore symmetrically [Pelnard-Considre, 1956; de Schipper et al., 2016], but rather were advected [Castelle et al., 2009] in the direction of the seasonally shifting alongshore

currents. Natural gains and losses in the total sand volume budget (integrated spatially from the back beach to 8m depth and over the entire alongshore survey span) are sometimes larger than the nourishment contributions.

The cost-benefit analysis of beach nourishment practices is complex. For low-lying homes at Imperial Beach, nourishment sand mitigated flooding by wave overtopping but elevated the water table, inducing groundwater flooding [Hargrove, 2015]. Nourishment sand affected intertidal invertebrate populations (often negatively, [Wooldridge et al., 2016]) and may have contributed to the clogging of the Tijuana River mouth that created hyper-polluted and anoxic conditions in the estuary. In the face of rising seas, limited sand resources [Roelvink, 2015], and increasing coastal populations, detailed monitoring of often-expensive beach nourishments provides crucial information for coastal managers attempting to protect coastal infrastructure and maintain thriving tourist economies [Pendleton et al., 2012; WorleyParsons, 2013; Alexandrakis et al., 2015].

4.7 Acknowledgements

The text of Chapter 4, in full, is a reprint with minor modifications of the paper "The evolution of four southern California beach nourishments", to be submitted to *Coastal Engineering*. The dissertation author was the primary researcher and first author with guidance provided by R.T. Guza and W.C. O'Reilly.

Appendices

4.A Coastline following coordinates and mapping scheme

A coastline following coordinate system was created using surveys without measurable influence of beach nourishment. This includes all surveys before the fall 2012 nourishment placements (gray shading, Figure 4.2b-d) at Imperial, Cardiff and Solana beaches, and (somewhat arbitrarily) all surveys after Jan 7 2004 at Torrey Pines. MOP lines, extending from backbeach locations spaced 100m apart in the alongshore, to the nearest offshore location on the 10m bathymetric contour, are used as the alongshore coordinate, $\tilde{y}$. Transect lines at Imperial and Solana beach (black lines, Figures 4.5a, 4.A.3a) are aligned with the MOP lines, as well as the surveys after 31 October 2011 at Cardiff beach (black lines, Figure 4.A.1a). Only the bathymetric surveys with transects aligned with MOP lines were used to calculate the coastline following coordinate system at Cardiff. The mean horizontal positions of contours spaced 15 centimeters in the vertical, are used as the cross-shore coordinate, $\tilde{x}$. These horizontal positions were extracted from interpolated profiles along the predetermined transect lines. Profiles from the quarterly bathymetric surveys were created by bin-averaging elevation data in 20m alongshore by 1m cross-shore bins centered on the transect lines, applying a 2m cross-shore moving average, and splining to a 1m grid wherever breaks in the data do not exceed 20m. Subaerial profiles from the monthly beach surveys were created using a Delaunay triangulation linear interpolation of observations within 20m wide alongshore swaths centered on the transect line. At Torrey Pines, transect lines (black lines, Figure 4.3a) are not aligned with MOP lines, so the mean horizontal contour locations were linearly interpolated to the MOP lines.

Data was binned into grid cells defined by this coastline following coordinate system. Bathymetry surveys at Imperial and Solana Beaches were binned to grid cells with 100 m $\Delta\tilde{y}$ alongshore resolution (centered on MOP lines), and cross-shore bins with mean vertical positions spaced 15 cm $\Delta\tilde{x}$ apart. Because of the sometimes higher alongshore resolution bathymetry surveys at Cardiff and Torrey Pines Beach, these observations were instead binned to grid cells with 50m and 20m $\Delta\tilde{y}$ alongshore resolution respectively. Additionally, subaerial surveys and the subaerial portions of bathymetry surveys at all sites were binned with 20m $\Delta\tilde{y}$ alongshore resolution. The spatially varying unnourished times mean (Figures 4.3a,4.5a,4.A.1a,4.A.3a) was then removed from the binned observations,

$$d' = d - < d > \tag{4.1}$$

where the data fluctuation is a combination of the true signal fluctuation, s, and noise, ε

$$d' = s' + \varepsilon. \tag{4.2}$$

We chose $< \varepsilon^2 >$ = 2cm, the typical mean standard error in each grid cell. This value is sometimes higher (7cm), however, over canyon, reef, or shoal.

These binned fluctuations were then smoothed, and empty grid cells filled in, using a simple mapping scheme. Each mapped fluctuation grid point, m', is calculated as a linear combination of the observed data fluctuations,

$$m' = a^T d'. \tag{4.3}$$

where the mean square error, $< e^2 >$,

$$< e^2 > = < (m' - s')^2 > \tag{4.4}$$

$$= a^T < d'd'^T > a - 2 < d's' > a + < s'2 > \tag{4.5}$$

is minimized with gain,

$$a = < d'd'^T > -1 < d's' > . \tag{4.6}$$

Typically, the covariance matrices are modeled by a functional fit to the observed autocovariance, where noise is assumed uncorrelated with the signal and uncorrelated from one gridpoint to the next [Bretherton et al., 1976],

$$< d'd'^T > = < s's'^T > + < \varepsilon^2 > . \tag{4.7}$$

Attempts to model the complex patterns of the observed autocovariance did not significantly improve results compared to assuming an arbitrary simple functional form. (This will be addressed in a future paper.) Therefore, a simple (and unrealistic) Gaussian is used to model the autocovariance,

$$< s's'^T > = < s'^2 > exp(-(\Delta\tilde{y}/L\tilde{y})^2 - (\Delta\tilde{x}/L\tilde{x})^2), \tag{4.8}$$

where Lỹ = 200m and Lx̃= 30 cm (mean vertical) are chosen simply to fill in gaps in a typical survey by doing minimal smoothing (similar to Plant et al. [1999]). Figures 4.3b-h, 4.5b-h, 4.C.1b-h and 4.C.3b-h show examples of these maps where grid points are only plotted if they have a normalized mean square error, NMSE $= < e^2 > / < s'^2 >$, that is less than 0.2. The maximum observed surface during unnourished times (Figures 4.4a,4.6a,4.B.2a,4.B.4a), and the minimum observed surface over the entire record (Figure 4.A.1), was calculated at each grid point from these maps, where only interpolated regions with NMSE$<$ 0.2 are considered.

4.B Nourishment evolution at Cardiff and Solana Beaches

The coarse-grained nourishment evolution at Cardiff and Solana Beaches was more similar to the behavior of the coarse-grained nourishment evolution at Imperial Beach than the native-grain-sized nourishment evolution at Torrey Pines. Nourishment sand was placed on already accreted beachfaces (Figures 4.C.1b and 4.C.3b), and largely remained subaerial for many years while being stretched and advected alongshore (Figures 4.C.1c-g and 4.C.3c-g). The persistent super-elevation of the nourished subaerial beach is highlighted (blue Figure 4.C.2c-g and C4c-g) when compared to the maximum elevations observed prior to nourishment (Figure 4.6a). The 2015-2016 El Niño winter transferred much of the remaining subaerial nourishment sand from the beachface to an offshore bar (Figures 4.C.1h and 4.C.3h). Offshore regions became more elevated than ever observed previously (Figures 4.C.2h and 4.C.4h); however, these large offshore bars might have developed whether or not these beaches were nourished, due to the significant wave attack of the El Niño.

4.C Volume error estimates

A GPS bias of 3 cm (a typical observed value at a known benchmark checked during every survey at Cardiff and Imperial Beach) over the entire domain was assumed as an upper limit on the cumulative error contribution of long-period GPS noise [Borsa et al., 2007].

The offshore bathymetry is measured as the distance from the sea floor to a GPS equipped jet ski, using the travel time of acoustic pings. The speed of sound is calculated using the assumption that the water column is unstratified, with the same

temperature throughout as measured at the surface. A four-month time series of summer temperature stratification (June-Sept 2012) measured at the Scripps Pier was used to quantify the errors associated with this assumption. The stratification was extrapolated in sigma coordinates until 3m depth, where it is assumed that breaking typically mixes the water column. (The breakpoint changes with the tide, but setup is not considered.) The calculated errors are typically less than a few centimeters even in the deepest observed waters (Figure 4.B.1a). The 68% error calculated at the mean depth of each cross-shore location (Figure 4.B.1b) is used as the sonar bias at each grid point and summed over the survey area. The cumulative sonar bias contribution to the volume divided by survey area estimate (Figure 4.12) is small (about 0.5cm at each site) and only biases the volume low, because warmer water is stable above colder water.

To estimate interpolation errors at Cardiff Beach, volume estimates from the higher resolution surveys with 50m alongshore resolution (black lines, Figure 4.B.1a) were compared to the volume estimate calculated from these same surveys when decimated to 100m alongshore resolution. The maximum difference between these volume estimates was used as the interpolation error estimate. Separate error estimates were calculated for unnourished and nourished times. At the other sites, higher resolution surveys are not available. (Torrey Pines had 20m alongshore resolution in the nourishment placement area as in Figure 4.3a, but not across the full domain.) Therefore, all surveys were decimated to 200m alongshore resolution and the maximum difference between the un-decimated and decimated volume estimates was used as the interpolation error estimate, where nourished and unnourished times were treated separately. Surveys spaced close in time during the first couple years of monitoring at Torrey Pines, and during the winters of 2010-11 and 2012-13 at Cardiff suggest that the typical quarterly sampling scheme is sufficient to capture much of the observed temporal variability.

Table 4.1: Nourishment statistics

Beach	Native Grain Size $[mm]^a$	Nourishment Grain Size $[mm]^b$	Nourishment Volume $[m^3]^c$	Subaerial Survey Area $[m^2]$	Jumbo Survey Area $[m^2]$
Torrey	0.23	0.2	187,000	171,715	1,094,546
Imperial	0.25	0.53	344,000	252,358	1,610,518
Cardiff	0.16	0.57	68,000	95,499	629,437
Solana	0.15	0.55	107,000	104,968	1,213,960

(*a*) At MSL. Torrey, Imperial and Cardiff from *Ludka et al.* [2015]. Solana from *Group Delta Consultants* [1998]
(*b*) Torrey from *Seymour et al.* [2005]. Imperial, Cardiff, and Solana from *Coastal Frontiers* [2015]
(*c*) *Coastal Frontiers* [2005, 2015]

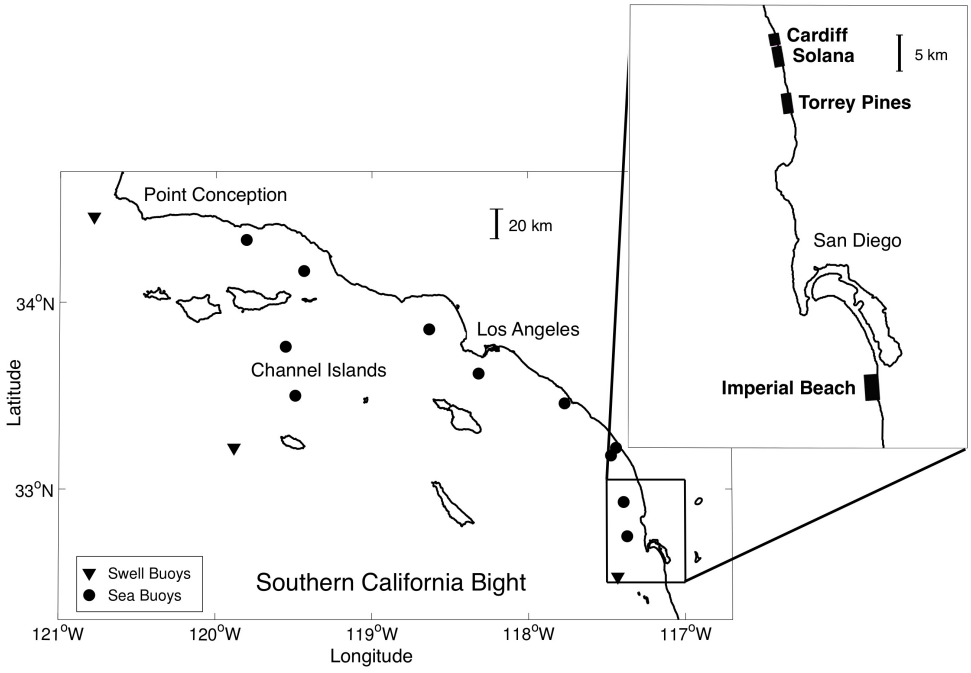

Figure 4.1: Map of the southern California Bight, with wave buoy locations indicated (circles are used for local seas, triangles for swell). The study beaches are indicated in the inset.

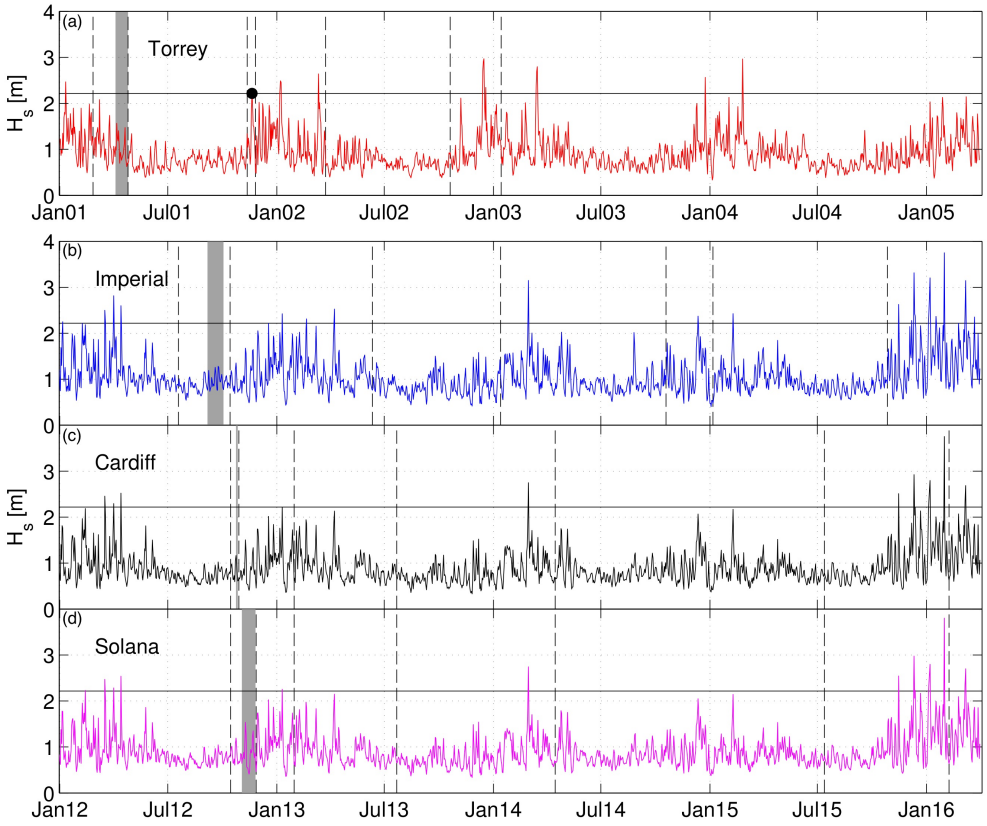

Figure 4.2: Daily averaged significant wave height, H_s, versus time at (a) Torrey Pines, (b) Imperial Beach (c) Cardiff and (d) Solana in 10m depth. Gray shading shows period of nourishment placement. The Cardiff nourishment placement period was short (25 Oct 2012 - 28 Oct 2012). Black vertical dashed lines mark surveys shown in Figs 3-6 and B1-B4. Black dot in (a) shows storm (H_s= 2.2m) that eroded the Torrey Pines nourishment pad. H_s=2.2 is shown in all panels with a black horizontal line.

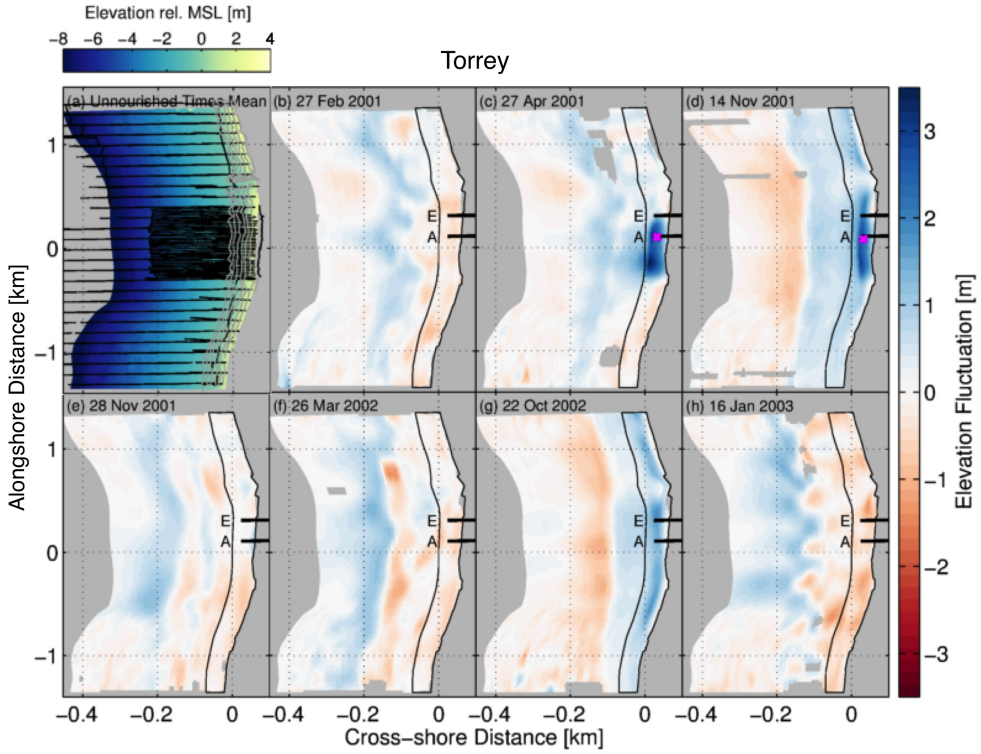

Figure 4.3: Nourishment evolution at Torrey Pines. (a) Map of mean elevation (relative to MSL) averaged over observations from unnourished times (all surveys after 7 Jan 2004). Example tracks are shown for a full survey (black) and a subaerial survey (gray). (b-h) Time sequential maps of sand elevation fluctuation relative to mean shown in (a). These maps have an alongshore resolution of $\Delta\tilde{y}$ = 20m and the interpolation is not plotted where NMSE > 0.2 (Appendix 4.A). The thin black line outlines subaerial region used in center of mass (Figure 4.8) and volume calculation (Figure 4.9). Magenta x marks subaerial center of mass (Figure 4.8), only trackable with continuous nourishment influence for the first few surveys. Thick black lines mark transects A and E in Figure 4.7.

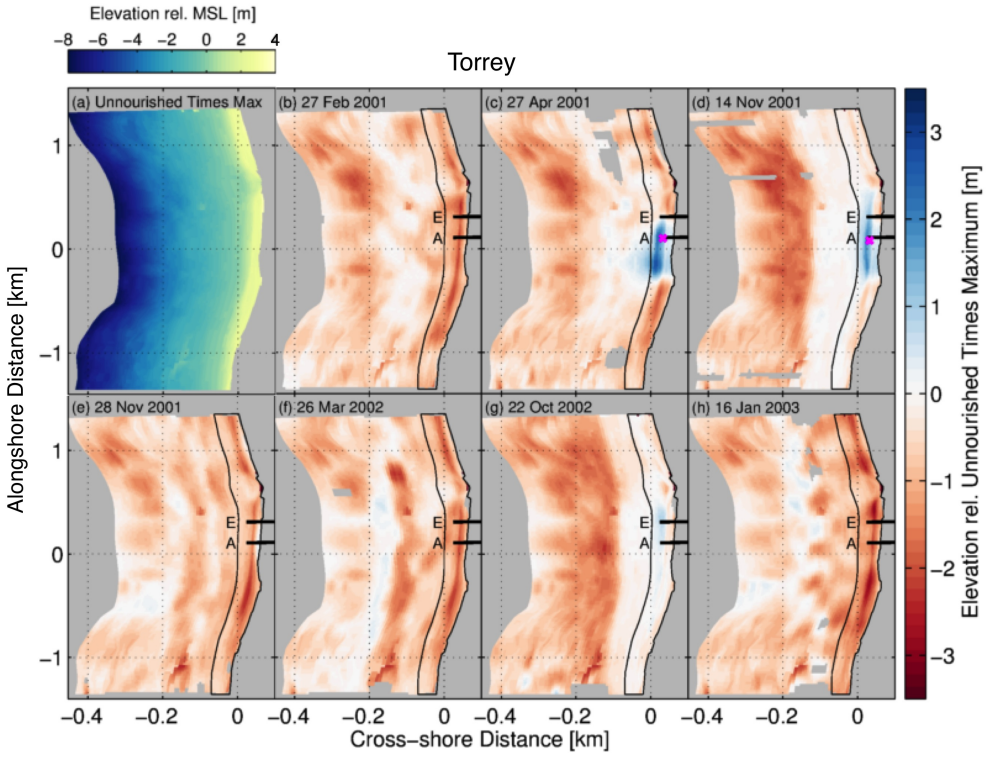

Figure 4.4: Nourishment evolution at Torrey Pines. (a) Map of maximum elevation (relative to MSL) over un-nourished observations (all surveys after 7 Jan 2004). (b-h) Time sequential maps of sand elevation fluctuation, relative to maximum un-nourished observation (a). These maps have an alongshore resolution of $\Delta\tilde{y}$ = 20m and the interpolation is not plotted where NMSE > 0.2 (Appendix 4.A). Thin black line outlines subaerial region used in center of mass (Figure 4.8) and volume calculation (Figure 4.9). Magenta x marks subaerial center of mass (Figure 4.8), only trackable with continuous nourishment influence for the first few surveys. Thick black lines mark transects A and E in Figure 4.7.

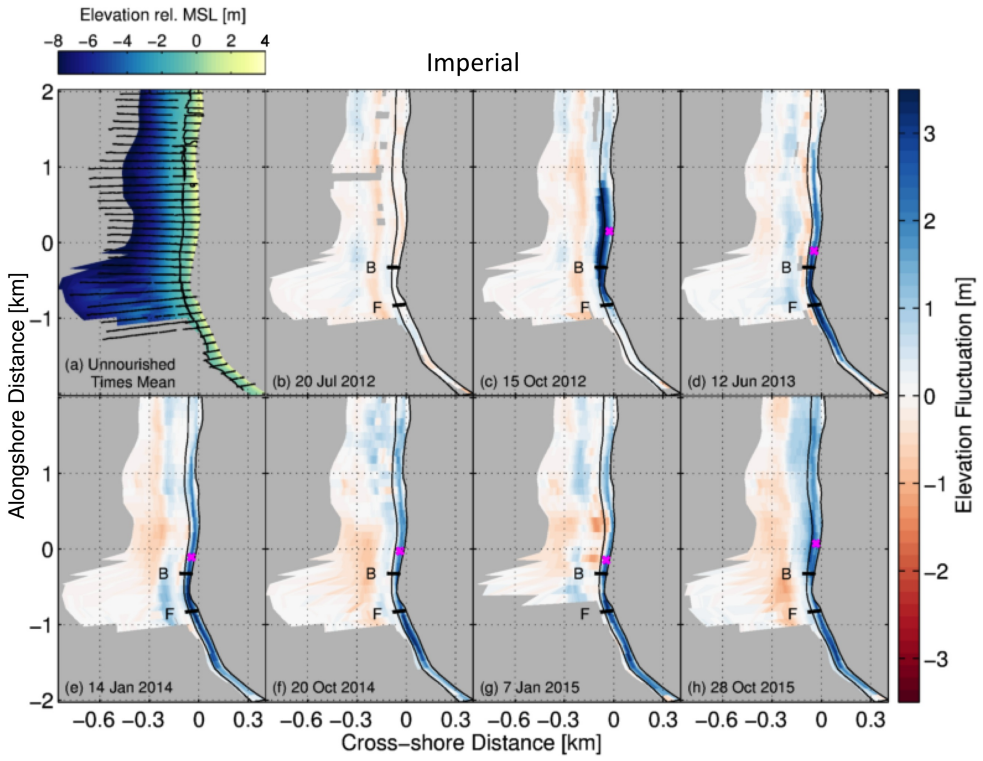

Figure 4.5: Nourishment evolution at Imperial Beach. (a) Map of mean elevation (relative to MSL) averaged over observations from unnourished times (all surveys before 7 Sept 2012). Example tracks are shown for a full survey (black). An example subaerial survey is not shown. (b-h) Time sequential maps of sand elevation fluctuation relative to mean shown in (a). These maps have an alongshore resolution of $\Delta\tilde{y}$ = 100m and the interpolation is not plotted where NMSE $>$ 0.2 (Appendix 4.A). Thin black line outlines subaerial region used in center of mass (Figure 4.8) and volume calculation (Figure 4.9). Magenta x marks subaerial center of mass (Figure 4.8). Thick black lines mark transects B and F in Figure 4.7.

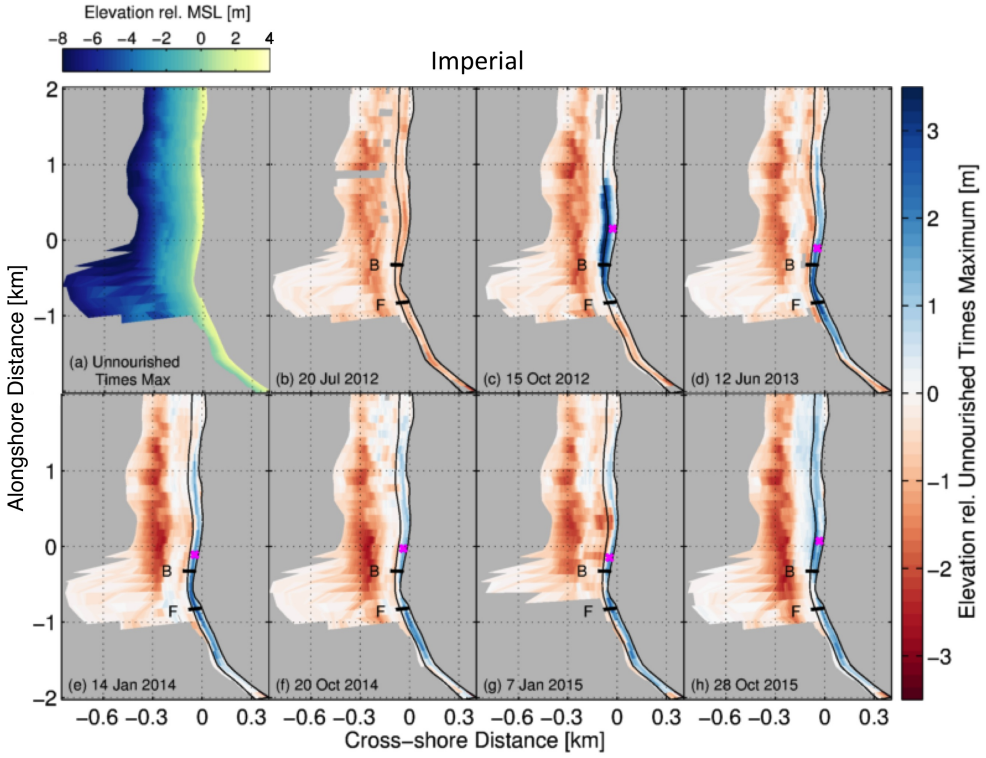

Figure 4.6: Nourishment evolution at Imperial Beach. (a) Map of maximum elevation (relative to MSL) over un-nourished observations (all surveys before 7 Sept 2012). (b-h) Time sequential maps of sand elevation fluctuation, relative to maximum un-nourished observation (a). These maps have an alongshore resolution of $\Delta\tilde{y}$ = 100m and the interpolation is not plotted where NMSE > 0.2 (Appendix 4.A). Thin black line outlines subaerial region used in center of mass (Figure 4.8) and volume calculation (Figure 4.9). Magenta x marks subaerial center of mass (Figure 4.8). Thick black lines mark transects B and F in Figure 4.7.

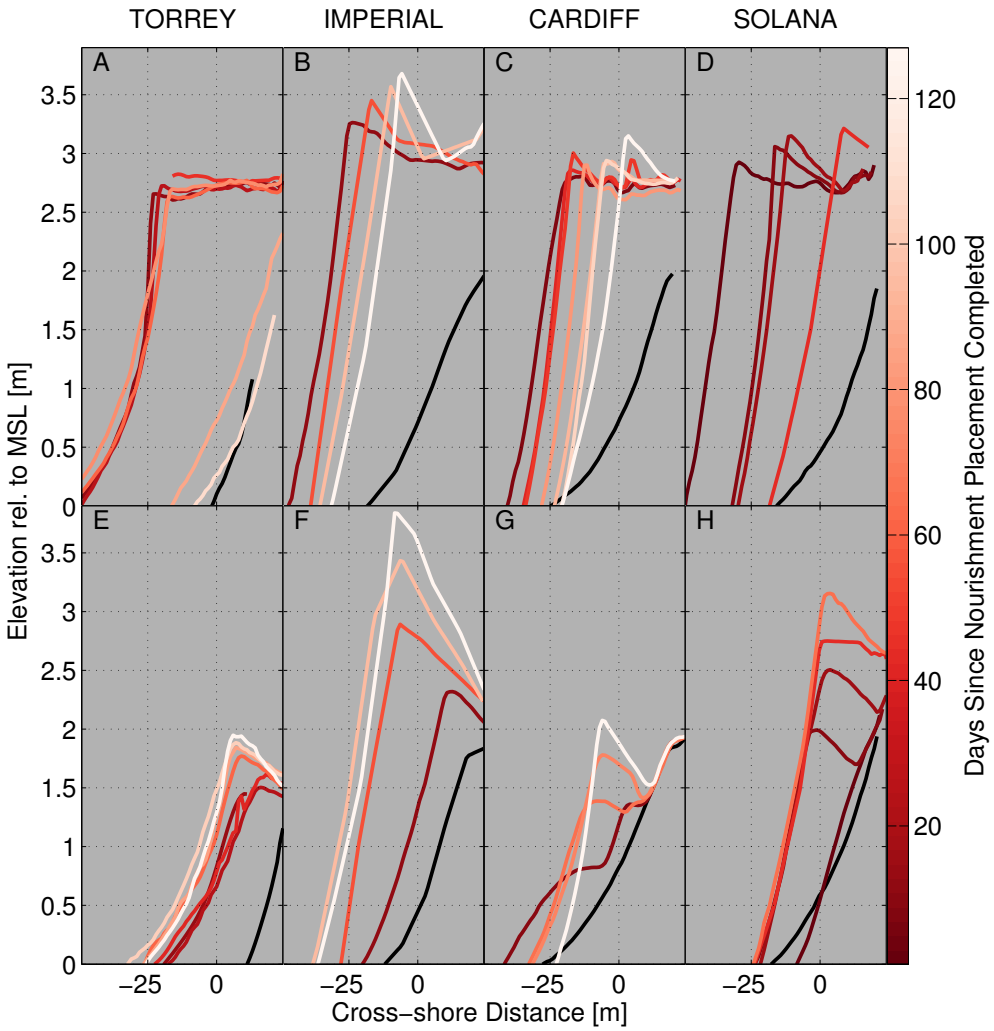

Figure 4.7: Subaerial beach elevation (above MSL) versus time since nourishment (color bar) at (left to right) Torrey, Imperial, Cardiff, and Solana Beach. (A-D) Original placement region. (E-H) Adjacent to original placement region. Transect line locations (A-H) are shown in Figures 4.3-6, and 4.B.1-B.4.

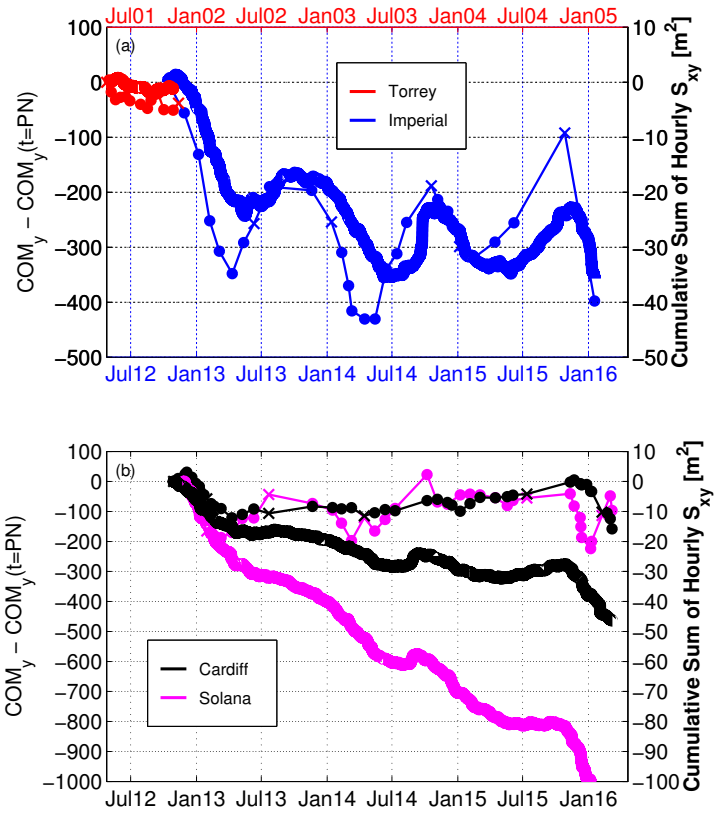

Figure 4.8: Thin lines in both panels show the alongshore position of the center of mass of subaerial sand "in play", COM_y, versus time. Center of mass is plotted relative to post-nourishment alongshore position, $COM_y(t = PN)$, and is in coastline following coordinates (Appendix 4.A). X marks surveys shown in Figs 3-6, B1-B4. Sand in play is defined as the volume of sand between the observed elevation at a given time and the minimum surface ever observed at each grid point (Figure 4.A.1). Locations with a mean elevation > -0.5 m MSL are considered subaerial (black outline Figures 4.3-6, 4.B.1-4), because this region is consistently measured in monthly subaerial surveys. This analysis is done using subaerial maps with an alongshore resolution of $\Delta\tilde{y}$ = 20m. The center of mass from surveys where more than 10% of the map has NMSE>0.2 is not plotted (Appendix 4.A). Thick lines in both panels show cumulative hourly wave S_{xy} radiation stress [Longuet-Higgens and Stewart 1964] versus time. S_{xy}, alongshore averaged over the entire alongshore reach, is a proxy for the wave-driven alongshore current [Longuet-Higgins 1970]. We will test the sensitivity (potentially strong) of the S_{xy} trend to tweaking the angle of coastline at Cardiff and Solana Beach (panel b).

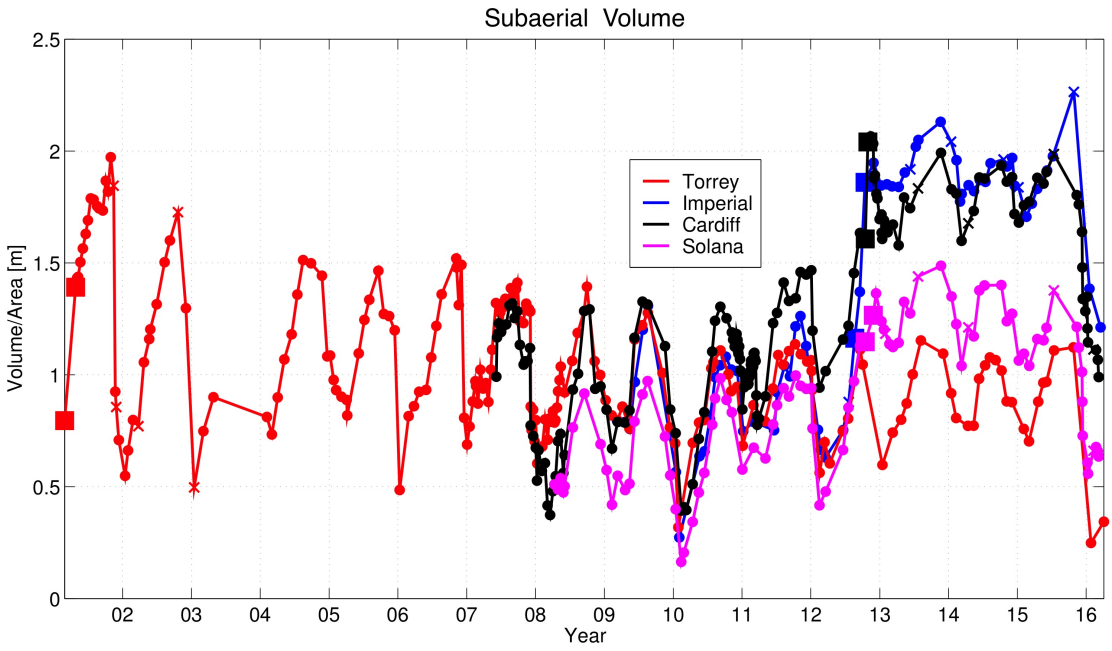

Figure 4.9: Subaerial volume divided by survey area versus time at four beaches (legend) relative to the minimum observed surface (Figure 4.A.1). Subaerial regions are outlined in Figures 4.3-6, 4.B.1-4. Nourishments occurred between the pre- and post-nourishment surveys (big squares). Xs show other surveys plotted in Figures 4.3-6, 4.B.1-4. This analysis is done using maps with an alongshore resolution of $\Delta\tilde{y}$ = 20m. Surveys where more than 10% of the map has NMSE>0.2 are not plotted (Appendix 4.A).

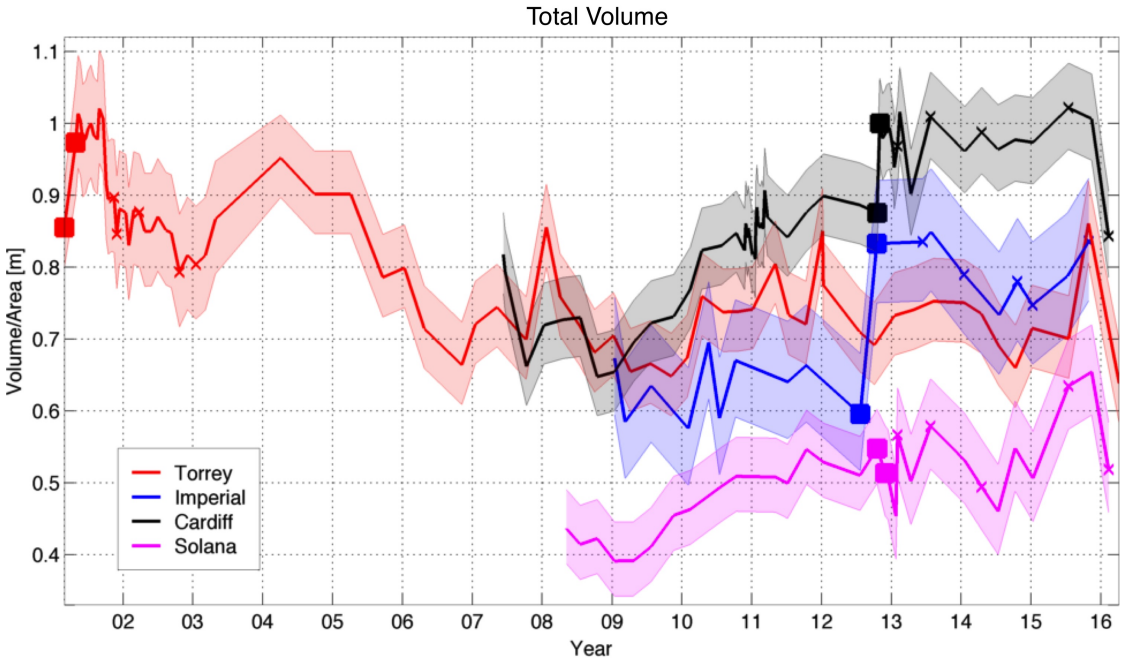

Figure 4.10: Total volume divided by survey area versus time at four beaches (legend) relative to the minimum observed surface (Figure 4.A.1). Nourishments occurred between the pre- and post-nourishment surveys (big squares). Xs show other surveys plotted in Figures 4.3-6, 4.B.1-4. Error bars are calculated using method in Appendix 4.C. This analysis is done using maps of the full surveys with an alongshore resolution of $\Delta\tilde{y}$ = 100m at Imperial and Solana Beach, $\Delta\tilde{y}$ = 50 at Cardiff, and $\Delta\tilde{y}$ = 20 at Torrey Pines. Surveys where more than 10% of the map has NMSE>0.2 are not plotted (Appendix 4.A).

Figure 4.11: Imperial Beach photographs. (a) landward tipping nourishment pad, (b) water pooled in backbeach on the nourishment pad [Hargrove, 2015], (c) nearby wet garage [Hargrove, 2015], (d) Tijuana River mouth after it was mechanically opened after clogging with sand [Baker, 2016]

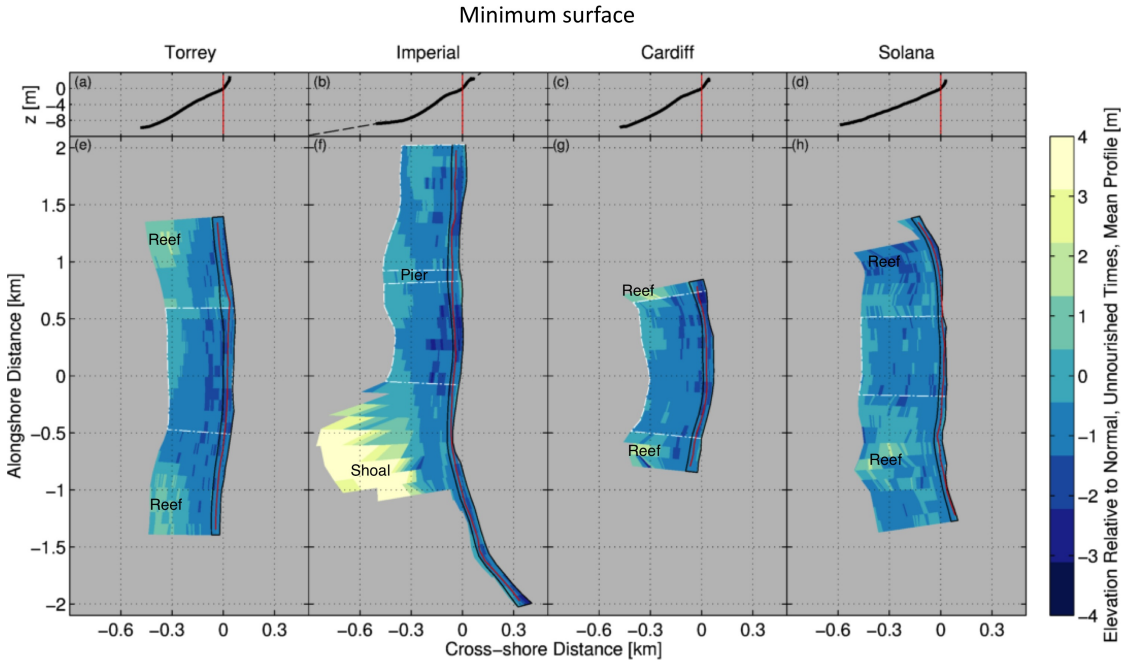

Figure 4.A.1: (a-d) Alongshore-averaged normal mean profiles are calculated during unnourished times and in regions outlined by white dashed lines in panels e-h, away from rocky reef, cobble relic shoal, and a recreation pier. The thin dashed line at Imperial Beach (b) is extrapolated. (e-h) Minimum surfaces observed at each grid point over the entire record (color scale bar), relative to the normal mean profiles in (a-d). At each alongshore location, the mean profile is aligned with the mean shoreline (solid red line in bottom panels) and subtracted from the minimum surface. Many of the regions identified as reef or shoal, have minimum elevations that are elevated above the normal mean profile. This analysis is performed using maps with an alongshore resolution of $\Delta\tilde{y}$ = 100m at Imperial and Solana Beach, $\Delta\tilde{y}$ = 50 at Cardiff, and $\Delta\tilde{y}$ = 20 at Torrey Pines, where interpolated regions with NMSE>0.2 are not considered.

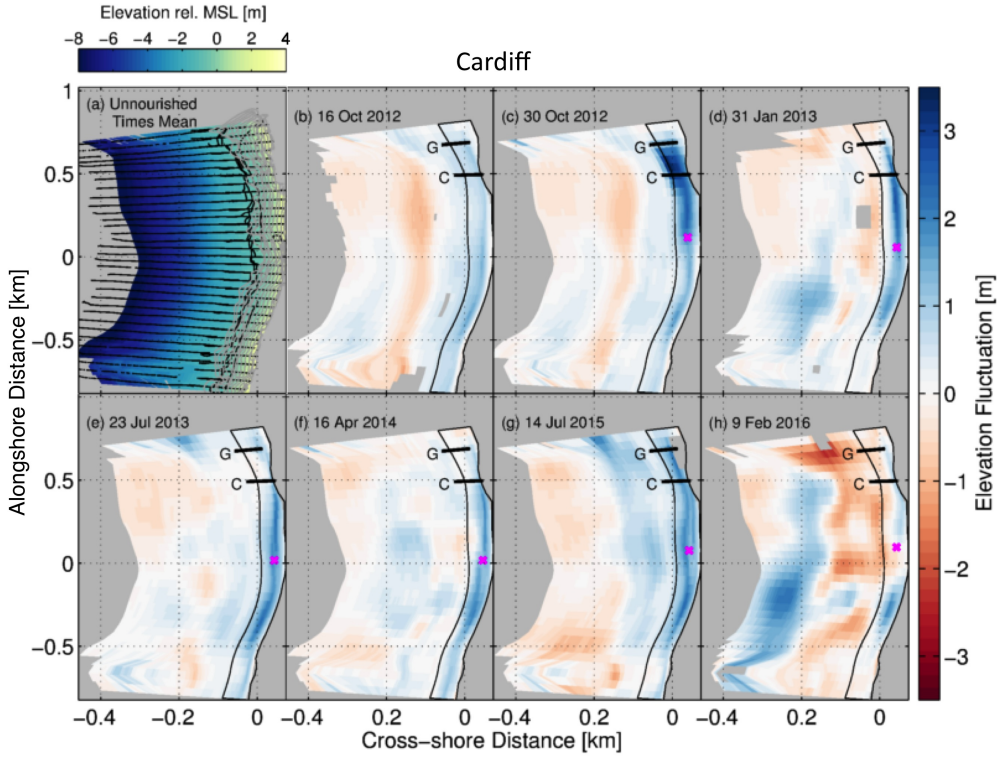

Figure 4.B.1: Nourishment evolution at Cardiff Beach. (a) Map of mean elevation (relative to MSL) averaged over observations from unnourished times (all surveys before 25 Oct 2012). Example tracks are shown for a full, high-resolution survey (black) and a subaerial survey (gray). (b-h) Time sequential maps of sand elevation fluctuation relative to mean shown in (a). These maps have an alongshore resolution of $\Delta\tilde{y} = 50$m and the interpolation is not plotted where NMSE > 0.2 (Appendix 4.A). Thin black line outlines subaerial region used in center of mass (Figure 4.8) and volume calculation (Figure 4.9). Magenta x marks subaerial center of mass (Figure 4.8). Thick black lines mark transects C and G in Figure 4.7.

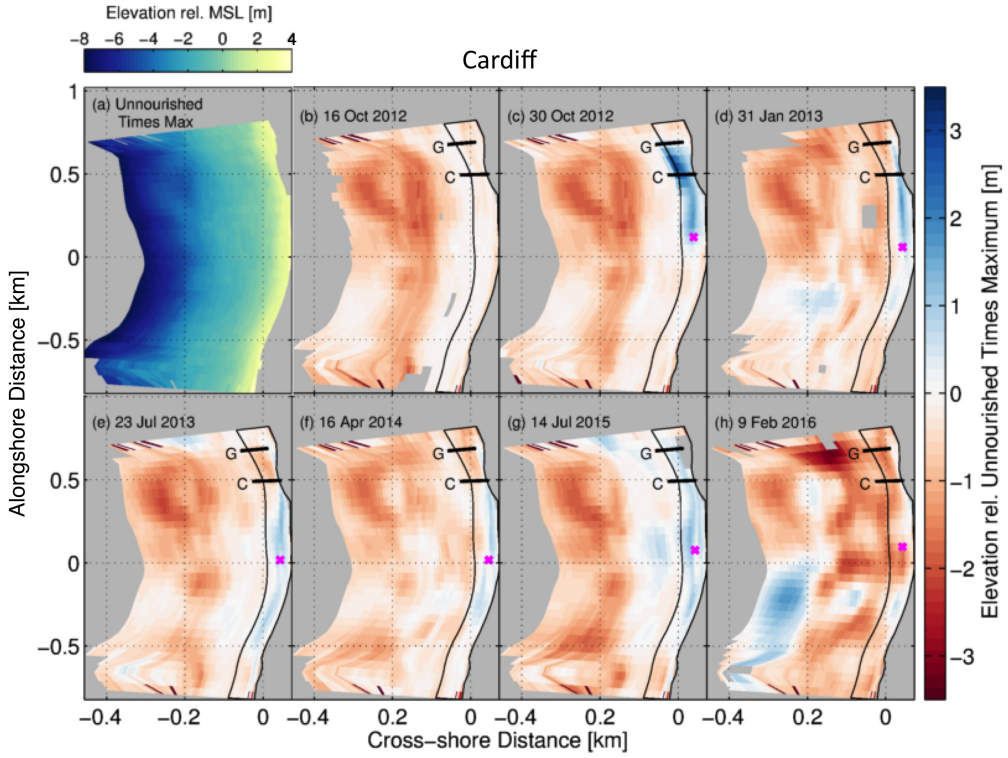

Figure 4.B.2: Nourishment evolution at Cardiff Beach. (a) Map of maximum elevation (relative to MSL) over un-nourished observations (all surveys before 25 Oct 2012). (b-h) Time sequential maps of sand elevation fluctuation, relative to maximum un-nourished observation (a). These maps have an alongshore resolution of $\Delta\tilde{y}$ = 50m and the interpolation is not plotted where NMSE > 0.2 (Appendix 4.A). Thin black line outlines subaerial region used in center of mass (Figure 4.8) and volume calculation (Figure 4.9). Magenta x marks subaerial center of mass (Figure 4.8). Thick black lines mark transects C and G in Figure 4.7.

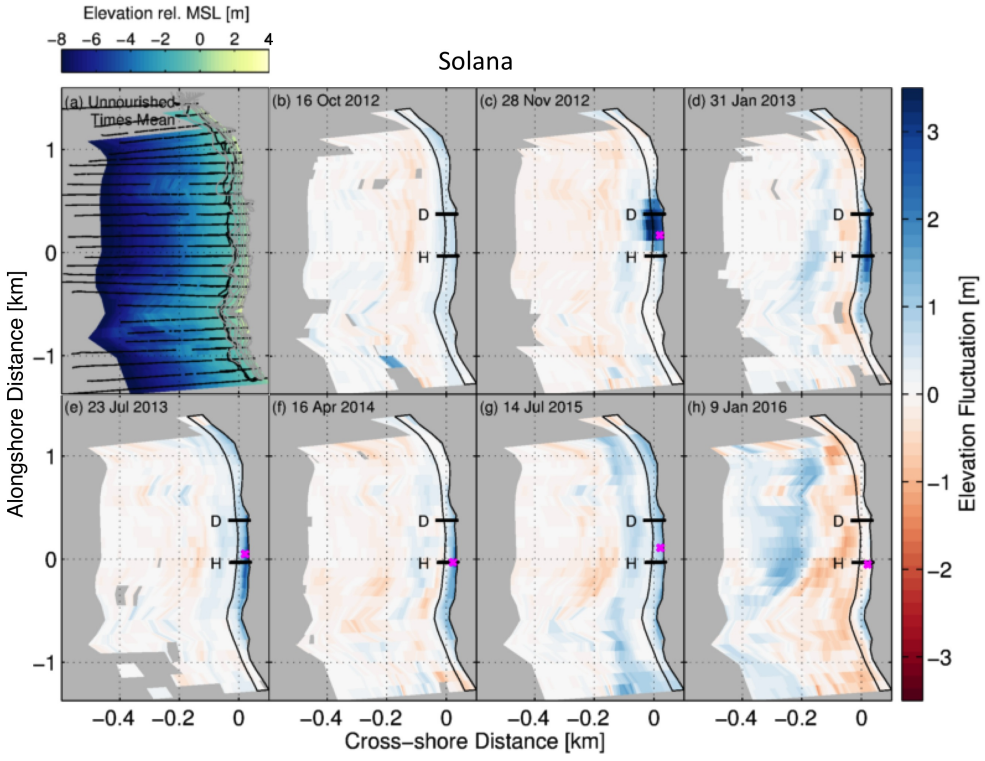

Figure 4.B.3: Nourishment evolution at Solana Beach. (a) Map of mean elevation (relative to MSL) averaged over observations from unnourished times (all surveys before 4 Nov 2012). Example tracks are shown for a full survey (black) and a subaerial survey (gray). (b-h) Time sequential maps of sand elevation fluctuation relative to mean shown in (a). These maps have an alongshore resolution of $\Delta\tilde{y}$ = 100m and the interpolation is not plotted where NMSE $>$ 0.2 (Appendix 4.A). Thin black line outlines subaerial region used in center of mass (Figure 4.8) and volume calculation (Figure 4.9). Magenta x marks subaerial center of mass (Figure 4.8). Thick black lines mark transects D and H in Figure 4.7.

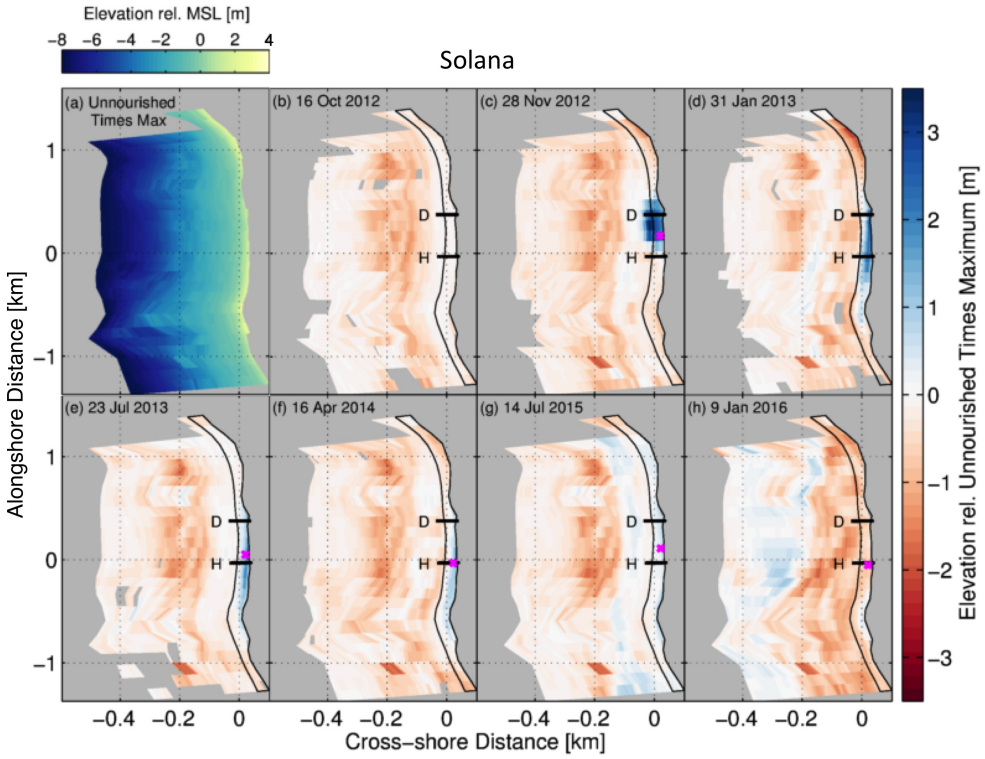

Figure 4.B.4: Nourishment evolution at Solana Beach. (a) Map of maximum elevation (relative to MSL) over un-nourished observations (all surveys before 4 Nov 2012). (b-h) Time sequential maps of sand elevation fluctuation, relative to maximum un-nourished observation (a). These maps have an alongshore resolution of $\Delta\tilde{y}$ = 100m and the interpolation is not plotted where NMSE > 0.2 (Appendix 4.A). Thin black line outlines subaerial region used in center of mass (Figure 4.8) and volume calculation (Figure 4.9). Magenta x marks subaerial center of mass (Figure 4.8). Thick black lines mark transects D and H in Figure 4.7.

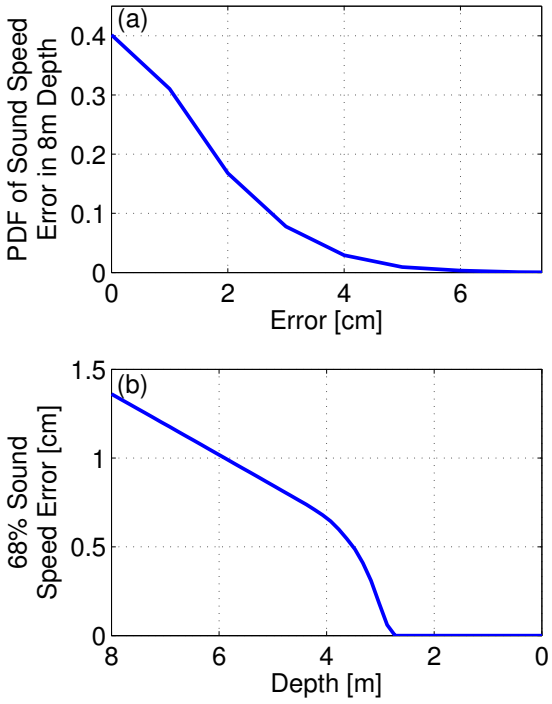

Figure 4.C.1: (a) PDF of speed of sound errors in 8m depth. (b) 68% speed of sound error across the profile, extracted from the PDF at each depth.

References

Alexandrakis, G., C. Manasakis, and N. A. Kampanis (2015), Valuating the effects of beach erosion to tourism revenue. A management perspective, *Ocean & Coastal Management*, *111*, 1–11.

Allan, J. C., and P. D. Komar (2006), Climate controls on US West Coast erosion processes, *Journal of Coastal Research*, pp. 511–529.

Anfuso, G., Benavente, J., and Gracia, F. J. (2001). Morphodynamic responses of nourished beaches in SW Spain. *Journal of Coastal Conservation*, *7*(1), 71-80.

Aubrey, D. G. (1979), Seasonal patterns of onshore/offshore sediment movement, *Journal of Geophysical Research*, *84*(C10), 6347–6354.

Aubrey, D. G., D. L. Inman, and C. D. Winant (1980), The statistical prediction of beach changes in southern California, *Journal of Geophysical Research*, *85*(C6), 3264–3276.

Bailard, J. A. (1981). An energetics total load sediment transport model for a plane sloping beach. *Journal of Geophysical Research: Oceans*, *86*(C11), 10938-10954.

Baker, D. (2016), Tijuana River reopened after blockage kills sharks, floods streets, *San Diego Union Tribune*, 12 April 2016.

Bakker, W. T., (1968), The dynamics of a coast with a groin system, in *Proceedings 11th Conference on Coastal Engineering*.

Barnard, P. L., J. Allan, J. E. Hansen, G. M. Kaminsky, P. Ruggiero, and A. Doria (2011), The impact of the 2009–10 El Niño Modoki on US West Coast beaches, *Geophysical Research Letters*, *38*(13).

Barnard, P. L., A. D. Short, M. D. Harley, K. D. Splinter, S. Vitousek, I. L. Turner, J. Allan, M. Banno, K. R. Bryan, A. Doria, et al. (2015), Coastal vulnerability across the Pacific dominated by El Niño Southern Oscillation, *Nature Geoscience*, *8*(10), 801–807.

Barth, N., and C. Wunsch (1990), Oceanographic experiment design by simulated annealing, *Journal of Physical Oceanography*, *20*(9), 1249–1263.

Benedet, L., Finkl, C. W., and Hartog, W. M. (2007). Processes controlling development of erosional hot spots on a beach nourishment project. *Journal of Coastal Research*, 33-48.

Bocamazo, L. M., Grosskopf, W. G., and Buonuiato, F. S. (2011). Beach nourishment, shoreline change, and dune growth at Westhampton Beach, New York, 1996-2009. *Journal of Coastal Research*, 181-191.

Borsa, A. A., Minster, J. B., Bills, B. G., and Fricker, H. A. (2007). Modeling long-period noise in kinematic GPS applications. *Journal of Geodesy*, 81(2), 157-170.

Bowen, A. J., D. Inman, and V. Simmons (1968), Wave set-down and set-up, *Journal of Geophysical Research*, *73*(8), 2569–2577.

Bretherton, F. P., Davis, R. E., and Fandry, C. B. (1976, July). A technique for objective analysis and design of oceanographic experiments applied to MODE-73. In Deep Sea Research and Oceanographic Abstracts (Vol. 23, No. 7, pp. 559-582).

Browder, A. E., and R. G. Dean (2000), Monitoring and comparison to predictive models of the Perdido Key beach nourishment project, Florida, USA, *Coastal Engineering*, *39*(2), 173–191.

Bruun, P. (1954), Coastal erosion and development of beach profiles, *Tech. Rep. Memo 44*, U.S. Army Corps of Engineers, Washington, D. C.

Bruun, P. (1995), The development of downdrift erosion, *Journal of Coastal Research*, pp. 1242–1257.

Bruun, P. (1962), Sea level rise as a cause of shore erosion, *Proceedings of the American Society of Civil Engineers, Journal of the Waterways Harbors and Coastal Engineering Division*, *88*, 117–130.

Callaghan, D. P., R. Ranasinghe, and D. Roelvink (2013), Probabilistic estimation of storm erosion using analytical, semi-empirical, and process based storm erosion models, *Coastal Engineering*, *82*, 64–75.

Carson, M., A. Köhl, D. Stammer, A. Slangen, C. Katsman, R. van de Wal, J. Church, and N. White (2016), Coastal sea level changes, observed and projected during the 20th and 21st century, *Climatic Change*, *134*(1-2), 269–281.

Castelle, B., V. Marieu, S. Bujan, S. Ferreira, J.-P. Parisot, S. Capo, N. Sénéchal, and T. Chouzenoux (2014), Equilibrium shoreline modelling of a high-energy meso-macrotidal multiple-barred beach, *Marine Geology*, *347*, 85–94.

Castelle, B., Turner, I. L., Bertin, X., and Tomlinson, R. (2009). Beach nourishments at Coolangatta Bay over the period 1987-2005: impacts and lessons. *Coastal Engineering*, *56*(9), 940-950.

[CDIP] Coastal Data Information Program (2016), University of California, San Diego, *https://cdip.ucsd.edu/*, Accessed: 4 Mar 2016

CERC (1984). Shore Protection Manual. Vicksburg, Mississippi: U.S. Army Coastal Engineering Research Center, Corps of Engineers.

Clayton, T. (1991), Beach replenishment activities on US Continental Pacific Coast, *Journal of Coastal Research*, pp. 1195–1210.

Coastal Frontiers (2005), 2004 regional beach monitoring program, report, San Diego Association of Governments, 401 B Street, Suite 800, San Diego, CA 92101, USA.

Coastal Frontiers (2015), 2014 regional beach monitoring program, report, San Diego Association of Governments, 401 B Street, Suite 800, San Diego, CA 92101, USA.

Climate Prediction Center, 2016 (2006), February 2016 ENSO diagnostic discussion. *http://www.cpc.ncep.noaa.gov*, Accessed: 4 Mar 2016

Coco, G., N. Senechal, A. Rejas, K. R. Bryan, and S. Capo (2014), Beach response to a sequence of extreme storms, *Geomorphology*.

Cooke, B. C., A. R. Jones, I. D. Goodwin, and M. J. Bishop (2012), Nourishment practices on Australian sandy beaches: a review, *Journal of Environmental Management*, *113*, 319–327.

Cooper, N. J. (1998), Assessment and prediction of Poole Bay (UK) sand replenishment schemes: application of data to Fuhrboter and Verhagen Models. *Journal of Coastal Research*, 353-359.

Davis Jr, R. A., Wang, P., and Silverman, B. R. (2000). Comparison of the performance of three adjacent and differently constructed beach nourishment projects on the Gulf Peninsula of Florida. *Journal of Coastal Research*, 396-407.

Davidson, M. A., and I. L. Turner (2009), A behavioral template beach profile model for predicting seasonal to interannual shoreline evolution, *Journal of Geophysical Research: Earth Surface*, *114*(F1).

Davidson, M. A., R. P. Lewis, and I. L. Turner (2010), Forecasting seasonal to multi-year shoreline change, *Coastal Engineering*, *57*, 620–629.

Davidson, M. A., K. D. Splinter, and I. L. Turner (2013), A simple equilibrium model for predicting shoreline change, *Coastal Engineering*, *73*, 191–202.

Davis, R. E. (1976), Predictability of sea surface temperature and sea level pressure anomalies over the North Pacific Ocean, *Journal of Physical Oceanography*, *6*(3), 249–266.

Delannay, R., Louge, M., Richard, P., Taberlet, N., and Valance, A. (2007). Towards a theoretical picture of dense granular flows down inclines. *Nature Materials*, *6*(2), 99- 108.

de Schipper, M. A., S. de Vries, G. Ruessink, R. C. de Zeeuw, J. Rutten, C. van Gelder-Maas, and M. J. Stive (2016), Initial spreading of a mega feeder nourishment: observations of the sand engine pilot project, *Coastal Engineering*, *111*, 23–38.

Dean, R. G. (1991), Equilibrium beach profiles: characteristics and applications, *Journal of coastal research*, pp. 53–84.

Dean, R. G., and Yoo, C. H. (1992). Beach-nourishment performance predictions. *Journal of waterway, port, coastal, and ocean engineering*, *118*(6), 567-586.

Diehl, P. (2015), Solana Beach, Encinitas OK sand replenishment, *San Diego Union Tribune*, 15 Oct 2015.

Dietrich, W. E. (1982). Settling velocity of natural particles. *Water resources research*, *18*(6), 1615-1626.

Dingler, J. R., and T. E. Reiss (2002), Changes to Monterey Bay beaches from the end of the 1982–83 El Niño through the 1997–98 El Niño, *Marine Geology*, *181*(1), 249–263.

Dubarbier, B., B. Castelle, B. Marieu, and B. G. Ruessink (2015), Process-based modelling of cross-shore sandbar behaviour, *Coastal Engineering*, *95*, 35–50.

Elko, N., F. Feddersen, D. Foster, C. Hapke, J. McNinch, R. Mulligan, H. T. Özkan-Haller, N. Plant, and B. Raubenheimer (Eds.) (2014), *The Future of Nearshore Processes Research*.

Elko, N. A., R. A. Holman, and G. Gelfenbaum (2005), Quantifying the rapid evolution of a nourishment project with video imagery, *Journal of Coastal Research*, pp. 633–645.

Elko, N. A., and P. Wang (2007), Immediate profile and planform evolution of a beach nourishment project with hurricane influences, *Coastal Engineering*, *54*(1), 49–66.

Enfield, D. B., and J. Allen (1980), On the structure and dynamics of monthly mean sea level anomalies along the Pacific coast of North and South America, *Journal of Physical Oceanography*.

Flick, R. E., and A. Badan-Dangon (1989), Coastal sea levels during the January 1988 storm off the Californias, *Shore and Beach*, *57*(4), 28–31.

Gallagher, E. L., S. Elgar, and R. T. Guza (1998), Observations of sand bar evolution on a natural beach, *Journal of Geophysical Research*, *103*(C2), 3203–3215.

Gallien, T. W., W. C. O'Reilly, R. E . Flick, and R. T. Guza (2015), Geometric properties of anthropogenic flood control berms on southern California beaches, *Ocean & Coastal Management*, *105*, 35–47.

Gares, P. A., Y. Wang, and S. A. White (2006), Using LIDAR to monitor a beach nourishment project at Wrightsville beach, North Carolina, USA, *Journal of Coastal Research*, pp. 1206–1219.

Griggs, G., and N. Kinsman (2016), Beach widths, cliff slopes, and artificial nourishment along the California coast, *Shore and Beach*, *84*(1).

Group Delta Consultants (1998), Shoreline erosion study North Solana Beach, California report, Solana Beach Coastal Preservation Association, 219 Pacific Avenue Solana Beach, California 92075, USA

Guza, R. T., and E. B. Thornton (1981), Wave set-up on a natural beach, *Journal of Geophysical Research*, *86*(C5), 4133–4137.

Haas, J. K. (2005), Grain size and mineralogical characteristics of beach sand in the Oceanside Littoral Cell, Southern California: implications for sediment provenance, Master's thesis, University of California, San Diego.

Haddad, T. C., and O. H. Pilkey (1998), Summary of the New England beach nourishment experience (1935-1996), *Journal of Coastal Research*, pp. 1395–1404.

Hamlington, B., R. Leben, K.-Y. Kim, R. Nerem, L. Atkinson, and P. Thompson (2015), The effect of the El Niño-Southern Oscillation on US regional and coastal sea level, *Journal of Geophysical Research: Oceans*, *120*(6), 3970–3986.

Hamm, L., M. Capobianco, H. Dette, A. Lechuga, R. Spanhoff and M. Stive (2002), A summary of European experience with shore nourishment, *Coastal Engineering*, *47*(2), 237–264.

Hanson, H., A. Brampton, M. Capobianco, H. Dette, L. Hamm, C. Laustrup, A. Lechuga, and R. Spanhoff (2002), Beach nourishment projects, practices, and objectives - a European overview, *Coastal Engineering*, *47*(2), 81–111.

Hargrove, D. (2015), What happens when you bring sand to the beach: IB homeowners claim SANDAG created flood hazard, *San Diego Reader*, 24 Jan 2015.

Hoefel, F., and S. Elgar (2003), Wave induced sediment transport and sandbar migration, *Science*, *299*(5614), 1885–1887.

Holland, K. T. (1998), Beach cusp formation and spacings at Duck, USA, *Continental Shelf Research*, *18*(10), 1081–1098.

Holman, R. A., D. M. Lalejini, K. Edwards and J. Veeramony (2014), A parametric model for barred equilibrium beach profiles, *Coastal Engineering*, *90*, 85–94.

Horel, J. D. (1984), Complex principal component analysis: Theory and examples, *Journal of climate and Applied Meteorology*, *23*(12), 1660–1673.

Huyer, A., and R. L. Smith (1985), The signature of El Niño off Oregon, 1982–1983, *Journal of Geophysical Research: Oceans*, *90*(C4), 7133–7142.

Inman, D. L. (1953), Areal and seasonal variations in beach and nearshore sediments at La Jolla, California, *Tech. Rep. Memo 39*, Beach Erosion Board, U.S. Army Corps of Engineers.

Inman, D. L., and G. A. Rusnak (1956), Changes in sand level on the beach and shelf at La Jolla, California, *Tech. Rep. Memo 82*, Beach Erosion Board, U.S. Army Corps of Engineers.

Kamphuis, J. W. (1991). Alongshore sediment transport rate. *Journal of Waterway, Port, Coastal, and Ocean Engineering*, *117*(6), 624-640.

Kana, T. W., and R. K. Mohan (1998), Analysis of nourished profile stability following the fifth hunting island (SC) beach nourishment project, *Coastal Engineering*, *33*(2), 117–136.

Kelly, K. A. (1988), Comment on "Empirical orthogonal function analysis of advanced very high resolution radiometer surface temperature patterns in Santa Barbara Channel" by GSE Lagerloef and RL Bernstein, *Journal of Geophysical Research: Oceans (1978–2012)*, *93*(C12), 15,753–15,754.

Kirkpatrick, S., and M. P. Vecchi (1983), Optimization by simmulated annealing, *Science*, *220*(4598), 671–680.

Konicki, K. M., and R. A. Holman (2000), The statistics and kinematics of transverse sand bars on an open coast, *Marine Geology*, *169*(1), 69–101.

Kriebel, D. L., and R. G. Dean (1985), Numerical simulation of time-dependent beach and dune erosion, *Coastal Engineering*, *9*(3), 221–245.

Kriebel, D. L., and R. G. Dean (1993), Convolution method for time dependent beach profile response, *Journal of Waterway, Port, Coastal, and Ocean Engineering*, *119*, 204–226.

Kuang, C., Pan, Y., Zhang, Y., Liu, S., Yang, Y., Zhang, J., and Dong, P. (2011). Performance evaluation of a beach nourishment project at West Beach in Beidaihe, China. *Journal of Coastal Research*, *27*(4), 769-783.

Kuriyama, Y. (2012), Process-based one-dimensional model for cyclic longshore bar evolution., *Coastal Engineering*, *62*, 48–61.

Larson, M., and N. C. Kraus (1989), SBEACH: Numerical model for simulating storm-induced beach change, *Tech. Rep. CERC-89-9*, U.S. Army Corps of Engineers, Vicksburg, Mississippi.

Larson, M., and N. C. Kraus (1994), Temporal and spatial scales of beach profile change, Duck, North Carolina, *Marine Geology*, *117*(1), 75–94.

Larson, M., M. Capobianco, and H. Hanson (2000), Relationship between beach profiles and waves at Duck, North Carolina, determined by canonical correlation analysis, *Marine Geology*, *163*(1-4), 275–288.

Lippmann, T. C., and R. A. Holman (1990), The spatial and temporal variability of sand bar morphology, *Journal of Geophysical Research*, *95*(C7), 11,575.

Longuet-Higgins, M. S. (1970). Longshore currents generated by obliquely incident sea waves, 1. *J. Geophys. Res*, *75*(33), 6778-6789.

Longuet-Higgins, M. S., and R. Stewart (1962), Radiation stress and mass transport in gravity waves, with application to surf beats, *Journal of Fluid Mechanics*, *13*(04), 481–504.

Lorenz, E. N. (1956), Empirical orthogonal functions and statistical weather prediction, *Tech. Rep. No. 1*, Department of Meteorology, Massachusetts Institute of Technology.

Ludka, B. C., T. Gallien, S. Crosby, R.T. Guza, (2016), Mid-El Niño erosion at nourished and unnourished southern California beaches. *Geophysical Research Letters*, *42*(9),4510–4516

Ludka, B., R. Guza, W. O'Reilly, and M. Yates (2015), Field evidence of beach profile evolution toward equilibrium, *Journal of Geophysical Research: Oceans*, *120*(11), 7574–7597.

Luo, S., F. Cai, H. Liu, G. Lei, H. Qi, and X. Su (2015), Adaptive measures adopted for risk reduction of coastal erosion in the People's Republic of China, *Ocean & Coastal Management*, *103*, 134–145.

McCall, R. T., J. S. M. Van Thiel de Vries, N. G. Plant, A. R. Van Dongeren, J. A. Roelvink, D. M. Thompson, and A. J. H. M. Reniers (2010), Two-dimensional time dependent hurricane overwash and erosion modeling at Santa Rosa Island, *Coastal Engineering*, *57*(7), 668–683.

McGranahan, G., D. Balk, and B. Anderson (2007), The rising tide: assessing the risks of climate change and human settlements in low elevation coastal zones, *Environment and Urbanization*, *19*(1), 17–37.

Miller, J. K., and R. G. Dean (2004), A simple new shoreline change model, *Coastal Engineering*, *51*(7), 531–556.

Moffatt and Nichol (2009), Coastal regional sediment management plan for the San Diego region, *Tech. rep.*, Prepared for the SANDAG and California Coastal Sediment Management Workgroup, 3780 Kilroy Airport Way, Suite 600, Long Beach, California 90806.

Nicholls, R. J. (2011), Planning for the impacts of sea level rise, *Oceanography*, *24*(2), 144–157.

O'Reilly, W. C., and R. T. Guza (1998), Assimilating coastal wave observations in regional swell predictions. Part I: Inverse methods, *Journal of Physical Oceanography*, *28*(4), 679–691.

Pape, L., N. G. Plant, and B. G. Ruessink (2010), On crossshore migration and equilibrium states of nearshore sandbars, *Journal of Geophysical Research: Oceans (1978–2012)*, *115*(F3).

Pawka, S. S. (1983), Island shadows in wave directional spectra, *Journal of Geophysical Research: Oceans (1978–2012)*, *88*(C4), 2579–2591.

Pelnard-Considére, R., (1956), Essai de theorie de l'evolution des formes de rivage en plages de sable et de galets, in *4th Journees de l'Hydraulique, Les Energies de la Mer, Paris*, vol. III-1, pp. 289298, Soc. de Hydrotech. de Fr., Paris.

Pender, D., and H. Karunarathna (2013), A statistical-process based approach for modelling beach profile variability, *Coastal Engineering*, *81*, 19–29.

Pendleton, L., C. Mohn, R. K. Vaughn, P. King, J. G. Zoulas (2011), Size matters: The economic value of beach erosion and nourishment in Southern California, *Contemporary Economic Policy*, *30*(2), 223–237.

Pianca, C., R. Holman, and E. Siegle (2015), Shoreline variability from days to decades: Results of long-term video imaging, *Journal of Geophysical Research: Oceans*

Plant, N. G., R. A. Holman, M. H. Freilich, and W. A. Birkemeier (1999), A simple model for interannual sandbar behavior, *Journal of Geophysical Research*, *104*(C7), 15,755.

Plant, N. G., M. H. Freilich, and R. A. Holman,(2001), Role of morphologic feedback in surf zone sandbar response, *Journal of Geophysical Research*, *106*(C1), 973–989.

Plant, N. G., K. T. Holland, and R. A. Holman,(2006), A dynamical attractor governs beach response to storms, *Geophysical Research Letters*, *33*, L17607.

Revell, D. L., J. E. Dugan, and D. M. Hubbard (2011), Physical and ecological responses of sandy beaches to the 1997-98 El Niño, *Journal of Coastal Research*, *27*(4), 718–730.

Ribberink, J. S. (1998). Bed-load transport for steady flows and unsteady oscillatory flows. *Coastal Engineering*, *34*(1), 59-82.

Roelvink, D., A. Reniers, A. P. van Dongeren, J. van Thiel de Vries, R. McCall, and J. Lescinski (2009), Modelling storm impacts on beaches, dunes and barrier islands, *Coastal Engineering*, *56*(11), 1133–1152.

Roelvink, D. (2015), Addressing local and global sediment imbalances: coastal sediments as rare minerals, *The Proceedings of the Coastal Sediments 2015*.

Roelvink, J. A., and I. Brøker (1993), Cross-shore profile models, *Coastal Engineering*, *21*(1), 163–191.

Ruessink, B. G. (2003), Intersite comparison of interannual nearshore bar behavior, *Journal of Geophysical Research*, *108*(C8), 3249.

Ruessink, B. G., Y. Kuriyama, A. J. H. M. Reniers, J. A. Roelvink, and D. J. R. Walstra (2007), Modeling cross-shore sandbar behavior on the timescale of weeks, *Journal of Geophysical Research*, *112*, F03010.

Ruessink, B. G., Miles, J. R., Feddersen, F., Guza, R. T., and Elgar, S. (2001). Modeling the alongshore current on barred beaches. *Journal of Geophysical Research*, *106*(C10), 22451-22463.

Ryan, H., and M. Noble (2002), Sea level response to ENSO along the central California coast: how the 1997–1998 event compares with the historic record, *Progress in Oceanography*, *54*(1), 149–169.

Sallenger, A. H., W. Krabill, J. Brock, R. Swift, S. Manizade, and H. Stockdon (2002), Sea-cliff erosion as a function of beach changes and extreme wave runup during the 1997–1998 El Niño, *Marine Geology*, *187*(3), 279–297.

Seymour, R., R. T. Guza, W. O'Reilly, and S. Elgar (2005), Rapid erosion of a small southern California beach fill, *Coastal Engineering*, *52*(2), 151–158.

Shepard, F. P. (1950), Beach cycles in southern California, *Tech. Rep. Memo 20*, U.S. Army Corps of Engineers, Washington, D. C.

Smith, J. E. (2016), El Niño raises concerns about coastal erosion, *San Diego Union Tribune*, 7 Feb 2016.

Speybroeck, J., D. Bonte, W. Courtens, T. Gheskiere, P. Grootaert, J. P. Maelfait, M. Mathys, S. Provoost, K. Sabbe, E. W. Stienen, et al. (2006), Beach nourishment: an ecologically sound coastal defence alternative? A review, *Aquatic Conservation: Marine and Freshwater Ecosystems*, *16*(4), 419–435.

Splinter, K. D., I. L. Turner, and M. A. Davidson (2013), How much data is enough? The importance of morphological sampling interval and duration for calibration of empirical shoreline models, *Coastal Engineering*, *77*, 14–27.

Splinter, K. D., I. L. Turner, M. A. Davidson, P. Barnard, B. Castelle, and J. Oltman-Shay (2014), A generalized equilibrium model for predicting daily to interannual shoreline response, *Journal of Geophysical Research: Earth Surface*, *119*(9), 1936–1958.

Stive, M. J., M. A. de Schipper, A. P. Luijendijk, S. G. Aarninkhof, C. van Gelder-Maas, J. S. van Thiel de Vries, S. de Vries, M. Henriquez, S. Marx, and R. Ranasinghe (2013), A new alternative to saving our beaches from sea-level rise: the sand engine, *Journal of Coastal Research*, *29*(5), 1001–1008.

Stockdon, H. F., R. A. Holman, and P. A. Howd (2006), Empirical parameterization of setup, swash, and runup, *Coastal Engineering*.

Stocker, T. F., D. Qin, G. K. Plattner, M. Tignor, S. K. Allen, J. Boschung, A. Nauels, Y. Xia, V. Bex, and P. M. Midgley (Eds.) (2013), *IPCC, 2013: Climate Change 2013: The Physical Science Basis. Contribution of Working Group I to the Fifth Assessment Report of the Intergovernmental Panel on Climate Change*, Cambridge University Press, Cambridge, United Kingdom and New York, NY, USA.

Stokes, C., M. Davidson, and P. Russell (2015), Observation and prediction of three-dimensional morphology at a high-energy macrotidal beach, *Geomorphology*, *243*, 1–13.

Thornton, E. B., and Guza, R. T. (1986). Surf zone longshore currents and random waves: Field data and models. *Journal of Physical Oceanography, 16*(7), 1165-1178.

Thornton, E. B., R. T. Humiston, and W. Birkemeier (1996), Bar/trough generation on a natural beach, *Journal of Geophysical Research*, *101*(C5), 12097–12110.

Trembanis, A. C., and O. H. Pilkey (1998), Summary of beach nourishment along the US Gulf of Mexico shoreline, *Journal of Coastal Research*, pp. 407–417.

Valverde, H. R., A. C. Trembanis, and O. H. Pilkey (1999), Summary of beach nourishment episodes on the US east coast barrier islands, *Journal of Coastal Research*, pp. 1100–1118.

van rijn, L. C., D. Walstra, B. Grasmeijer, J. Sutherland, S. Pan, and J. P. Sierra (2003), The predictability of cross-shore bed evolution of sandy beaches at the time scale of storms and seasons using process-based profile models, *Coastal Engineering*, *47*(3), 295–327.

Van Rijn, L. C. (2007a). Unified view of sediment transport by currents and waves. I: Initiation of motion, bed roughness, and bed-load transport. *Journal of Hydraulic Engineering*, *133*(6), 649-667.

van Rijn, L. C. (2007b). Unified view of sediment transport by currents and waves. II: Suspended transport. *Journal of Hydraulic Engineering*, *133*(6), 668-689.

Walstra, D. J. R., A. J. H. M. Reniers, R. Ranasinghe, J. A. Roelvink, and B. G. Ruessink. Sierra (2012), On bar growth and decay during interannual net offshore migration, *Coastal Engineering*, *60*, 190–200.

Warner, J. C., Armstrong, B., He, R., and Zambon, J. B. (2010). Development of a coupled ocean-atmosphere-wave-sediment transport (COAWST) modeling system. *Ocean modelling*, *35*(3), 230-244.

Wengrove, M. E., M. Henriquez, M. A. de Schipper, R. Holman, and M. J. F. Stive (2013), Monitoring morphology of the sand engine leeside using argus cbathy, in *Coastal Dynamics*.

Winant, C. D., D. L. Inman, and C. E. Nordstrom (1975), Description of seasonal beach changes using empirical eigenfunctions, *Journal of Geophysical Research*, *80*(15), 1979–1986.

Wooldridge, T., H. J. Heather, and J. R. Kohn (2016), Effects of beach replenishment on intertidal invertebrates: A 15-month, eight beach study, *Estuarine, Coastal and Shelf Science*, *175*(1), pp. 24–33.

WorleyParsons (2013), Assessing the value of coastal resources in Victoria, report, Level 6, 8 Nicholson St, East Melbourne VIC 3002, Australia.

Wright, L. D., and A. D. Short (1984), Morphodynamic variability of surf zones and beaches: a synthesis, *Marine Geology*, *56*(1), 93–118.

Wright, L. D., A. D. Short, and M. O. Green (1985), Short-term changes in the morphodynamic states of beaches and surf zones: An empirical predictive model,

Marine Geology, *62*(3-4), 339–364.

Yates, M. L., R. T. Guza, and W. C. O'Reilly (2009a), Equilibrium shoreline response: Observations and modeling, *Journal of Geophysical Research: Oceans (1978–2012)*, *114*(C9).

Yates, M. L., R. T. Guza, W. C. O'Reilly, and R. J. Seymour (2009b), Overview of seasonal sand level changes on Southern California beaches, *Shore and Beach*.

Yates, M., R. Guza, W. O'reilly, and R. Seymour (2009c), Seasonal persistence of a small southern California beach fill, *Coastal Engineering*, *56*(5), 559–564.

Yates, M. L., R. T. Guza, W. C. O'Reilly, J. E. Hansen, and P. L. Barnard (2011), Equilibrium shoreline response of a high wave energy beach, *Journal of Geophysical Research: Oceans (1978–2012)*, *116*(C4).

Young, A. P., R. T. Guza, P. N. Adams, W. C. O'Reilly, and R. E. Flick (2012), Cross-shore decay of cliff top ground motions driven by local ocean swell and infragravity waves, *Journal of Geophysical Research: Oceans (1978–2012)*, *117*(C6).